F

RECLAMATION

Managing Water in the West

Desalination and Water Purification Research and Development Program Report No. 134

Pilot-Scale Studies for Direct Contact Membrane Distillation-Based Desalination Process

U.S. Department of the Interior
Bureau of Reclamation

September 2009

REPORT DOCUMENTATION PAGE

Form Approved
OMB No. 0704-0188

1. REPORT DATE *(DD-MM-YYYY)*	2. REPORT TYPE	3. DATES COVERED *(From - To)*
September 2009	Final	October 2004–June 2007

4. TITLE AND SUBTITLE
Pilot-Scale Studies for Direct Contact Membrane Distillation-Based Desalination Process

5a. CONTRACT NUMBER
Agreement No. 04-FC-81-1037

5b. GRANT NUMBER

5c. PROGRAM ELEMENT NUMBER

6. AUTHOR(S)
Kamalwah K. Sirkar and Liming Song

5d. PROJECT NUMBER

5e. TASK NUMBER
Task G

5f. WORK UNIT NUMBER

7. PERFORMING ORGANIZATION NAME(S) AND ADDRESS(ES)
New Jersey Institute of Technology, Center for Membrane Technologies
Room 362 Tiernan Hall
323 Dr. King Blvd.
Newark NJ 07102

8. PERFORMING ORGANIZATION REPORT NUMBER

9. SPONSORING / MONITORING AGENCY NAME(S) AND ADDRESS(ES)
U.S. Department of the Interior, Bureau of Reclamation,
Technical Service Center, Environmental Services Division,
Water Treatment Engineering and Research Group, 86-68230,
PO Box 25007, Denver CO 80225-0007

10. SPONSOR/MONITOR'S ACRONYM(S)
Reclamation

11. SPONSOR/MONITOR'S REPORT NUMBER(S)
DWPR Report No. 134

12. DISTRIBUTION / AVAILABILITY STATEMENT
Available from the National Technical Information Service
Operations Division, 5285 Port Royal Road, Springfield VA 22161

13. SUPPLEMENTARY NOTES
Final report can be downloaded from Reclamation Web site:
http://www.usbr.gov/pmts/water/publications/reports.html

14. ABSTRACT ***(Maximum 200 words)***

A small pilot plant for direct contact membrane distillation- (DCMD) based desalination was built and operated successfully on a daily basis at United Technologies Research Center, East Hartford, Connecticut, for 3 months. The operation employed hot brine at 90–93 degrees Celcius (°C) and distillate at 20–54 °C. The hot brine was either city water and city water containing salt at the level of 3.5 percent (%), 6%, or 10% or seawater trucked in from Long Island Sound, Connecticut. One to ten horizontal, crossflow hollow fiber membrane modules, each having either 2,448 or 2,652 hollow fibers and 0.61 or 0.66-square-meter surface area, were combined in various configurations to study the plant performance. The highest water vapor flux of 55 kilograms per square meter per hour ($kg/m^2/h$) was achieved with two modules in series; the flux varied between 15 to 33 $kg/m^2/h$ for configurations employing 6 to 10 modules. The highest distillate production rate achieved was 0.62 gallons per minute. The membrane modules never showed any sign of distillate contamination by salt. The plant operated successfully with a very limited flux reduction at salt concentrations up to 10% from city water or seawater. The cost of water by DCMD process is cheaper than or competitive with that for reverse osmosis depending on the steam cost.

15. SUBJECT TERMS
membrane distillation, pilot plant, hollow fiber membrane, crossflow, seawater

16. SECURITY CLASSIFICATION OF:			17. LIMITATION OF ABSTRACT	18. NUMBER OF PAGES	19a. NAME OF RESPONSIBLE PERSON
UL			U		Glenn Howard
a. REPORT	b. ABSTRACT	c. THIS PAGE			19b. TELEPHONE NUMBER *(include area code)*
U	U	U			303-445-2252

Standard Form 298 (Rev. 8/98)
Prescribed by ANSI Std. 239-18

Desalination and Water Purification Research and Development Program Report No. 134

Pilot-Scale Studies for Direct Contact Membrane Distillation-Based Desalination Process

Prepared for Reclamation Under Agreement No. 04-FC-81-1037

by

Dr. Kamalesh K. Sirkar
Dr. Liming Song
New Jersey Institute of Technology
Newark, New Jersey

U.S. Department of the Interior
Bureau of Reclamation
Technical Service Center
Environmental Services Division
Water Treatment Engineering and Research Group
Denver, Colorado

September 2009

MISSION STATEMENTS

The mission of the Department of the Interior is to protect and provide access to our Nation's natural and cultural heritage and honor our trust responsibilities to Indian tribes and our commitments to island communities.

The mission of the Bureau of Reclamation is to manage, develop, and protect water and related resources in an environmentally and economically sound manner in the interest of the American public.

Disclaimer

The views, analysis, recommendations, and conclusions in this report are those of the authors and do not represent official or unofficial policies or opinions of the United States Government, and the United States takes no position with regard to any findings, conclusions, or recommendations made. As such, mention of trade names or commercial products does not constitute their endorsement by the United States Government.

Acknowledgement

The research conducted under this contract was sponsored by the Desalination and Water Purification and Development Program, Bureau of Reclamation, Denver, Colorado.

We acknowledge the considerable assistance and participation by United Technologies Research Center, East Hartford, Connecticut, in building and operating the pilot plant. The contributions by Dr. Zidu Ma, Dr. Xiaohong Liao, and Mr. Jim Irish, in particular, were invaluable. We acknowledge the significant reduction in the charge for the membrane module manufacturing cost by Applied Membrane Technology, Inc. Praveen Kosaraju helped substantially during the pilot plant data taking in the months of March and April 2006. We acknowledge the effort by Membrana Inc. in developing the polymeric hollow fiber heat exchanger.

Table of Contents

List of Figures

List of Figures (continued)

List of Figures (continued)

List of Figures (continued)

List of Figures (continued)

List of Figures (continued)

List of Tables

Glossary

AMT	Applied Membrane Technology Inc.
A_{rf}	membrane area ratio for heat transfer through fiber outside surface, $= d_o/d_i$
A_{rln}	membrane area ratio for heat/mass transfer through the fiber based on logarithmic mean diameter - based surface, $= d_{lm}/d_i$
A_{rp}	membrane area ratio for heat transfer through fiber inside surface, $= d_i/d_i$
Ca	calcium
Cl	chlorine
cm^2	square centimeter
C_0	initial salt concentration in the distillate tank (t =0)
C_t	salt concentration in the distillate tank at the operation time t, ppm
C_p	salt concentration in the permeate, ppm; heat capacity, J/kg/K
CSTR	continuous stirred tank reactor
°C	degrees Celcius
DCMD	direct contact membrane distillation
d_i	fiber inside diameter, m
d_{lm}	logarithmic mean diameter of fiber, m
Dn	dilution factor (=P/V)
do	fiber outside diameter, m
F_c	correction factor
ft^2	square foot
°F	degrees Fahrenheit
g_c	Newton's law conversion factor
GCAOTR	Grants and Cooperative Agreements Officer's Technical Representative
gfd	gallon per square feet per day (gallon/ft^2/d)
gpd	gallons per day
gpm	gallon per minute
h_f	shell side feed heat transfer coefficient, W/m^2/K
Hg	mercury
h_m	membrane heat transfer coefficient, W/m^2/K
h_{mg}	heat transfer coefficient across the membrane pore gas phase, W/m^2/K
h_{ms}	heat transfer coefficient for the solid polymeric matrix, W/m^2/K
HNO_3	nitric acid
h_p	tube side heat transfer coefficient, W/m^2/K

Glossary (continued)

HX	heat exchanger
ΔH_v	heat of vaporization of water, J/kg
I.D.	inside diameter
$kg/m^2/h$	kilograms per square meter per hour
k_m	membrane mass transfer coefficient, $kg/m^2/h/Pa$
k_{mg}	thermal conductivity of the gas phase, W/m/K
k_{ms}	thermal conductivity of the matrix material, W/m/K
kPa	kilopascal
kWh	kilowatthour
L	fiber total length, m
l_o	inactive fiber length in tube sheet at permeate outlet, m
L/min	liter per minute
l_w	active fiber length, m
m	number of fiber layers
MD	membrane distillation
mg	milligram
mg/L	milligram per liter
mM	millimolar
mol/s	mole per second
MSF	multistage flash
n	fiber number per layer
N_2	nitrogen
Na	sodium
NaCl	sodium chloride
NJIT	New Jersey Institute of Technology
Nu	Nusselt number
N_v	water vapor flux, $kg/m^2/h$
O.D.	outside diameter
p	vapor pressure, Pa; permeate side pressure, Pa
P	feed side pressure, Pa; distillate production rate, L/min
Pa	Pascal
p_{fm}	water vapor partial pressure at the membrane surface on the shell side, Pa
p_{fm}^0	vapor pressure of water at the membrane surface on the shell side, Pa
PHFHEs	polymeric hollow fiber heat exchangers
p_{pm}	water vapor partial pressure at the membrane surface on the tube side, Pa

Glossary (continued)

p_{pm}^{0}	vapor pressure of water at the membrane surface on the tube side, Pa
p_o	permeate outlet pressure, Pa
PP	polypropylene
Pr	Prandtl number, $C_p\mu/k$
PTFE	polytetrafluoroethylene
PVDF	polyvinylidene fluoride
p_w	permeate pressure at the junction of active and inactive fiber lengths near permeate outlet, Pa
Δp_{br}	breakthrough pressure, Pa
ΔP_{N_2}	pressure difference across the membrane, Pa
Q	heat transfer rate, W
Q_{N_2}	permeability coefficient of N_2 permeation through the membrane, mol/(m/s/Pa)
R	gas constant
Re	Reynolds number
Reclamation	Bureau of Reclamation
RO	reverse osmosis
s	membrane surface area, cm^2
SO_4^{2}	sulfate
t	DCMD operation time, min
T	temperature, K
T_{b0}	brine feed temperature, ºC
TBNDRF	Tularosa Basin National Desalination Research Facility
T_{d0}	distillate feed temperature, ºC
T_{d1}	distillate outlet temperature, ºC
TDS	total dissolved solids
T_f	brine bulk temperature
T_{f0}	brine feed temperature, ºC
T_{fm}	brine temperature at the membrane surface, ºC
T_p	distillate bulk temperature
T_{p0}	distillate feed temperature for one layer, ºC
T_{p1}	distillate outlet temperature for one layer, ºC
T_{pm}	distillate temperature at the membrane surface, ºC
u_I	interstitial velocity on shell side, m/s
µm	micrometer
µS	microsiemens

Glossary (continued)

u_L	linear velocity on tube side, m/s
UTRC	United Technologies Research Center
V	volume of brine solution in the distillate tank, L; permeate-side flow rate, mol/s
V_{b0}	brine inlet volumetric flow rate, m^3/h
V_{b1}	brine outlet volumetric flow rate, m^3/h
V'_{f0}	local brine inlet volumetric flow rate per unit length of fiber, $m^3/h/m$
V'_{f1}	local brine outlet volumetric flow rate per unit length of fiber, $m^3/h/m$
VMD	vacuum membrane distillation
V_{d0}	distillate inlet volumetric flow rate, m^3/h
V_{d1}	distillate outlet volumetric flow rate, m^3/h
V_{p0}	distillate inlet volumetric flow rate for one fiber layer, m^3/h
V_{p1}	distillate outlet volumetric flow rate for one fiber layer, m^3/h
V_w	permeate product flow rate, mol/s
x	position along the fiber length, m; water mole fraction
ZLD	zero liquid discharge

Greek Letters

α	membrane surface area based on fiber inside diameter per unit length per fiber layer
γ	activity coefficient
δ_M	membrane thickness, m
ε_m	membrane porosity
μ	viscosity, Pa/s
ρ	density, kg/m^3

Subscript

0	inlet (flow rate, temperature, density, heat capacity)
1	outlet (flow rate, temperature, density, heat capacity)
b	brine
d	distillate
f	brine or shell side
i	distillate or fiber lumen side
j	the *j*th fiber layer
m	liquid-vapor interfaces on the brine side and distillate side
o	brine or shell side

Glossary (continued)

p	distillate or fiber lumen side
w	wall or membrane surface

1. Executive Summary

Although research and development studies to improve commercialized reverse osmosis and thermally driven desalination processes are continuing, there exists a need to develop and evaluate alternate desalination technologies (e.g., membrane distillation [MD]), which utilize waste heat. In one variety of MD, direct contact membrane distillation (DCMD), hot brine flows on one side of a gas-filled porous, hydrophobic hollow fiber membrane and cold distillate flows on the other side of the membrane; water vapor evaporated from hot brine is recovered in the cold distillate stream by condensation. This technique is of interest here. The primary deficiencies of this technique are flux reduction due to long-term pore wetting and reduced brine-side heat and mass transfer coefficients. These deficiencies were overcome in Phase II of this research on the DCMD process (Sirkar and Li, 2003) by employing rectangular crossflow of the hot brine around porous hydrophobic hollow fiber membranes having a thin hydrophobic microporous coating of a silicone-fluoropolymer plasma polymerized on the fiber outside diameter on the hot brine side to prevent pore wetting. Further, the hydrophobic porous hollow fibers had thick walls, high porosity, and larger diameter. These combinations yielded a stable and a highly productive DCMD process with water vapor fluxes reaching as high as 79 kilograms per square meter per hour ($kg/m^2/h$) (46.5 gallons per square foot per day [gfd]) at 90 degrees Celsius (°C) in the module MXFR #3 having a membrane surface area of 119 square centimeters (cm^2). In the Phase III project (Sirkar and Li, 2005), the membrane surface area was scaled up by more than an order of magnitude to 2,864 cm^2 (3.08 square feet [ft^2]) using 1,088 similar hollow fibers in the rectangular crossflow module design; for brine feed of 90 °C at a high feed velocity over the fibers, a water permeation flux as high as 60 $kg/m^2/h$ was achieved in DCMD through the module S/N 1004.

This level of successful performance led to building a small DCMD pilot plant at United Technologies Research Center, East Hartford, Connecticut, in the present pilot plant project. In this project, individual modules scaled up to 2,448/2,652 hollow fibers (similar to those used in Phase III project) and having 0.61/0.66-m^2 surface area were utilized to build a small pilot plant containing up to 10 modules. A distilled water production rate of 0.62 gallons per minute (gpm) was achieved for hot brine feeds at around 90 °C, flowing at 17 gpm; this amounts to 3.64-percent (%) water recovery in a single pass. Tests with 3%, 6%, and 10% salt in city water indicated a minor drop in water vapor flux. The water vapor fluxes achieved in different configurations of the modules varied from 55 $kg/m^2/h$ to 15 $kg/m^2/h$ depending on the brine velocity, module configurations, distillate velocity, and flow configurations. Tests with seawater trucked in from Long Island Sound, Connecticut, substantiated these observations; fluxes were

relatively unaffected as the seawater was concentrated three times over a few days' runs. Tests with city water as well as seawater and spanning a period of 3 months did not lead to any fiber leakage in any of the modules.

A model describing the performance of individual crossflow hollow fiber modules was also developed. It was able to successfully predict the DCMD performances of these modules at three levels of membrane surface area: MXFR #3 (119 cm^2); S/N 1004 (0.28 square meters [m^2]); S/N 1006–1015 (0.61–0.66 m^2). The DCMD performances of a combination of a number of modules in the pilot plant were also predicted satisfactorily. Cost estimates developed indicate that DCMD based on these types of membranes and modules are competitive with reverse osmosis. There is considerable interest at United Technologies Research Center where the pilot plant was located to go beyond the pilot plant stage and explore further larger-scale development of this technology for desalination.

2. Background and Introduction to Potential Solution

Cost reduction of desalination technologies is now considered to be the singlemost important factor to increase using desalination to enhance water supplies in the United States. The *Desalination Roadmap* (2003), for example, indicates that in reverse osmosis (RO) desalination, energy consumption (44 percent [%]) and fixed charges (37%) together consume more than 81% of the desalination cost. Similarly, it is known that in thermally driven desalination processes, including multistage flash and multiple effect distillation, capital cost of the large metallic tube-based evaporators is very high in the range of 40–50% of the total water cost (Steinbruchel and Rhinesmith, 1980). Therefore, alternate desalination processes and techniques which are not yet commercialized but may be potentially more economical from the perspective of capital and energy costs, easier to use and can use low-grade waste heat, are of considerable interest.

Membrane distillation (MD) is potentially one such process. In one variety of the MD process, namely, direct contact membrane distillation (DCMD), a hot nonvolatile solute—containing aqueous solution (e.g., hot brine) is passed on one side of a porous hydrophobic membrane as a colder aqueous distillate stream flows on the other side. Diffusion of water vapor evaporated from the hot brine at the brine—membrane interface takes place through the gas-filled hydrophobic membrane pores; the water vapor is condensed in the cold distillate on the other side of the membrane, the distillate-membrane interface (figure 1a). In another variety of MD, namely, vacuum membrane distillation (VMD), there is no cold distillate stream on the other side of the membrane; instead, a vacuum is maintained. The water vapor is condensed and recovered as the distillate in a separate condenser. Of these two MD processes, DCMD is quite attractive since it eliminates the need for a separate condenser. It operates at around atmospheric pressure and can treat brines of various salt concentrations since it is not subject to the osmotic pressure-driven limitations of RO.

Such a desalination process has an inherent advantage if hot brine is available at anywhere between 99 degrees Celcius (°C) and 35 °C (210.2–95 degrees Fahrenheit [°F]) from existing low grade heat sources: geothermal brines; hot rejected seawater/hot brine blowdown from thermal distillation; hot industrial waste aqueous streams; low-pressure steam, etc. Cheaper, renewable solar energy-based heating may provide hot brine at a significant cost advantage. The membrane distillation process utilizes sensible heat of the hot feed brine to evaporate pure water which is collected by the cold distillate stream on the other side of the membrane.

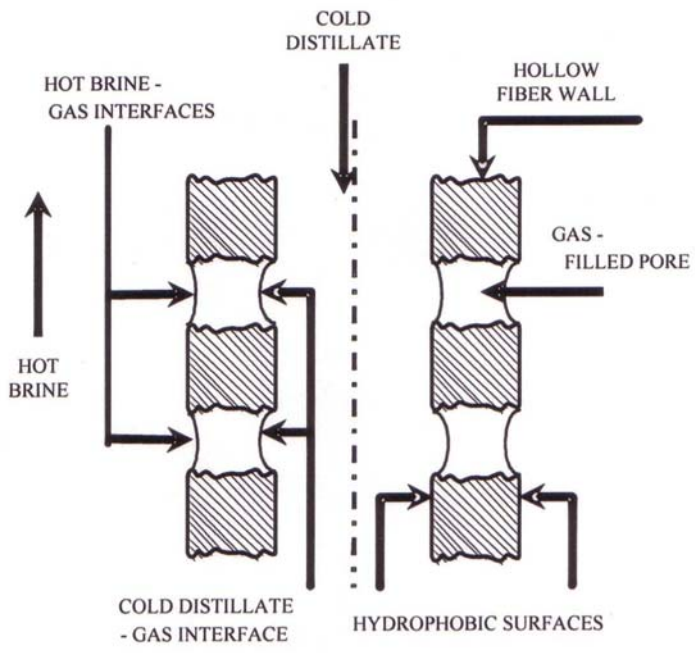

Figure 1a. Conventional direct contact membrane distillation.

However, the water vapor flux must be high to retain the advantages of low energy cost and lower capital cost for simple operation at a low pressure. In the DCMD process using a porous hydrophobic membrane, surface tension forces withhold the brine from the pores and prevent the penetration of the liquid and, thus, contact between the two liquids on two sides of the polymer membrane. Generally, the solution/brine surface tensions are higher than the critical surface tension of the polymer.

In the DCMD process for a hot brine feed, the temperature difference, causing a corresponding vapor pressure difference across the porous membrane, provides the driving force of water evaporation at the feed-membrane interface and condensation at the much colder distillate-membrane interface. This process has many advantages (Lawson and Lloyd, 1997; Schneider et al., 1988):

1. Complete rejection of nonvolatiles (e.g., salts, ions, colloids, cells, and organic nonvolatiles).

2. Operation at near-atmospheric pressure compared to the high operating pressures of membrane processes like RO, etc., and lower operating temperatures (50–100 °C) than conventional multiple-effect distillation.

3. Much reduced need for vapor space compared to conventional distillation processes.

4. Much reduced mechanical strengths needed for the membrane and the module (compared to RO). Corrosion problems are also avoided since the modules are made of polymer.

5. Use of relatively inert hydrophobic membranes limits interactions of the feed with the membrane.

6. Droplets cannot be entrained by the vapor stream due to the membrane.

7. Modular membrane system allows easy extension of capacity.

Laboratory experiments on DCMD using different microporous hydrophobic membranes have yielded water fluxes in the range of 25–75 kg/m^2/h (14.7–44.2 gallons per square foot per day [gfd]) (Lawson and Lloyd, 1997; Schneider et al., 1988; Schofield et al., 1990a, 1990b). These values are quite attractive and are in the range of the highest practical values of water fluxes achieved in RO (Bhattacharyya et al., 2001). Further, these values have been achieved with 100% salt rejection which is not possible in RO.

Since the earliest report of DCMD by Findley (1967) and Gore (1982), many studies have been made; and reviews have been published (Schofield et al., 1987, 1990a, 1990b, 1990c; Schneider et al., 1988; Sirkar, 1992; Lawson and Lloyd, 1997; Martinez-Diez et al., 1996, 2001; Phattaranawik et al., 2003). These studies have identified the need to reduce temperature polarization on the hot brine side (figure 1b): the value of T_{fm} should be as close to the bulk brine temperature T_f as possible so that water vapor pressure at the hot brine-pore interface is as high as possible. This ensures a high partial pressure difference of water vapor across the gas-filled membrane pore. However, the conductive heat loss through the solid polymeric wall of the membrane as well as the gas-vapor pathway in the membrane pore should also be reduced drastically to ensure that the sensible heat of the hot brine is primarily utilized to vaporize water at the brine-membrane surface. These conditions dictate thicker wall membranes having as high a porosity as possible: conductive heat flux is reduced; the water vapor transport coefficient through the membrane may be potentially increased. In addition, the distillate temperature should remain low to maintain a high water vapor pressure difference between the two sides of the membrane pore.

Most studies mentioned earlier used hydrophobic membranes of polypropylene (PP), polytetrafluoroethylene (PTFE), polyvinylidene fluoride (PVDF), etc., having a high porosity, 0.3–0.8, and larger pore size, 0.1–0.6 micrometers (μm). Such membranes are not supposed to get wetted by hot brine flowing at atmospheric pressure as long as the pressure difference between the two sides does not exceed the breakthrough pressure (Δp_{br}) (Schneider et al., 1988; Sirkar, 1992). Pore wetting would lead to salt leakage increasing the salinity of the distillate stream.

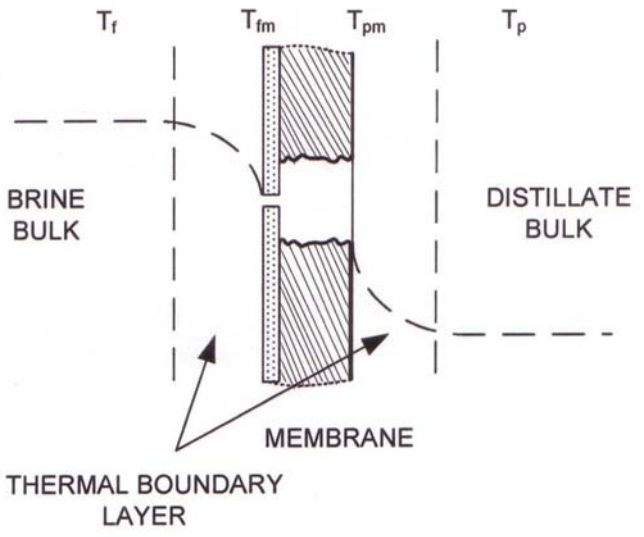

Figure 1b. Temperature profile across the DCMD membrane.

Often, however, the water vapor flux has been observed to suffer from a decay with time. Investigators have surmised that this is due to pore fouling, scaling, etc. (Schneider et al., 1988; Lawson and Lloyd, 1997; Calabro et al., 1994; Van Gassel et al., 1986; Drioli and Calabro, 1987; Banat and Simandl, 1994). Pore fouling, scaling, etc., can also lead to pore wetting. Preventing/controlling such wetting/fouling via suitable membrane design is of considerable interest.

Porous membranes having pore sizes in the range of 0.03–0.6 μm have to be made permanently nonwettable. One could solve this problem using porous PTFE membranes; however, the module cost will go up by a factor of 10 (Schneider et al., 1988). To prevent pure distillate contamination by leakage of feed saline water through wetted pores, one can increase the distillate liquid pressure above that of the feed brine at a loss of the purified distillate. Alternately, one can adopt/develop economically attractive membranes which are made almost permanently nonwettable under the operating conditions—for example, by plasma polymerization of a porous coating of silicone-fluoropolymer. Figure 1b shows the schematic for DCMD where a thin microporous coating on the outside diameter of the porous polypropylene hollow fiber makes the membrane almost permanently nonwettable.

To address these issues, we carried out preliminary DCMD investigations on a very small scale using hollow fiber membranes and modules having a number of novel features (Li and Sirkar, 2004; Sirkar and Li, 2003); in addition, VMD studies were also carried out (Li and Sirkar, 2005; Sirkar and Li, 2003). First, a crossflow module design was implemented in which the hot brine flowed perpendicular to the axis of the hollow fibers to ensure a high heat transfer

coefficient (figure 1c) at a low Reynolds number. It is known that crossflow can enhance mass transport coefficients by a few times at quite low Reynolds numbers compared to parallel flow (Wickramasinghe et al., 1992). Second, an ultrathin, highly porous layer of silicone-fluoropolymer was deposited on the outside surface of hydrophobic porous hollow fibers of polypropylene by plasma polymerization (figure 1d). The selected porous PP hollow fibers had large pore size greater than (>) 0.2 μm. Applying the coating was not to reduce this PP substrate pore size but to provide an additional porous, highly hydrophobic layer (having a higher hydrophobicity than that of PP). Further, if this layer has larger pores, it will act as a buffer layer. Should there be accidental wetting via wetting precursors/deposits, the buffer layer will get wetted but not the substrate PP layer. To be noted is that the critical surface tension of this coating was much less than that of a PP surface.

There were additional features in the small modules/devices studied in DCMD (Li and Sirkar, 2004; Sirkar and Li, 2003). The hollow fibers selected had a wall thickness of 150 μm, considerably larger than that in conventional porous hydrophobic hollow fibers; this substantially reduced the conductive heat loss. Further, the fiber walls were highly porous—the porosity being around 0.65. The high porosity reduced the conductive heat flux while reducing the resistance for water vapor diffusion through the pores. In addition, the hollow fibers employed had a much larger internal diameter of 330 μm to reduce the distillate pressure drop. It is highly important to maintain a large distillate flow rate through the fiber bore so that the distillate temperature rise can be controlled with a limited expenditure of pressure energy. Distillate temperature rise should be controlled to maintain as high a vapor pressure difference between the hot brine and the colder distillate; the latter is essential to achieving a high water vapor flux.

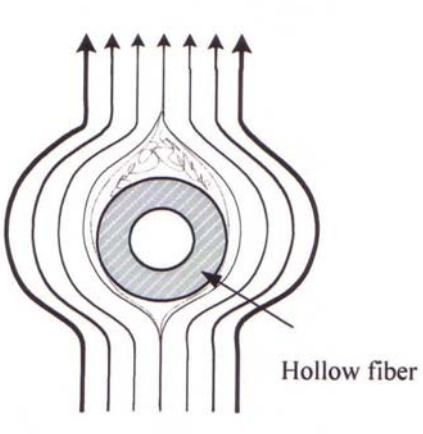

Figure 1c. Crossflow over hollow fiber outside diameter.

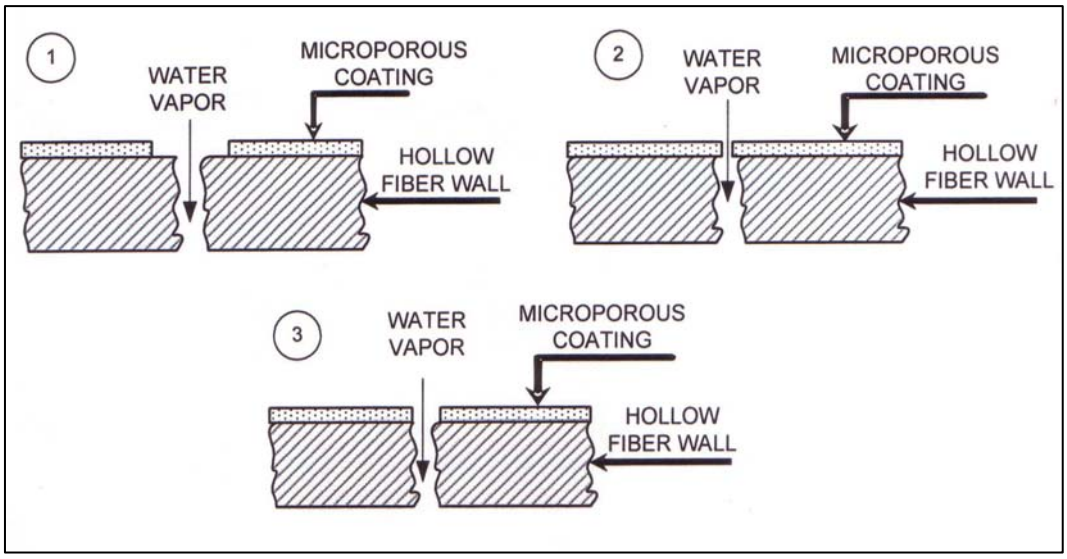

Figure 1d. Water vapor flowing through porous hydrophobic coating on the surface of porous hollow fiber membrane.

The synergistic combination of these novel features yielded very high water vapor fluxes in DCMD of as much as 60–79 kg/m^2/h (35.3–46.5 gfd) from hot brine feeds of 85–90 °C in a small module having a hollow fiber membrane surface area of 119 square centimeters (cm^2) (0.128 square feet [ft^2]) (based on fiber inside diameter) (Li and Sirkar, 2003; Sirkar and Li, 2003). This is more than a few times what is achieved in conventional seawater RO. Hollow fiber membrane devices are relatively simple, can pack considerable surface area per unit volume, and may be scaled up without great difficulty. Therefore, these high flux results are of considerable importance. A number of issues naturally arise. Can one achieve such high water vapor fluxes in larger membrane modules? Is there any scale-dependence in this behavior? How does fouling, etc., affect the water vapor flux over an extended period of time? Sirkar and Li (2003) studied desalination in their small DCMD module using a hot brine concentration of 1% sodium chloride (NaCl). What is the effect of increasing brine concentration on the observed water vapor flux? Could one make progress toward zero liquid discharge (ZLD) by going to high brine concentrations?

In Phase III of the project (Sirkar and Li, 2005), we successfully scaled up the hollow fiber membrane device by increasing the membrane surface area from 119 cm^2 to 2,864 cm^2 (0.28 square meters [m^2]) in a single module. Two such modules were developed. The water vapor flux behavior was investigated as the salt concentration in brine was increased from 1% to 3%, 6%, and 10%. There was a small decrease (around 5–10%) in flux as the salt concentration was increased to 10%. We varied the distillate inlet temperature to observe how the water vapor flux was reduced with an increase in distillate inlet temperature. We studied the relatively constant behavior of the large module over 5 days.

Therefore, this DCMD technique may be used to successfully recover water at a high rate from concentrated salt solutions (e.g., the rejected hot seawater/the hot brine blowdown from a thermal distillation plant). In addition, the concentrate volume from existing desalination plants may be reduced and more water recovered. Further, the two larger modules S/N 1004 and S/N 1005 were placed back-to-back and operated successfully; hot brine exiting one module at a temperature lower than the feed brine temperature entered immediately into the next module. This experiment illustrated how one could stack the horizontal crossflow modules in a small volume and extract as much water vapor as possible from a given hot brine stream. Conceptually, one can stack 3, 4, 5, 6 or more of such modules back-to-back. The only shortcoming is that the water vapor flux will decrease as the feed brine temperature decreases. Thus, the productivity per unit membrane area will decrease. One can partially compensate for this decrease by starting with as high a feed brine temperature as possible in the first module in the stack of modules. Phase III results (Sirkar and Li, 2005) show that one can successfully extract around 10 $kg/m^2/h$ of water from a feed at as low a temperature as 55 °C. These results led us to propose a pilot plant study of the DCMD process at a suitable site with a production capacity of 1 gallon per minute (gpm) (3.785 liters per minute [L/min]) of distillate water.

Such a pilot plant study was expected to provide answers to many questions in this novel DCMD technology.

1. Can a larger number of membrane modules be fabricated reproducibly?

2. Does the membrane performance deteriorate with time? What is the reason for deterioration, if any?

3. How does stacking of horizontal crossflow modules work? Will a separate design be needed for a much larger scale?

4. What are the extents of pressure drops in the tube side and the shell side to reduce heating up of the tube side distillate stream and extract an increasing amount of heat from the hot brine in the shell side?

5. What are the ranges of feed brine temperature over which the membrane stability and the water flux level are acceptable?

6. What is the extent of water extraction in one pass of the hot brine through a stack of modules?

7. What are the pretreatment needs for such a membrane technology vis-a-vis the feed stream used?

The pilot plant was expected to be set up at the Tularosa Basin National Desalination Research Facility (TBNDRF). Among a number of hot brine sources, geothermal sources in Tularosa Basin in New Mexico was of interest. Dr. Michael Hightower of Sandia National Laboratory, Albuquerque, New Mexico (telephone: 505-844-5499; mmhight@sandia.gov) and the project Grants and Cooperative Agreements Officer's Technical Representative (GCAOTR), Mr. Glenn T. Howard Jr., P.E., provided the following information. The "geothermal well" on the TBNDRF site was well number (#)1 which had the following characteristics: total dissolved solids (TDS) 1,000 to 1,900 milligrams per liter (mg/L); temperature: 41 °C (105 °F); production capacity: 100 to 120 gpm. There were no solar heating facilities at the TBNDRF. If provided, they would most likely be part of a research project.

In this pilot plant, initially, an amount of cold distilled (or tap) water is needed to start operation on the permeate side (available at TBNDRF). Afterwards, the distillate product stream may be cooled to the extent needed; and a fraction recycled to the permeate side to condense the water vapor coming from the hot brine side. The remaining fraction of the distillate stream will be the final product stream. The fraction of the feed brine recoverable in such an operation depends on the feed brine temperature (inlet enthalpy) and the cooled feed brine temperature (exiting enthalpy). If the hot feed brine enters at around 92–93 °C (197.6–199.4 °F) and exits at around 40 °C, theoretically about 8.5–9% of the feed water may be recovered. In practice, it may be reduced by 10–20% due to conductive heat loss. Therefore to produce 1 gpm of net distilled water product, 12 gpm of hot saline should flow on the shell side. (The fractional recovery in a multistage flash plant in one pass is only around 11–12% [Howe, 1974]). Note that in Phase III project (Sirkar and Li, 2005), 25 L/min (6.6 gpm) of 3 weight (wt) % brine was flowing on the shell side. The cooled brine exiting the module stack will be reused by reheating it with some heat recovery from the hot distillate.

The Western, Southwestern, and intermountain States of the continental United States suffer from extensive drought conditions. Other regions of the country, including the eastern seaboard, suffer from periodic drought conditions. Geothermal brines, industrial waste streams, hot blowdowns from thermal desalination, and other processes, if treated by a DCMD process, can yield pure distilled water. If local sources of waste heat are available, brackish water, seawater, and water contaminated by nonvolatiles may be conveniently heated up and used as feed to a DCMD plant. The scale of DCMD plant can be small, medium, or large since DCMD units are modular. Decentralization of facilities is easily achieved for providing safe water. DCMD-based water production may be cheaper than RO, even if local waste heat is not available (Sirkar and Li, 2005).

Successful pilot plant tests will indicate that, potentially, a new desalination technology may be at hand. Waste streams available in thermal desalination plants via the rejected hot seawater/brine blow down, etc., may provide feed for additional water recovery. In fact, the DCMD process could compete with multistage flash distillation plants! Waste heat available in such plants and others (powerplants or otherwise) may be used to heat up waste water streams and implement a DCMD process to recover water. Smaller geothermal water sources may be treated to recover water. Further, expenses for low-grade heat input, that has been factored in, may still yield an economic process vis-a-vis RO (Sirkar and Li, 2005).

The manufacturer of the hollow fiber devices for the proposed pilot plant, Applied Membrane Technology (AMT) Inc., Minnetonka, Minnesota, is interested in larger-scale commercialization of such devices. Large-scale effort by them in the future will be part of a natural progression in developing this technology.

The pilot plant project objectives adopted to achieve our goal of a successful pilot plant were as follows:

1. Select a suitable site for a DCMD-based desalination pilot plant having a distilled water capacity of 1 gpm using locally available hot brine as feed.

2. Design the 1-gpm capacity DCMD pilot plant for the selected site.

3. Collaborate with AMT Inc., to develop larger-scale rectangular, crossflow hollow fiber membrane modules for DCMD based on experiences in prior research projects.

4. Build the pilot plant.

5. Develop pilot plant test procedures.

6. Gather test data and analyze pilot plant performance.

7. Develop correlations for membrane device performances.

8. Develop different cost items of a production plant based on pilot plant performance.

3. Conclusions and Recommendations

1. A small DCMD pilot plant was built and operated successfully by New Jersey Institute of Technology (NJIT) at United Technologies Research Center (UTRC), East Hartford, Connecticut, for a period of 3 months. The plant utilized hot brine at 90–93 °C (194–199.4 °F) and distillate at 20–54 °C. The hot brine was **either** city water **or** city water containing salt at the level of 3.5%, 6%, or 10% **or** seawater trucked in from Long Island Sound, Connecticut; the seawater had a TDS around 29,000 parts per minute (ppm). One to ten larger-scale horizontal crossflow hollow fiber membrane modules, each having a membrane surface area of either 0.61 or 0.66 m^2 (6.57 or 7.10 ft^2), were combined to build the pilot plant in various flow configurations for both the hot brine and the cold distillate. The pilot plant operation was successful. The highest distillate production rate achieved was 0.62 gpm. Lack of enough distillate cooling capacity prevented using a higher brine flow rate which would have yielded a 1-gpm distillate production rate.

2. Ten rectangular crossflow hollow fiber membrane modules (S/N1006– S/N1015) in picture frame configuration were built by AMT Inc. Each module, having either 2,448 or 2,652 fibers and membrane surface areas of 0.61 or 0.66 m^2, was tested using the face plates and distributor plates designed and built at NJIT. None of the modules showed any salt leakage. Only one of the modules had fiber breakage very early in the program, potentially resulting from excessive plasma polymerization. Each such module had more than twice the membrane surface area of the modules employed in the Phase III project (Sirkar and Li, 2005). Further, two such modules were used back-to-back to make **one unit pair** and potentially a fiber depth of 48–52 layers of fibers, each layer having 102 fibers facing the hot brine. The overall volume occupied by 10 modules was 0.06 cubic meters (m^3) providing a volumetric productivity of 10.3-gpm-per-m^3 membrane volume. Thus, crossflow hollow fiber membrane module scale up was successfully implemented.

3. The water vapor flux level depended on the module configurations vis-à-vis the brine flow and the distillate flow at given flow rates and inlet temperatures. The highest flux achieved was 55 kilograms per square meter per hour ($kg/m^2/h$) (32.4 gfd) for lower number of modules. For pilot plant configurations employing 6–10 modules, the water vapor flux varied between 15 to 33 $kg/m^2/h$. Higher brine crossflow velocity and exposure to higher brine temperature facilitated achievement of higher water vapor fluxes.

4. The pilot plant operated successfully with very limited flux reduction at the highest salt concentration tested, namely, 10% NaCl. When the seawater TDS exceeded 18%, there was significant precipitation; this happened since the Long Island Sound seawater had a very high calcium content (resulting from the high-scale content of the discharge from a nearby nuclear powerplant). At the time of precipitation, the calcium concentration was almost 48 times that normally found in seawater.

5. For 3 months of pilot plant operation, the membrane modules never showed any distillate contamination by salt. Operation of the nine membrane modules did not show any module deterioration.

6. The membrane module design displayed some channeling and bypassing by the brine. Future module designs should use fiber mats to eliminate such channeling. Further, we observed oscillations of the fibers on the brine side. Although this led to improved heat transfer and very little fouling, this oscillation should be controlled in future module design to prevent fiber failure at the potting location.

7. Although successful and complete prevention of the distillate contamination by salt was achieved in fibers having the fluorosilicone coating, nitrogen (N_2) permeation tests indicated that the coatings were thicker/less porous than membranes of Phases II/III. Additional control of the coating thickness and porosity will yield higher water vapor flux.

8. Successful modeling of the performance of the crossflow DCMD modules has been achieved. This suggests that one could design a larger plant with confidence.

9. Cost calculations have been carried out for the production of 1 million gallons of distillate per day employing the saline water source to provide distillate cooling requirement. The cost of water by the DCMD process is competitive with RO at higher energy cost levels for the steam in the brine heater. At lower energy cost levels, the DCMD process is cheaper.

10. United Technologies Research Center has undertaken further development of this desalination technology. They are interested in acquiring the pilot plant built in the project for continued testing and development pending the approval of the Bureau of Reclamation (Reclamation), Denver, Colorado.

4. Work Performed

The project objectives were implemented by executing the following nine tasks. A brief description of each major task is provided below.

Task 1 Select a site for pilot plant.

Task 2 Design the pilot plant for 1-gpm distilled water production rate at the selected site.

Task 3 Design, order, and procure large-scale rectangular crossflow hollow fiber membrane modules (from AMT Inc.) and other equipment needed.

Task 4 Build the pilot plant at the selected site.

Task 5 Test the pilot plant for operability.

Task 6 Gather test data and analyze pilot plant performance.

Task 7 Project the cost of water production in a large-scale plant based on pilot plant data and analysis.

Task 8 Dismantle pilot plant.

Task 9 Prepare and submit data, progress reports, and a final report.

Following is a detailed explanation of the work performed under each task.

4.1 TASK 1: Select a Site for Pilot Plant

Our original understanding during pre-award telephone discussions on August 27, 2004, with Drs. Thomas Jennings and Frank Leitz was that there was a scheduling problem in locating the pilot plant facilities at the TBNDRF; the site would be ready for us by the July–August 2005 period. It was, therefore, decided that our site activity would be rescheduled in that context to the July–August 2005 period.

However, on January 4, 2005, the project GCAOTR, Mr. Glenn T. Howard Jr., P.E., indicated that there was a continuing problem on the availability of the TBNDRF site due to some unforeseen funding constraints. As a result, exploration of potential alternate sites was initiated immediately. The following provides a summary of our site explorations involving seven sites. It also indicates Site 7 at United Technologies Research Center, East Hartford, Connecticut, as our choice for the pilot plant.

Site 1. Port Hueneme, California

Mr. Theodore Kuepper
Director, Seawater Desalination Test Facility
NFESC, ESC 32
Port Hueneme, California 93043
Telephone: (805) 982-1631
Fax: (805) 982-1641
Email: theodore.kuepper@navy.mil

Mr. Mark C. Miller
U.S. Army – TARDEC
C/O NFESC, ESC 32
Port Hueneme, California 93043

At the recommendation of Mr. Mark C. Miller, we contacted Mr. Kuepper in early July 2005. Mr. Kuepper was the manager of the Seawater Desalination Test Facility at Port Hueneme. After discussing the details of the proposed larger-scale demonstration, he came to the following conclusions. They did not have any direct inhouse facility for heating and cooling. So we needed to have a brine heat source via electricity, brine heater (via an immersion heater), and a chiller for the distillate. He would not allow the discharge of the hot distillate. It had to be cooled by a chiller and recycled. He could use reverse osmosis to desalinate tap water and potentially provide water having around 10-ppm salt for use as distillate. Further, he suggested that our brine/distillate flow rates of around 15 gpm for 1-gpm distillate production rate was quite high. He recommended operating at 1-gpm flow rates of brine and distillate. (This was at variance with our project proposal.) However, he did come around to the idea of our higher flow rates after several discussions. He also projected the facility cost to be at least $17,748 based on a labor cost of $96 per hour, electricity cost of $0.15 per kilowatthour (/kWh), and 15-day operation of the facility at $100 per day. However, our projected site usage was going to be for at least 2 months, and that cost had to be added. The lack of any heat source created a significant constraint. Required equipment purchase costs were also very high. His recommendation, especially, for the chiller was for rental. At that time, most chillers (available from renters) were in the South due to Katrina. So, this site was held in reserve.

Site 2. Universal Entech, LLC, Phoenix, Arizona

We had identified another facility in Phoenix, Arizona, in January 2005 belonging to Universal Entech, LLC. The person who communicated with us was Mr. Daniel Musgrove:

Mr. Daniel Musgrove
VP – Technology & Business Development
Universal Entech, LLC
5501 N. 7th Avenue, PMB 233
Phoenix, Arizona 85013-1756
Telephone: (602) 268-8849
Fax: (602) 268-9742
Email: dmusgrove@uesolutions.com

In early December 2004, we came across this company in Phoenix, Arizona, and contacted its vice president, Mr. Daniel Musgrove. This company has a Solar Cogeneration Technology which could potentially be used to provide heat for heating brine for membrane distillation. We shared with him a complete flow sheet with details of individual equipment needed. They carried out calculations, etc., about the extent and cost of their involvement. Their solar heating facility, however, could provide heat of no more than 20 kilowatts (kW). Thus, other heat sources were needed. They suggested a boiler to be based on waste wood products. This was not an attractive arrangement from a resource point of view since we needed to provide a costly heat exchanger. Further, no direct brine source was available. If, in fact, brines from wells had to be shipped out, then there were other facilities with more resources. So we discounted this site.

Site 3. Unit Operations Bay Laboratories at NJIT

During our continuing explorations in early March 2005, Harry Remmers of Reclamation identified an arrangement practiced quite often, namely, 55-gallon drums of saline/other waters are shipped from the site to the testing facility. Such an arrangement would have allowed the membrane distillation unit to be set up in the Unit Operations Bay Area in the second floor of Tiernan Hall at NJIT, Newark, New Jersey. The brine heating could be implemented during winter season via steam available during the winter in the laboratories. The challenge was to develop an arrangement for cooling the heated distillate stream via a chiller. The chiller had to have a substantial capacity and was, therefore, going to be quite costly. It appears that a chiller of appropriate capacity, if purchased, would have cost around $35,000–$40,000.

After extensive inhouse consultation, it was decided that NJIT Lab was to be pursued as a last resort. The biggest single obstacle was the cost of cooling distillate. The equipment cost of $40,000 was not available in the budget. However, if a chiller could be rented, it could be implemented. Hot distillate could not be discharged at 13–14 gpm (49.2–53 L/min) at this location. Companies in New Jersey renting chillers were out of rentable chillers since all available chillers were shipped to the South/Southwest due to Katrina.

Site 4. New Mexico State University, Las Cruces, New Mexico

Dr. S. Sikdar
Acting Associate Director for Health
National Risk Management Research Laboratory
U.S. Environmental Protection Agency (USEPA)
26 W. Martin Luther King Dr., MS 235
Cincinnati, Ohio 45268
Telephone: (513) 596-7528
Fax: (513) 596-7787
Email: sikdar.subhas@epa.gov

We contacted him for a potential site. He informed us of the site at New Mexico State University, Las Cruces, New Mexico. We contacted Professor Fernando Cadena and Professsor Shuguang Deng at this university. Discussions were initiated to explore whether we could visit them to develop greater details. The most severe problem at this site, according to Harry Remmers of Reclamation, was potential uranium and radon contamination of the brine (from wells) to be shipped to the university site. The problem of heat supply remained to be solved. The New Mexico State University at Las Cruces and our team at NJIT did not, therefore, consider this site to be appropriate.

Site 5. Nalco, Chicago, Illinois

Mr. Stephen Conover
President & CEO
Applied Membrane Technology, Inc.
Minnetonka, Minnesota 55343
Telephone: (952) 933-5121
Email: spconover@appliedmembranetech.com

Through his contacts, he had been looking for a potential site at Nalco Inc., in the Chicago area. He did not succeed in locating a site at Nalco Inc. We, therefore, removed this site from our consideration.

Site 6. Site at Salton Sea Location

It was recommended to us by the GCAOTR that we contact Mr. Herb Hines ((915) 549-6809, cell phone) who was located at the Salton Sea area in California where Sefton Water Technologies are carrying on larger-scale activities in collaboration with Cal Energy. After a number of conversations with him as well as with Harry Remmers, the following conclusions were made:

1. The permitting process, namely, permits to take saline water out of Salton Sea and putting the concentrated brine as well as any other waste/water

streams back into the Salton Sea required a lengthy permitting process in California of as much as 6 months.

2. Independent trailers had to be established to carry out the work there.

3. Mr. Hines was going to be out of the country (to Australia) by January–February 2006. Lack of a local facilitator would be a significant obstacle.

The resources that were available in the contract were unlikely to be enough for extended stays, many trips to Salton Sea location and infrastructural requirements. We decided to abandon consideration of this site; the requirements of the site were beyond the limits of the project budget and timeline.

Site 7. United Technologies Research Center, East Hartford, Connecticut

Mr. James R. Irish and Dr. Zidu Ma, Staff Research Scientist
Gr. Leader, Materials Integration
Physical Sciences Department
United Technologies Research Center
411 Silver Lane, MS 129-22
East Hartford, Connecticut 06108
Telephone: (860) 610-1651; (860) 660-1182
Email: irishjr@utrc.utc.com

After studying our publications on DCMD, Dr. Ma and Mr. Irish contacted us in early April 2005. Then they visited NJIT Labs, borrowed one of our small DCMD modules used in the earlier Phase II project, and demonstrated its performance at the United Technologies Research Center (UTRC). UTRC upper management became quite interested in this technology and offered to be the host site for the large-scale demonstration of this DCMD technology.

We visited their facilities at UTRC. We shared with them a complete flow sheet as well as the sizes of individual process equipment discussed under Task 2. They had virtually everything we needed for the larger-scale DCMD testing. These include:

1. Large amount of heat available from microturbines for heating the brine.

2. Heat exchanger for brine heating.

3. Cooling tower and absorption chiller to cool the heated distillate and recirculate it.

4. Adjacent facility to receive actual ocean water via a tanker truck and connecting it to the brine tank.

This site was selected for our tests. Should other facilities become available in the early part of 2006, they might be considered also as a potential site for additional testing, provided appropriate resources are available.

4.2 TASK 2: Design the Pilot Plant for 1-gpm Distilled Water Production Rate at the Selected Site

In the first quarter of the project, we initiated design activity to specify the membrane area needed for a distillate production rate of 1 gpm. This was based on an assumed membrane flux from the DCMD devices. We assumed a vapor flux of 40 kg/m^2/h. However, to some extent, this will be influenced by the highest brine temperature available which is not known at this time as well as how low the hot brine temperature is allowed to go down. We may safely assume that, for hot brine temperatures from 90 °C to 80 °C or even lower, the water fluxes obtained will be higher than 40 kg/m^2/h. Therefore, lower fluxes obtained with brines cooled down further will be compensated for by these higher fluxes, and the average assumed water flux is acceptable. However, it also depends on hot brine flow rate and the product recovery desired. The rest of the design activity is, to a large extent, influenced by the availability of cooling water supply in the physical facility. Such calculations were made in concurrence with Dr. Zidu Ma at UTRC.

The material and energy balance for the proposed system as well as sizing of the equipment were developed. These are provided in figure 2 and table 1, respectively. This was based on the assumption that the available brine had to be heated up in the pilot plant facilities. From site-oriented considerations, the distillate stream was completely recycled via cooling in an absorption cooler. The information on plastic storage tanks, plastic centrifugal pumps, sensors for measuring temperature and electrical conductivity, flow meters, and valves from different vendors is provided next.

The brine storage tank was made of polypropylene having a 275-gallon capacity (catalog number C-06317-44, Cole-Parmer, Vernon Hills, Illinois 60061); it could withstand a temperature up to 222 °F (104 °C). The distillate storage tank was also made of PP having a 275-gallon capacity and capable of withstanding up to 222 °F (104 °C). The brine recycle pump (catalog number EW-07085-00, Cole-Parmer, Vernon Hills, Illinois 60061) had a maximum flow rate of 40 gpm at 100 °C and a working flow rate of 14 gpm; it was made of a plastic material and could handle highly corrosive fluids. The distillate recycle pump similarly had a maximum flow rate of 40 gpm at 100 °C and a working flow rate of 16 gpm at a maximum system pressure of 30 pounds per square inch (psi).

Table 1. Mass and Energy Balances for the DCMD Pilot Plant of Figure 2

Mass Balance

Stream Number in Figure 2	Description	Flow Rate (gpm)	Temperature (ºC [ºF])	Piping Size (inches)
A	Tap water or distillate	1	20 (68)	1¼
B	Hot brine feed	14	80 (176)	1¼
C	Hot brine feed	14	92 (197.6)	1¼
D	Hot brine concentrate	13	53 (127.4)	1¼
E	Tap water (optional)	15	20 (68)	1¼
F	Distillate outlet	16	66 (150.8)	1¼
G	Recycled distillate	1	30 (86)	1¼
H	Tap water (optional)	15	20 (68)	1¼
I	Drained water including distillate (optional)	16	66 (150.8)	1¼
J	Distillate inlet (optional)	15	30 (86)	1¼

List of Equipment and Energy Balance

Energy Balance

Equipment (Figure 2)	Description	Capacity Requirement
HE-1	Brine preheating heat exchanger	110 kW
HE-2	Hot brine heat exchanger	45 kW
HE-3	Distillate cooler (in the case of recycle)	150 kW
BST-1	Hot brine storage tank	250 gallon
DST-1	Distillate storage tank (in the case of recycle)	250 gallon
P-1	Hot brine recycle pump	0.2 kW at 14 gpm
P-2	Distillate feed pump	0.2 kW at 15 gpm
DCMD	Membrane distillation modules	–
Miscellaneous	Flow meter, temperature meter, conductivity meter, pressure gauge, piping, fittings, valves, etc.	–

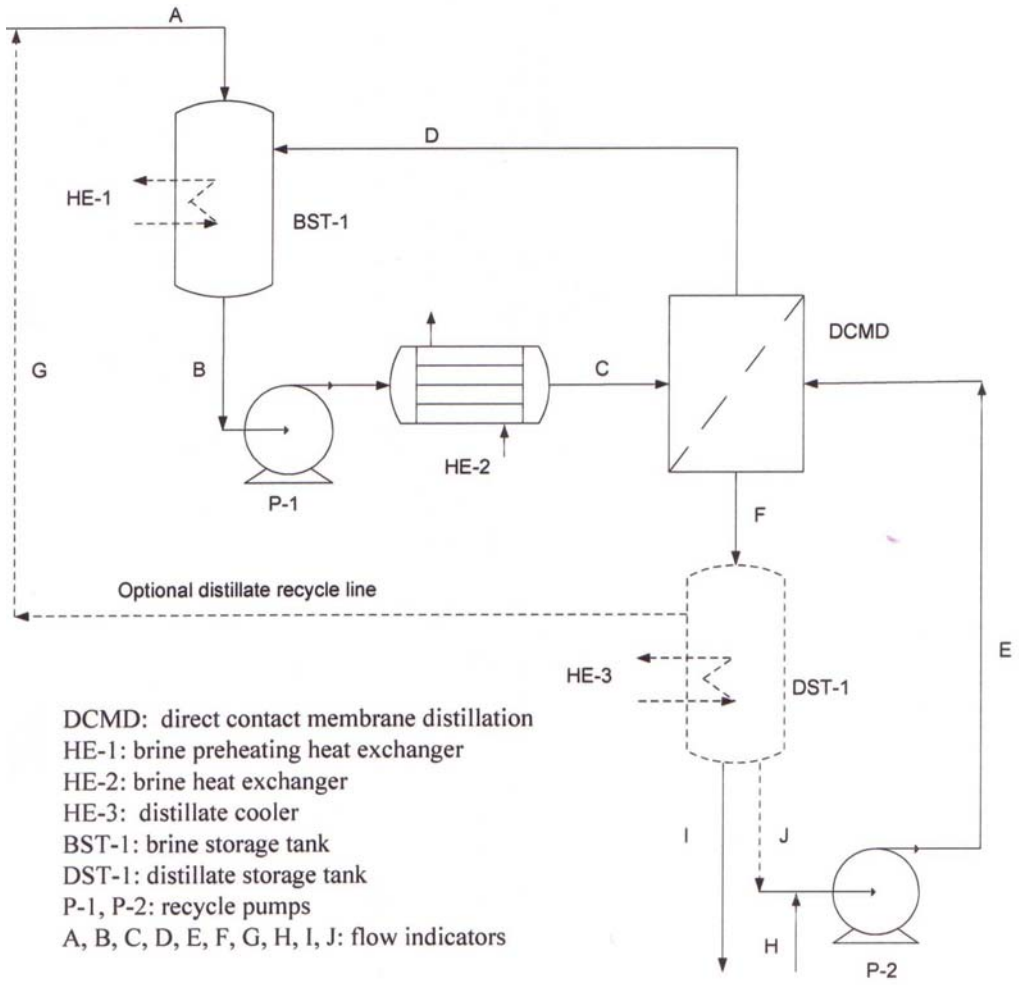

Figure 2. Schematic of DCMD process.

The conductivity monitor and controller were of the following type: conductivity controller (EW-19505-00, Cole-Parmer, Vernon Hills, Illinois 60061); conductivity cell for conductivity controller (EW-19500-00, Cole-Parmer, Vernon Hills, Illinois 60061). The temperature monitoring was done with four-channel thermometers (EW-94461-30, Cole-Parmer, Vernon Hills, Illinois 60061) as well as Type-K thermocouple probes (EW-93785-02, Cole-Parmer, Vernon Hills, Illinois 60061). The pressure gauges were 63-millimeter (mm) dual-scale gauges (EW-68007-01, Cole-Parmer, Vernon Hills, Illinois 60061), 30-inch mercury (Hg) to 30 psi and 100 to 200 kilopascal (kPa) dual-scale gauge. The brine side flow meters were in-line flow meters with a maximum operating temperature of 100 °C and a flow rate range of 2.0–20.0 gpm (EW-32472-01, Cole-Parmer, Vernon Hills, Illinois 60061) or 1.0–10.0 gpm (EW-32470-04, Cole-Parmer, Vernon Hills, Illinois 60061). The distillate side flow meters were also in-line flow meters with a maximum operating temperature 100 °C and a flow rate range of 2.0–20.0 gpm (EW-32472-01, Cole-Parmer, Vernon Hills, Illinois 60061) or 0.5–5.0 gpm (EW-32470-04, Cole-Parmer, Vernon Hills, Illinois 60061).

4.3 TASK 3: Design, Order, and Procure Large-Scale Rectangular Crossflow Hollow Fiber Membrane Modules (from AMT Inc.) and Other Equipment Needed

The large membrane modules were obtained from Applied Membrane Technology Inc., Minnetonka, Minnesota. AMT Inc. obtained fibers from Membrana, Charlotte, North Carolina, and Wuppertal, Germany. They first coated the fibers using appropriate formulations and plasma polymerization conditions used earlier successfully but with much smaller batches of fibers. This was done to test the epoxies in small shells with these fibers. The objective was to reduce first the possibilities of leakage at the potting locations; these leakages were somewhat frequent in Phase III research (Sirkar and Li, 2005). Five smaller test modules prepared by AMT Inc with appropriate epoxy potting are listed in table 2. Table 2 also lists the N_2 permeation results of these five different small modules received from AMT Inc. As one can see, the N_2 permeance values were high; these values are about 1.5–2 times higher than one of the most productive modules of the Phase II study, MXFR #3 (Li and Sirkar, 2003).

The brine leakage characteristics of the five small modules were also tested at different pressures. The salt leakage characteristics at varying transmembrane pressures for different modules are provided in figure 3. The DCMD separation characteristics in terms of water vapor flux are provided in figure 4. Both of these figures include an additional module #4 from our earlier Phase I and Phase II studies. As one can see from these figures, Module MPFM #23 had the least amount of salt leakage of the five modules (MPFM #21, 22, 23, 24, 25) received from AMT Inc. Further, the DCMD water vapor flux values in the modules were quite high—right in the desired range. We note that there was a tendency for increased salt leakage as the pressure difference between the two sides of the membranes started edging toward 10 psi (68,950 Pascals [Pa]). However, the extent of leakage was low, but so were the fiber numbers as shown in table 2. Module #4 from our Phase I and Phase II studies was from membranes having much smaller pores and a much thicker coating. So it was obvious that the proposed membranes for the pilot plant appeared to do quite well from all perspectives. These results were communicated to AMT Inc. Based on these results, AMT Inc. developed large modules using the same fibers having the following dimensions: inside diameter (I.D.) 330 μm; outside diameter (O.D.) 660 μm (PP 150/330). Note that the small-scale testings were done using the same fibers. The details of the 10 larger membrane modules are provided in table 3.

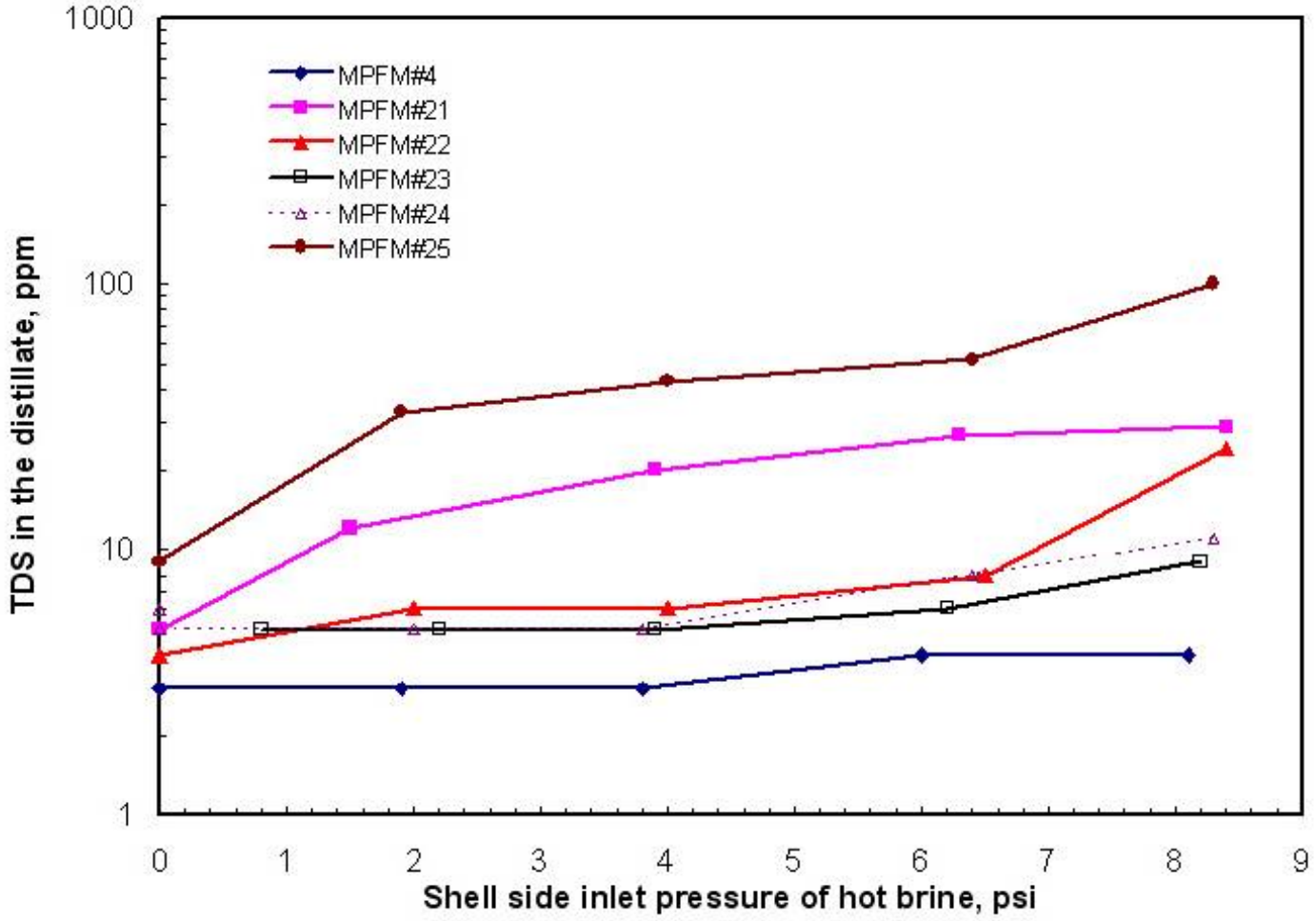

Figure 3. Variation of TDS concentration in the distillate with inlet pressure of hot brine (1% NaCl) as feed flowing through the shell side at an inlet temperature of 97 ºC (tube side, deionized (DI) water, 21–23 ºC, 3,000 centimeters per minute (cm/min) (600 cm/min for MPFM #4)).

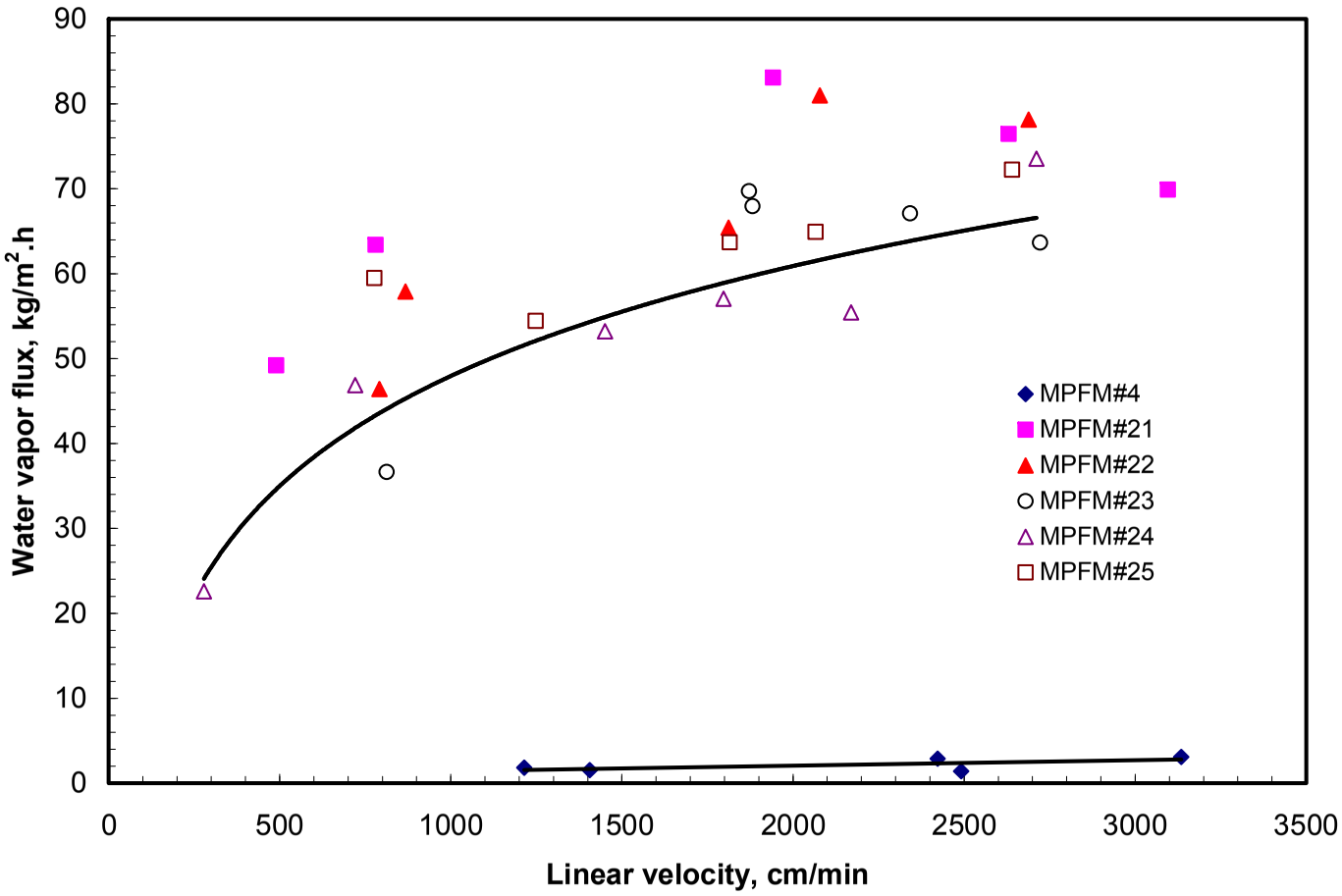

Figure 4. DCMD: Variation of water vapor flux with linear velocity of hot brine (1% NaCl) as feed flowing through the shell side (parallel flow) of smaller test modules at an inlet temperature of 97 ºC (tube side: DI water, 21–23 ºC, 3,000 cm/min (600 cm/min for MPFM #4)).

Table 2. Nitrogen Gas Permeance of Small Modules from AMT

Membrane Module	Module #4	MPFM #21	MPFM #22	MPFM #23	MPFM #24	MPFM #25
Support membrane type	PP50/200	PP 150/330 Accurel Membrana				
Support membrane	PP					
Fiber O.D. (μm)	300	630				
Fiber I.D. (μm)	200	330				
Wall thickness (μm)	50	150				
Coating [1]	Silicone fluoropolymer					
Number of fiber	300	20				
Effective fiber length (centimeters [cm])	16.51					
Effective membrane surface area (cm^2) [2]	311.2	34.23				
Gas	N_2					
Permeance (cm^3 (STP)/cm^2/s· cm/Hg) [3]	[4] 0.013	0.3990	0.4112	0.4008	0.4129	0.4233

[1] All membranes represent a recipe similar to the copolymer coating on MXFR #3 of Phase II project. Coating developed by ATM Inc., Minnetonka, Minnesota. The coating on module #4 was different and much less porous.

[2] Based on fiber internal diameter.

[3] Experimental conditions: temperature: 24.8 °C; gas inlet: tube side; gas outlet: shell side; a bubble flow meter was used for the flow rate measurements; pressure difference: 0.5 psi.

Calculation of permeance: $P = \frac{V_0}{s \cdot t \cdot \Delta p}$, $V_0 = \frac{p_1 V_1}{T_1} \cdot \frac{T_0}{p_0}$

STP: T_0 = 273.25 K, P_0 = 760 Torr

where P: permeance
s: membrane surface area
t: time (s)
Δp: pressure difference across membrane
P_1: local atmospheric pressure
T_1: room temperature
V_1: volume of permeated gas
V_o: volume of permeated gas at STP.

[4] From the reference: Li and Sirkar, 2004.

Table 3. Details of the Larger Membrane Modules and the Hollow Fibers

Particulars	S/N1006	S/N1015	S/N 1007–1014
Support membrane type	PP 150/330 Accurel MEMBRANA		
Support membrane	PP		
Fiber O.D. (μm)	630		
Fiber I.D. (μm)	330		
Wall thickness (μm)	150		
Maximum pore size (μm)	0.60		
Membrane porosity	~0.6–0.8		
Coating	Silicone fluoropolymer [1]		
Arrangement of fibers	Staggered		
Number of fibers	24 × 102 = 2,448		26 × 102 = 2,652
Effective fiber length (cm)	24.1		
Effective membrane surface area (cm^2) [2]	6,124.0		6,634.3
Effective cross -sectional area for shell side liquid flow (cm^2) [3]	59.70		
Rectangular module frame (internal dimensions)	L: 25.4 cm, W: 8.9 cm, H: 4.45 cm		
Packing fraction of fibers	0.209		0.193
Shell side flow mode	Crossflow		
Fabricated at	AMT Inc., Minnetonka, Minnesota		

[1] All membranes represent a recipe similar to the copolymer coating on MXFR #3 of Phase II project. Coating developed by AMT Inc., Minnetonka, Minnesota.

[2] Based on fiber internal diameter.

[3] Based on open area for flow = effective frame cross sectional area (24.1 × 8.9 cm^2) – fiber projected area (number of fibers in one layer × fiber O.D. × length of fiber cm^2).

Note: Face box: L: 42.5 cm, W: 16.5 cm, H: 3.5 cm; face plate: L: 30.2 cm, W: 12.7 cm, H: 0.65 cm.

These 10 modules were designated S/N 1006, S/N 1007, S/N 1008, S/N 1009, S/N 1010, S/N 1011, S/N 1012, S/N 1013, S/N 1014, and S/N 1015. The fiber numbers in these modules varied between 2,448 and 2,652 with either 24 layers or 26 layers of fibers; each layer contained 102 fibers. The effective fiber length was 24.1 cm; the substrate hollow fibers continue to be of polypropylene from Membrana having the dimensions of 330 μm I.D./150-μm wall thickness/630 μm O.D. with a maximum pore size of 0.60 μm and membrane porosity in the range of 0.6–0.8. The silicone fluoropolymer coating was supposed to be similar to that of the module MXFR #3 of Phase II project (Sirkar and Li, 2003). The packing fraction of fibers in the 10 modules varied between 0.193–0.209.

Figure 5a illustrates two of the larger modules of this project vis-à-vis the tiny module, MXFR #3, of the Phase II project (Sirkar and Li, 2003). Figure 5b illustrates the larger module S/N 1004 of the Phase III project (Sirkar and Li, 2005) vis-à-vis the module MXFR #3. The modules S/N 1006–1015 of this

project had similar frontal dimensions vis-à-vis S/N 1004 but had much deeper layers of fibers. Further, the fiber potting method adopted by AMT Inc. was also quite different for the modules S/N 1006–1015. There is an extremely remote possibility that many fiber bores were blocked by epoxies during potting at AMT Inc. It is highly unlikely as will be shown later in the DCMD results.

We should indicate that the cover plate and the distributor plate designs (figures 5c and 5d) for these modules were developed at NJIT. Further, the designs for sealing were somewhat changed; all of these plates were machined from polypropylene plates of appropriate thickness (1.5-inch thick plates for the face plate and ¼ inch for the distributor plate).

Each of the 10 larger modules was first tested for N_2 permeation. The experimental setup is shown schematically in figure 6a. Figure 6b provides a photo of the setup. The results are provided in table 4a. The N_2 permeance was calculated from the following equation:

$$\frac{Q_{N_2}}{\delta_M} = \frac{P_1 V_1 T_0}{P_0 T_1 \cdot s \cdot \Delta P_{N_2}} \qquad (1a)$$

In equation (1a), $T_0 = 273.15$ K; $P_0 = 760$ Torr; ΔP_{N_2} corrected to STP is the pressure difference across the membrane; s is the inside membrane surface area; P_1 is the atmospheric pressure; T_1 is the room temperature; V_1 is the volume flow rate of gas through the membrane during measurement at room temperature: and Q_{N_2} is the permeability coefficient of N_2 permeation through the membrane of effective thickness δ_M.

One notices that the N_2 permeances for the fibers in these larger modules are much smaller than those obtained with similar coated fibers in the much smaller MPFM modules (as shown in table 2); the reduction is by more than an order of magnitude. There is a possibility that this is most likely due to the significant pressure drop encountered by N_2 as it flows through the fiber bore. Long hollow fiber length, small fiber diameter, and high permeate flow may lead to high permeate pressure drop inside the fiber. This pressure drop in gas flow would affect the ΔP_{N_2} used in the calculations. We used a mathematical model developed by Pan and Habgood (1978) to determine pure gas permeabilities of hollow fiber modules by considering the permeate pressure drop inside the fiber. We assumed that such a procedure would substantially correct the estimate of N_2 permeance obtained from equation (1a).

N_2 permeance measurements were carried out in two deadend configurations (figure 6c). Both were considered here for pressure drops and N_2 permeance calculations using the model of Pan and Habgood (1978).

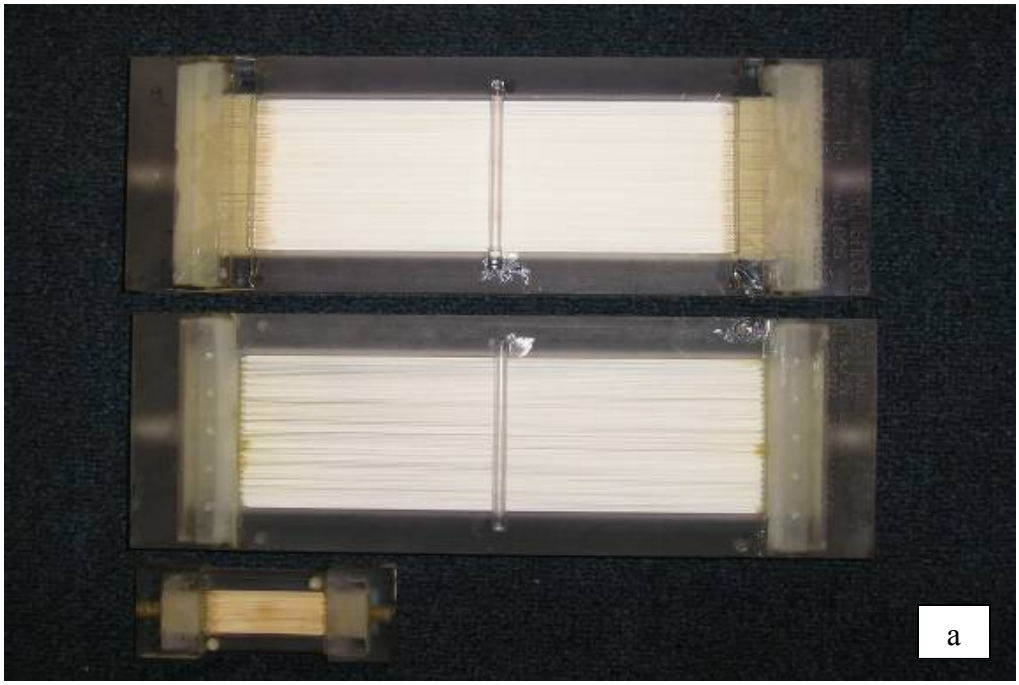
a

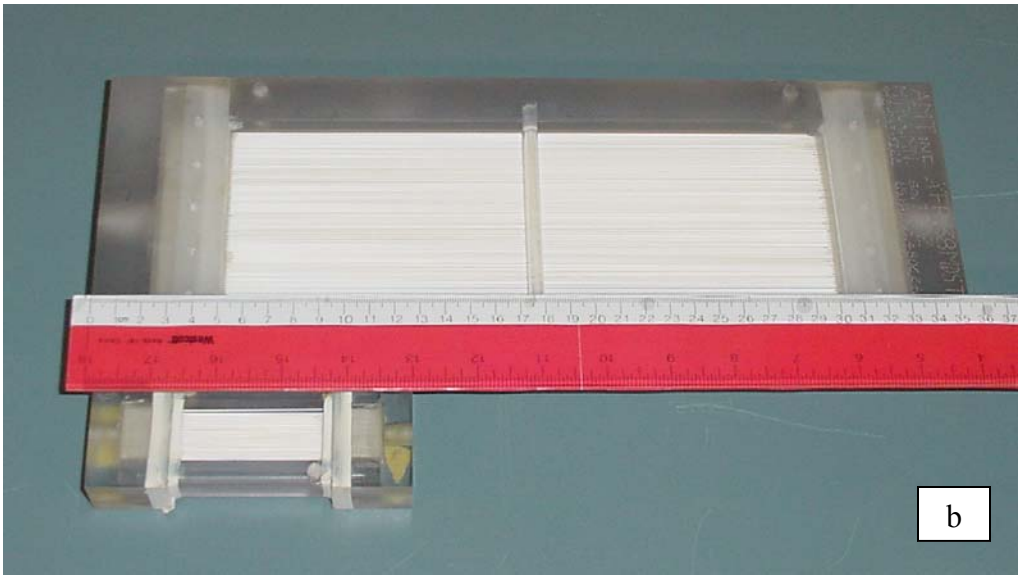
b

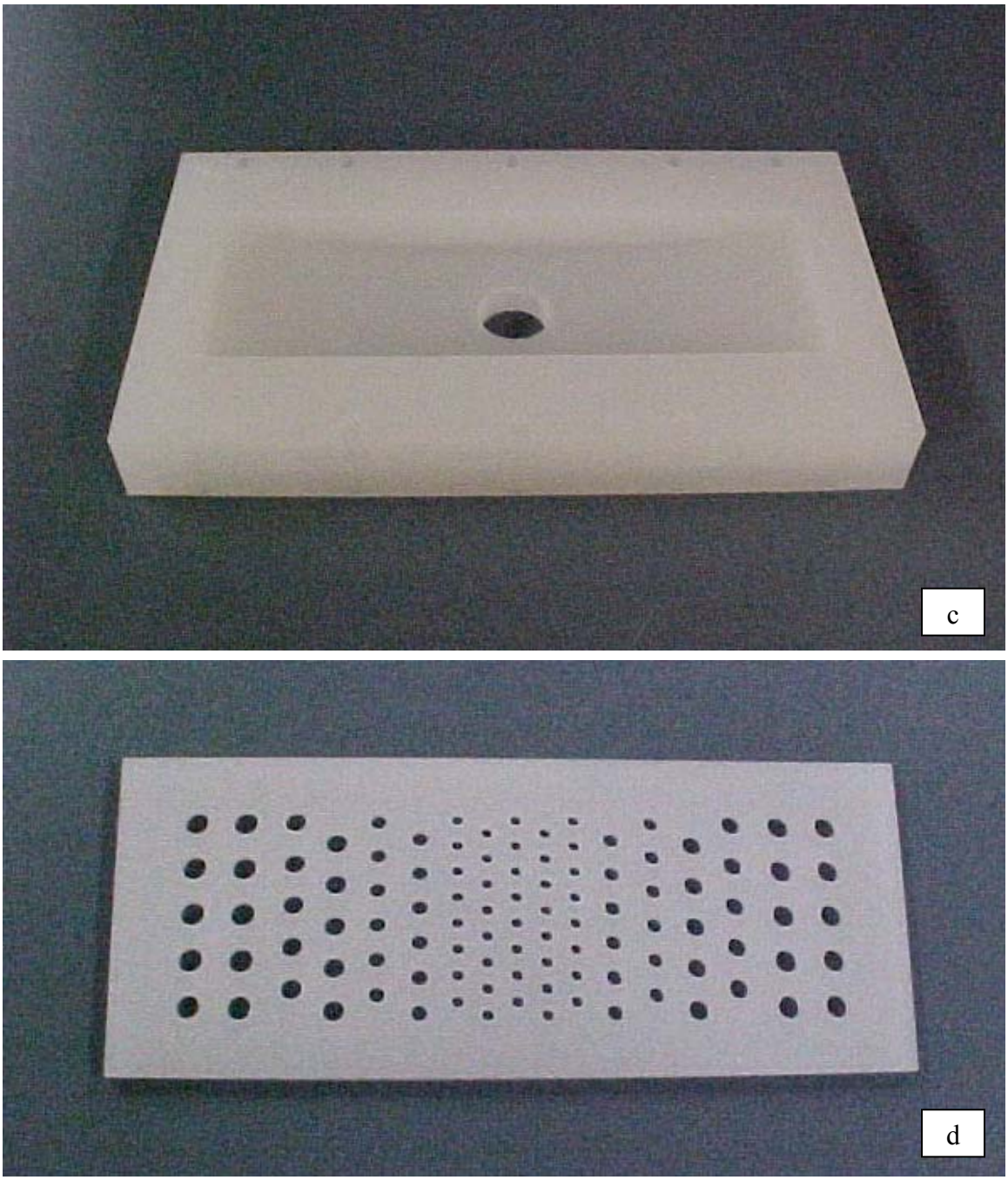

Figure 5. Photographs of various parts of a membrane module:

a. Two large-size membrane modules of this work along with the much smaller MXFR #3.

b. S/N 1004 comparing with MXFR #3.

c. The cover plate.

d. The distribution plate.T.

Table 4a. Characteristics of Larger Hollow Fiber Membrane Modules, Their Gas Permeation Propterties, and Performances in DCMD

Particulars	S/N 1006	S/N 1007	S/N 1008	S/N 1009	S/N 1010
Support membrane type	PP 150/330				
Coating	Silicone fluoropolymer				
Shell side flow mode	Cross flow				
Permeance of N_2 (cm^3 (STP)/cm^2·s· cmHg)[1]	0.0124	0.0071	0.0072	0.0072	0.0071
F(DCMD) ($kg/m^2/h$) [2]	32.0	17.4	16.0	20.1	14.9
Shell side flow rate (mL/min)	25,000	12,320	12,552	12,170	11,764
Shell side Re_s	156	69	69	72	67
Tube side flow rate (mL/min)	9,375	7,281	278	7,160	7,281
Tube side Re_t	473	280	173	288	261
TDS in the distillate (ppm)	1.13	1.56	1.80	1.61	1.80
Particulars	S/N 1011	S/N 1012	S/N 1013	S/N 1014	S/N 1015
Support membrane type	PP 150/330				
Coating	Silicone fluoropolymer				
Shell side flow mode	Cross flow				
Permeance of N_2, (cm^3 (STP)/cm^2·s· cmHg)[1]	0.0067	0.0066	0.0067	0.0067	0.0072
F(DCMD) ($kg/m^2/h$) [2]	18.4	17.9	20.7	20.1	10.7
Shell side flow rate (mL/min)	12,170	12,793	11,696	12,072	12,631
Shell side Re_s	67	76	65	67	66
Tube side flow rate (mL/min)	6,772	4,213	9,404	8,645	4,304
Tube side Re_t	260	178	401	362	163
TDS in the distillate (ppm)	1.94	1.61	1.47	2.61	2.57

[1] Experimental conditions: Temperature: 25.0 ^oC; atmospheric pressure: 76 cmHg; N_2 inlet: shell side; N_2 outlet: tube side.

[2] F(DCMD): Water vapor flux (DCMD), experimental conditions: shell side: 3.6% brine water at an inlet temperature 72–83.7 ^oC; tube side: DI water at 20.7–44.5 ^oC.

4.3.1 Configuration 1

The pressurized gas was fed into the shell side (outside of the fibers) through the center of the face plate and the permeated gas was collected from both ends of the fibers. For calculation purposes, only half of the module was considered in the following fashion. The fibers are closed at one end of this half (the end is actually the center of the module), and the permeate is collected from the other end. The feed is pressurized in the shell side from the closed end of the fibers, and the permeate flows in the lumen side.

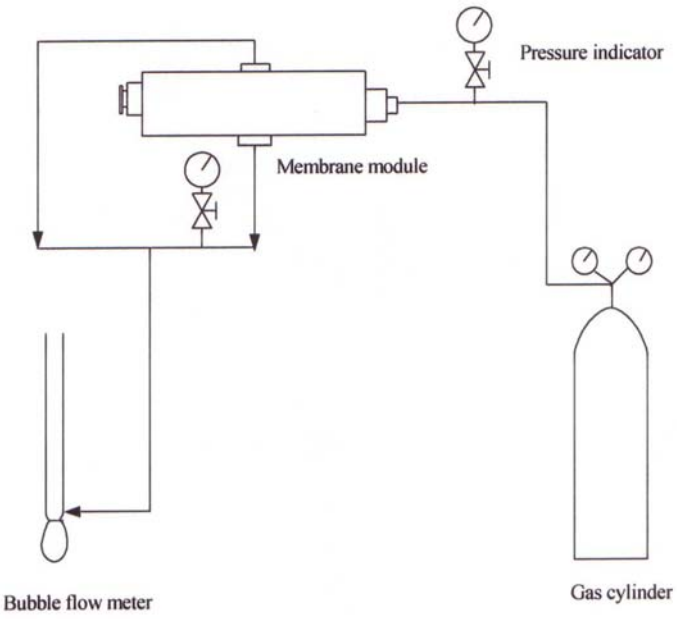

Figure 6a. Experimental setup for membrane gas permeation measurement.

Figure 6b. Photograph of the membrane gas permeation measurement experimental setup of figure 6a.

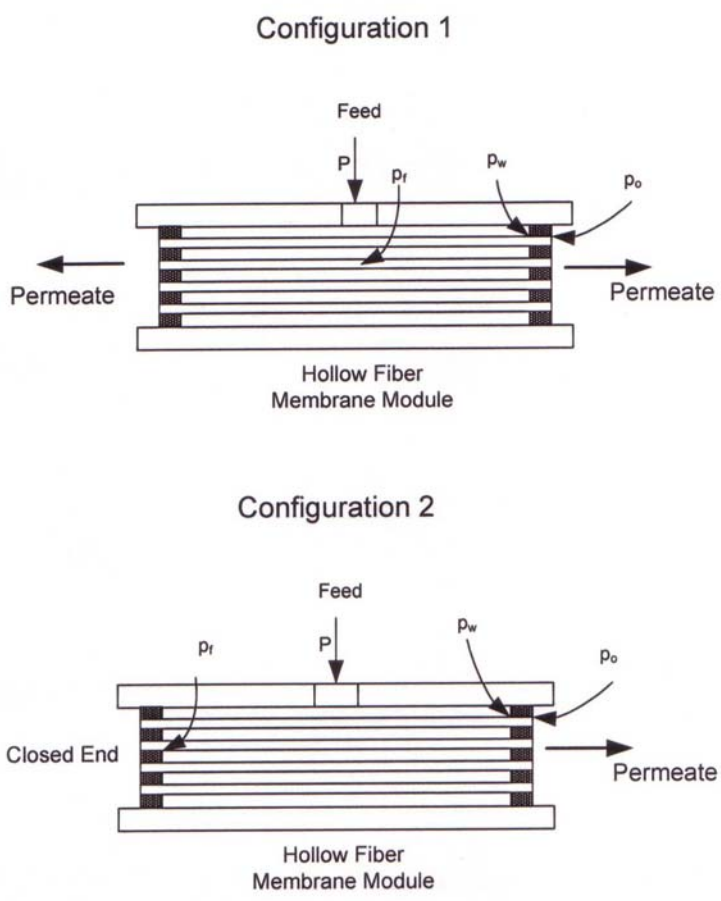

Figure 6c. Permeation through hollow fibers: Configuration 1 – both ends are open; Configuration 2 – one end is open and the other end is closed.

The numerical calculation program takes the permeate flow rate per fiber in mole per second (mol/s) and the feed pressure in Pascals as input values and returns the Q_{N2}/δ_m value in mole per square meter per second per Pascal (mole/m^2/s/Pa). The length of the fiber used in the program is half the actual length since only half of the module is considered for the calculation. Hence, one should input the permeate collected from one end of the module (or half of the total permeate flow rate).

4.3.2 Configuration 2

The pressurized gas was fed into the shell side (outside of the fibers) through the center of the face plate; the gas permeate was collected from one end of the fibers, and the other end was blocked. Modeling for this configuration is essentially the same as that of Configuration 1. In this case, the length of the fibers is the total fiber length (24 cm) instead of half of the total fiber length (12 cm) in Configuration 1.

4.3.3 Modeling of N_2 Permeance

An iteration method (Pan and Habgood, 1978) was developed using the following equations to calculate the pressure drop inside the fiber and N_2 permeance:

$$p_w^2 - p_o^2 = \frac{256\mu RTV_w l_o}{\pi g_c d_i^4} \tag{1b}$$

$$3P\left(p^2 - p_w^2\right) - 2\left(p^3 - p_w^3\right) = \frac{384\mu RT}{\pi^2 g_c d_i^4 \left(Q_{N_2}/\delta_m\right)}\left(V_w^2 - V^2\right) \tag{1c}$$

$$d_o\left(Q_{N_2}/\delta_m\right) = \frac{1}{\pi l_w}\int_0^V \frac{dV}{P-p} \tag{1d}$$

Equation (1b) was derived to calculate the permeate pressure drop over the inactive fiber length l_o in the inactive section of the module (potting). The quantities, p_w and p_o, are respectively the permeate pressure at the junction of active and inactive fiber lengths near the permeate outlet and the permeate outlet pressure; V_w is the observed permeate product flow rate. Equations (1c) and (1d) were used to calculate the permeate pressure drop over the active fiber length l_w, which was correlated with the permeance Q_{N2}/δ_m. Here P is the feed-side total pressure, and p is the local permeate-side total pressure. Further, V is the local permeate flow rate. Calculations were carried out to determine the value of Q_{N2}/δ_m following the procedure outlined below:

1. Calculate p_w from equation (1b) (this step accounts for the pressure drop in the inactive section of the module (potting) of length l_o.

2. As a first approximation, assume the permeate pressure at the closed end of the fiber p_f to be equal to $\left(P + p_w\right)/2$. Calculate the corresponding Q_{N2}/δ_m by equation (1c) ($p=p_f$ and $V=0$).

3. Calculate a new Q_{N2}/δ_m by numerically integrating the right-hand side of equation (1d) with the aid of equation (1c), in which the previously calculated Q_{N2}/δ_m was used.

4. Repeat step 3 until the value of Q_{N2}/δ_m converges to the desired accuracy (step 3 was repeated four times in the program).

Permeance values predicted from the model (table 4b) were found to be close to the values calculated by neglecting the pressure drop in the fibers. Pressure drop in the lumen side of the fibers appears to be negligible. The difference in permeance values from the model and from the experiments was very close when the permeate was collected from both ends rather than when permeate was collected from one end, as expected. This validates the model. This suggests that the coatings of these fibers were less porous and thicker than those in earlier modules.

Table 4b. N_2 Permeance and Modeling Results

Module Configuration	Shell Side Pressure	Lumen Side Pressure		Permeate Flow Rate in the Module	Permeance (mol/m^2/sec/Pa)	
		p_{in}* (from the Model)	p_{out}		Neglecting the Pressure Drop in the Fiber (Experimental)	Including the Pressure Drop in the Fiber (Modeling)
Permeate from only one end (length = 24 cm)	0.25 pounds per square inch gauge (psig) or 103,048.6 Pa	10,1593 Pa or 0.0388 psig	1 atm or 101,325 Pa or 0 psig	4.7 lit/min	$2.81*10^{-6}$	$3.168*10^{-6}$
Permeate from two ends (length = 12 cm)		101,415 Pa or 0.013 psig		4.7/2 lit/min	$2.81*10^{-6}$	$2.91*10^{-6}$
Permeate from only one end (length = 24 cm)	1 psig or 108,219.7 Pa	101,943 Pa or 0.0896 psig		10.7 lit/min	$1.6*10^{-6}$	$1.71*10^{-6}$
Permeate from two ends (length = 12 cm)		101,544 Pa or 0.0317 psig		12.5/2 lit/min	$1.87*10^{-6}$	$1.91*10^{-6}$

* p_{in} = the pressure on the lumen side at the blocked end (Configuration 2) or at the middle of the fiber (Configuration 1).

Figure 7a illustrates the process flow diagram employed to test the large DCMD modules for their DCMD performance at NJIT. Figure 7b shows the photograph of the experimental setup (corresponding to figure 7a) employed to achieve that goal at NJIT.

A number of DCMD runs were carried out using the large module S/N 1006 which was received first. Performance results of this module were communicated in general terms to AMT Inc. before the complete picture-frame type module fabrication was initiated by AMT Inc. for the rest of the modules (nine in total). Figure 8 illustrates the variation of inlet/outlet temperatures for the hot feed brine side and the colder distillate side; in this figure, instead of any brine, city water was employed. Figure 9 illustrates the water flux levels obtained in the run illustrated in figure 8. The water vapor flux values reached the level of 26 kg/m^2/h. The volume of the distillate collected in a certain time was used to calculate the water vapor flux through the membrane under the given experimental conditions. Water vapor flux was calculated from the following relation:

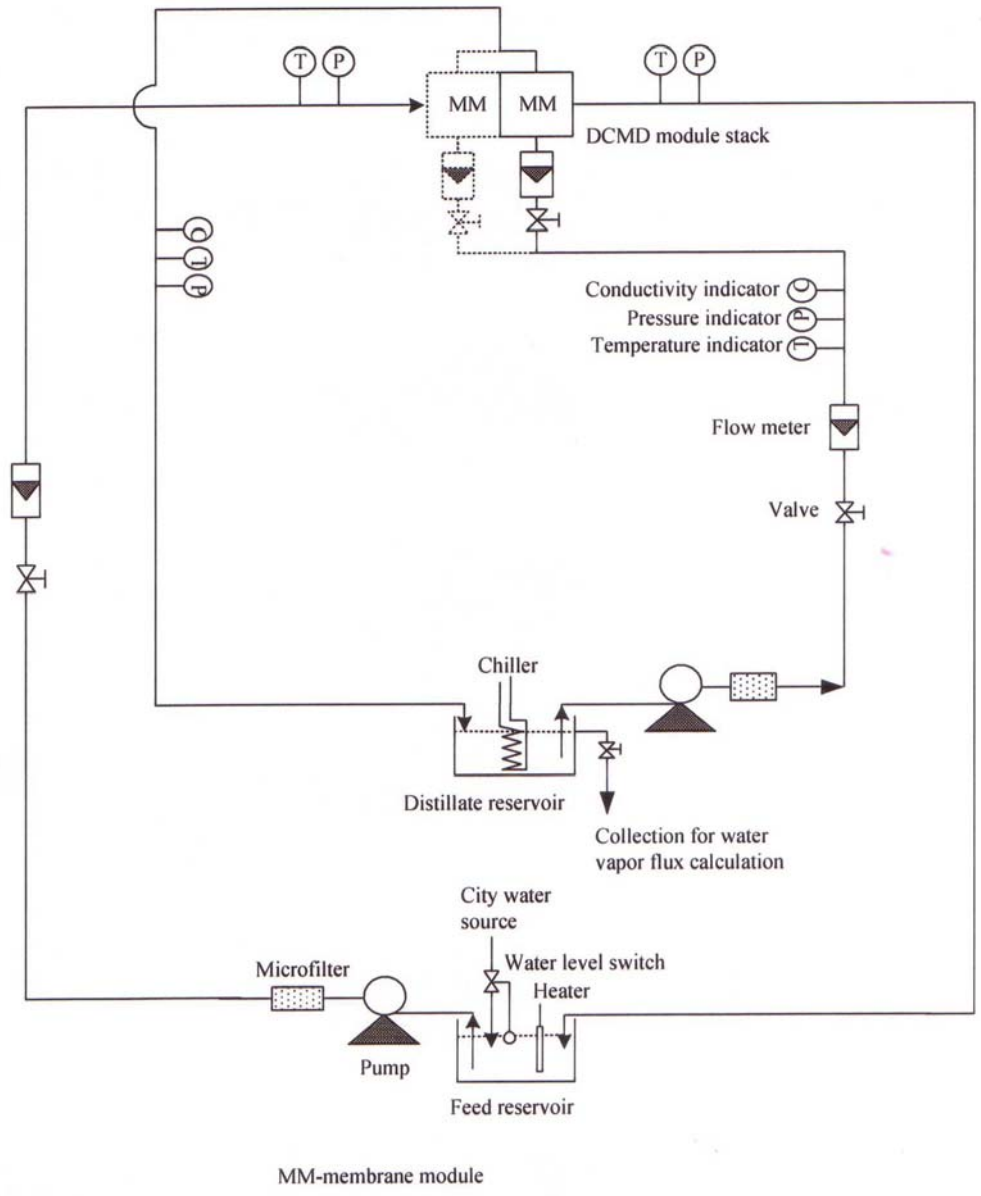

Figure 7a. Process flow diagram for DCMD.

Figure 7b. Photograph of the experimental setup of figure 7a.

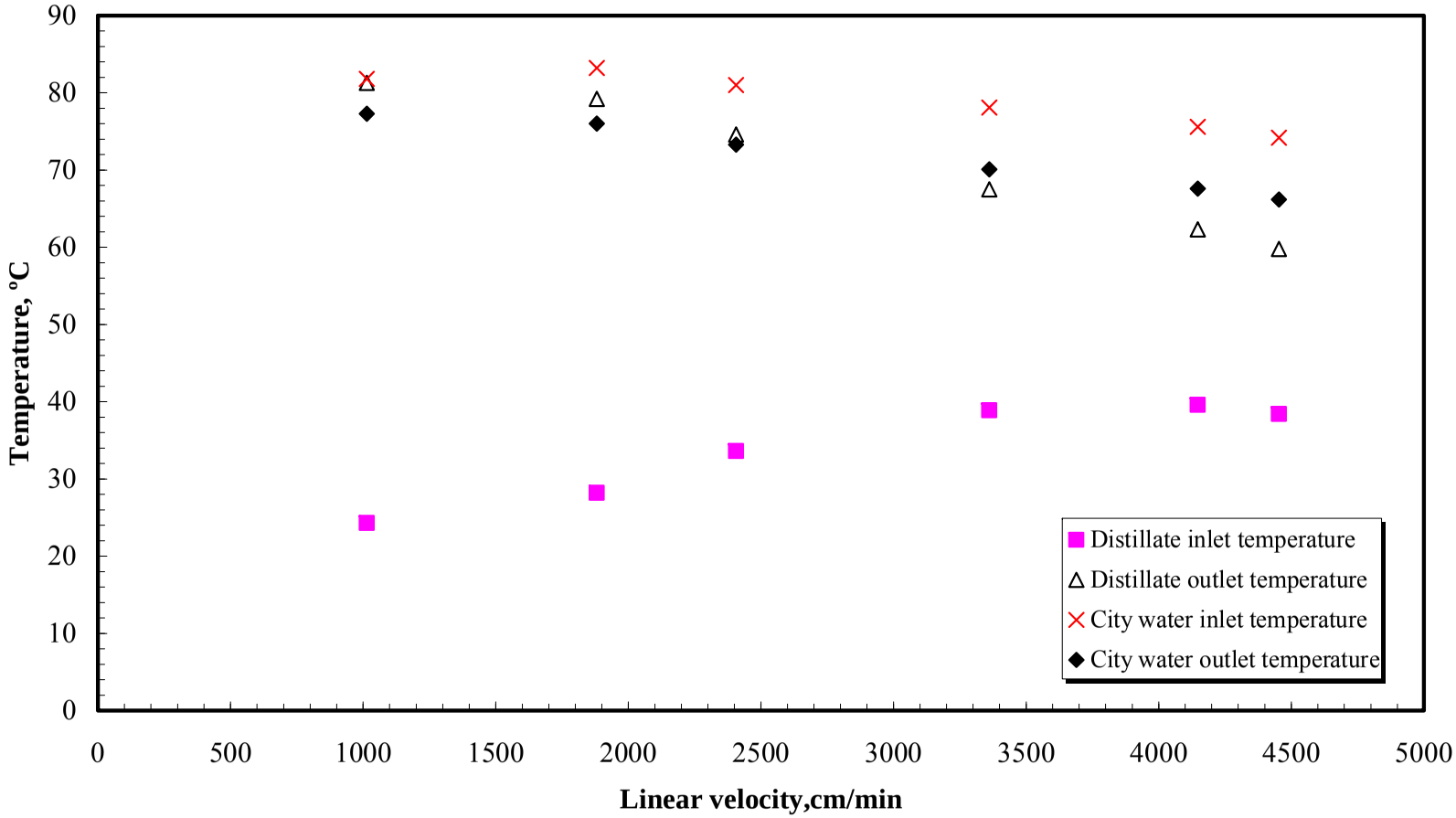

Figure 8. Variation of shell side and tube side outlet temperatures with linear velocity of DI water flowing on the tube side (DCMD module: S/N 1006; shell side: city water at 609 cm/min of interstitial velocity; shell side and tube side inlet temperatures are also shown in the graph).

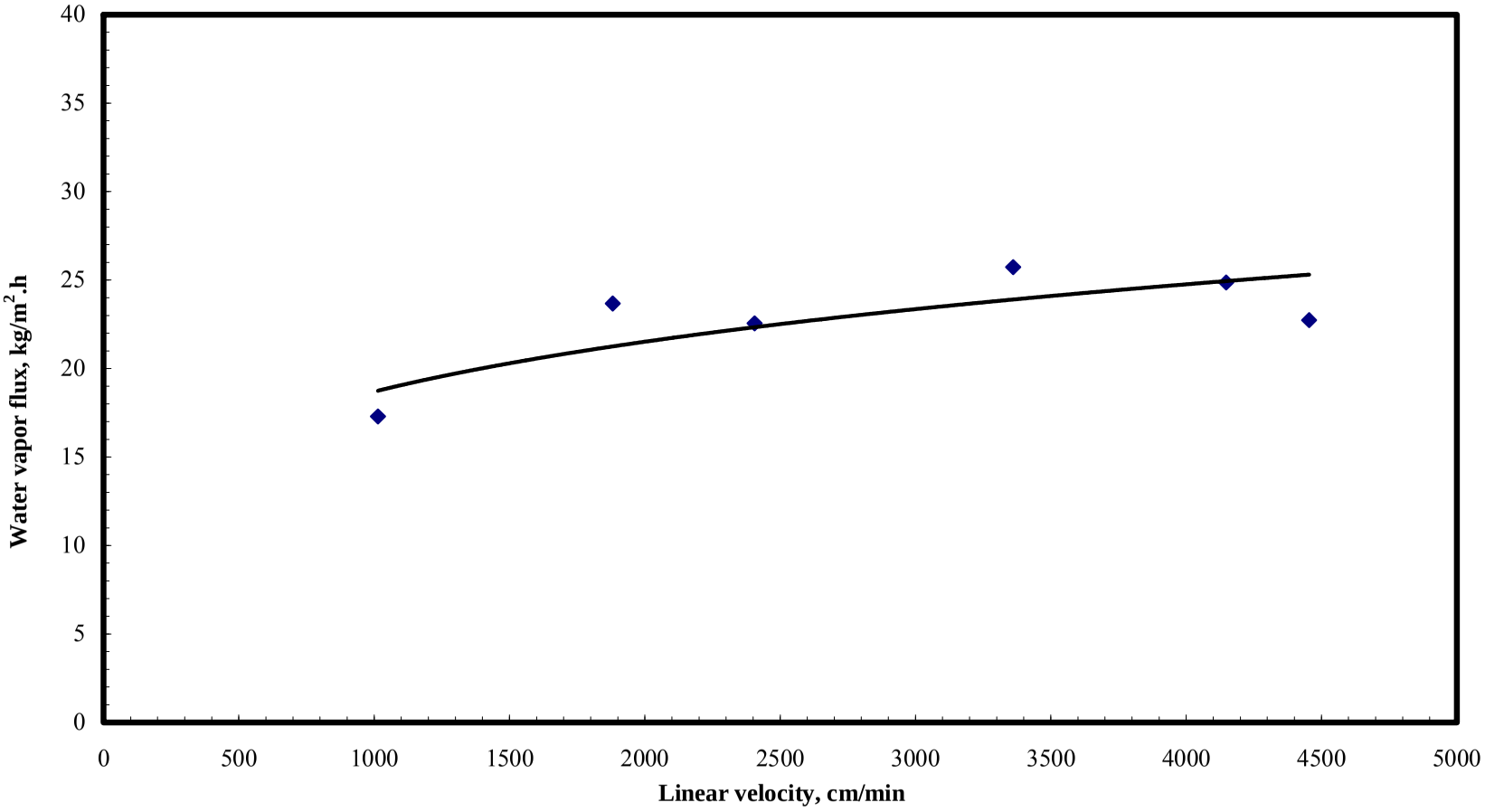

Figure 9. Variation of water vapor flux of module S/N 1006 with linear velocity of DI water flowing on the tube side (shell side: city water at 609 cm/min of interstitial velocity at a temperature of 74–83 °C; tube side: inlet temperature, 24–40 °C; outlet temperature, 60–81 °C).

Water vapor flux $(\frac{kg}{m^2 - h}) =$

$$\frac{\text{volume of water transferred (l)} \times \text{density of water (kg/l)}}{\text{membrane area (m}^2\text{)} \times \text{time (h)}} \quad (2a)$$

Here, the membrane area was calculated based on the hollow fiber inside area,

$$s = nm\pi d_i L \quad (2b)$$

where n is the number of fibers in a given layer in a membrane module having m layers; d_i is the fiber inside diameter; L is the fiber length.

Reynolds number is normally defined in the following way:

$$\text{Re} = \frac{D \times u \times \rho}{\mu} \quad (3a)$$

Here Re: Reynolds number; D: characteristic dimension; u: velocity; ρ: density; μ: dynamic viscosity (absolute viscosity). The Reynolds numbers of the hot feed or the cold distillate flowing through the shell or the tube side were defined as diameter-based Reynolds number (Re_d). In the calculation of Re_d based on equation (3a), fiber I.D. (d_i) and linear velocity were used for tube side parallel flow, and fiber O.D. and interstitial velocity for shell side crossflow; the highest interstitial velocity achievable was around 240 cm/min (7.87 feet per minute [ft/min]):

Interstitial velocity (u_I) =
brine flow rate/open area for flow through the shell side (3b)

The open area for flow through the shell side has been defined at the bottom of table 3.

Linear velocity (u_L) =
flow rate/open area for flow through the tube side (3c)

The lower values of the water vapor flux in figure 9 reflect the limited heat transfer capabilities of the setup at NJIT. This was observed earlier in the Phase III research (Sirkar and Li, 2005): when a module having about half of the amount of membrane area (0.28 m^2) of current larger modules was utilized, the flux levels were quite high. However, when two such smaller modules were placed back to back (S/N 1004 and S/N 1005), the flux levels achieved were lower almost by a factor of 2. The setup at NJIT did not have the thermal power to handle the cooling needed for high flow rates and high temperature drops.

The following two illustrations provide the results of DCMD runs for the large module S/N 1006 using hot brine (3.6% NaCl) as feed instead of heated city water. Figure 10 illustrates the inlet/outlet temperatures of the hot brine as well as those of the colder distillate stream. Figure 11 provides the water vapor flux data for the runs presented in figure 10. Water vapor fluxes achieved go up to 32 kg/m^2/h (18.85 gfd). The reason why higher values were not achieved was again the capacity limitation of the cooling system installed in this loop at NJIT. However, there is another piece of important information in figure 11. TheTDS measured in the distillate via the conductivity meter (ORION 115A+) was around 1 ppm. This indicated that there was no salt leakage to the distillate from the hot brine side. The module assembly design developed at NJIT and the fiber potting by AMT in the picture frame were working satisfactorily. Each and every large module sent by AMT was checked for leakage as well as applicability in DCMD. Table 4 provides the DCMD fluxes for modules S/N 1006 to S/N 1015, 10 modules in all. None of the modules leaked as shown by the distillate TDS values.

4.4 TASK 4: Build the Pilot Plant at the Test Site

The building of the pilot plant began in the fourth week of October 2005 and was completed by early February 2006. In very early December 2005, module S/N 1006 was shipped to the UTRC pilot plant site to test out in a cold water system. Then all 10 modules S/N 1006–1015 were shipped to the pilot plant. Figure 12a illustrates a photograph of the DCMD pilot-scale demo setup; figure 12b provides a view from a longer distance. Figure 12c provides a close up view of some of the membrane modules and the associated piping and connections. This figure shows two types of assemblies—one at the top where two modules are back-to-back in the same assembly; the second one at the bottom has only one module. Figure 13 illustrates the actual schematic of the pilot plant. There are two large plastic tanks (volume of each tank, 250 gallons). The cold distillate water is pumped from the distilled water tank by a centrifugal pump through a microfiltration unit (1 μm, Cole-Parmer) into the modules. Prior to introduction into the modules, the pressure, temperature, conductivity, and flow rate of this stream are measured. Then this flow is split and introduced into the distillate side of each of the 10 membrane modules shown in figure 2. Other flow schemes have also been pursued and will be so indicated. After measuring the conductivity, pressure, temperature, and flow rate of each distillate stream from the modules, they were combined and sent to a heat recovery heat exchanger where the heated distillate stream (obtained by combining individual streams) is cooled down by the spent brine stream from the modules. The cooled distillate stream is further cooled in a chilled water exchanger by chilled water source from the UTRC facility. The chilled distillate is discharged into the distillate water tank.

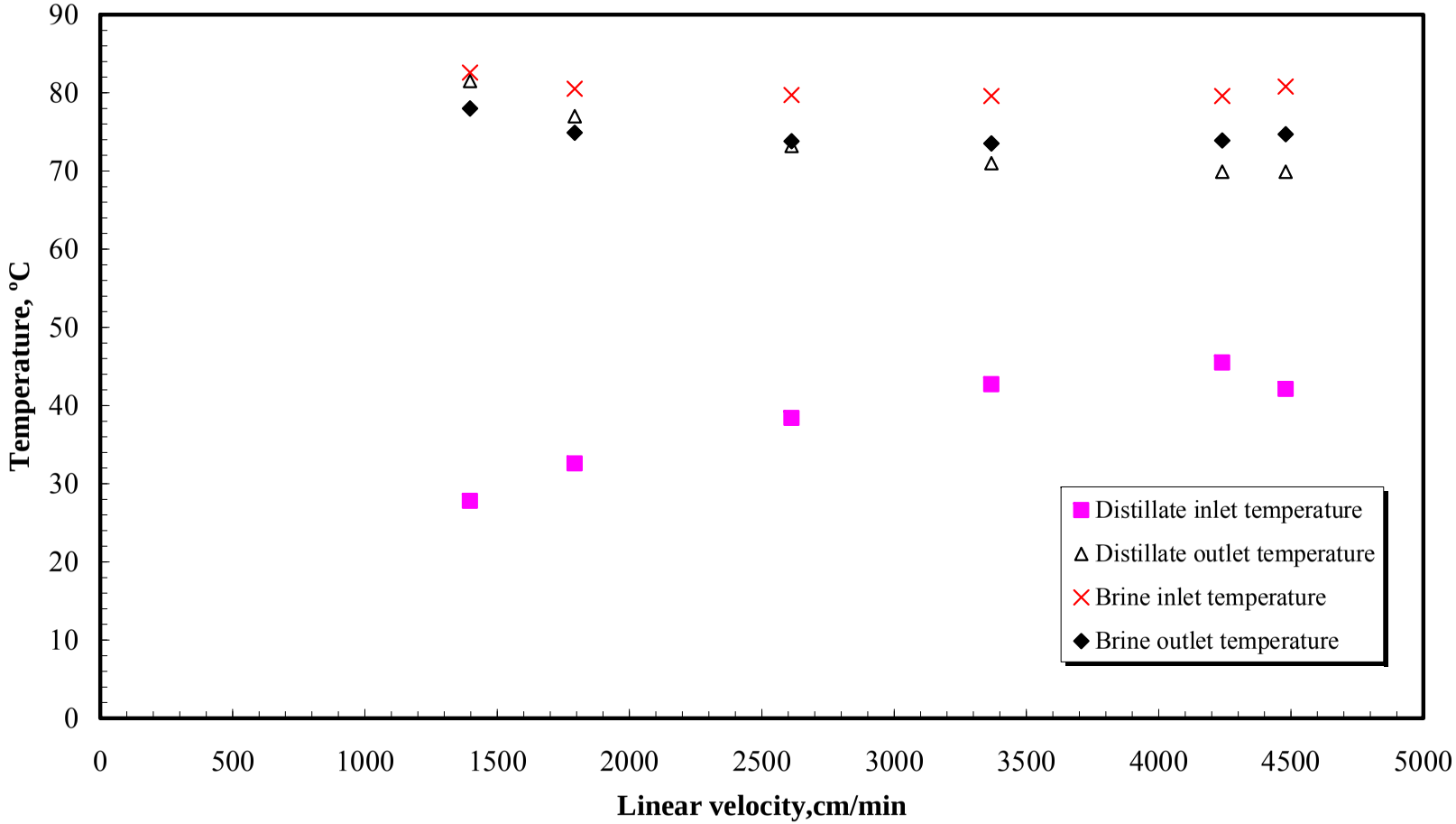

Figure 10. Variation of shell side and tube side outlet temperatures with linear velocity of DI water flowing on the tube side (DCMD module: S/N 1006; shell side: 3.6% brine at 609 cm/min of interstitial velocity; shell side and tube side inlet temperatures are also shown in the graph).

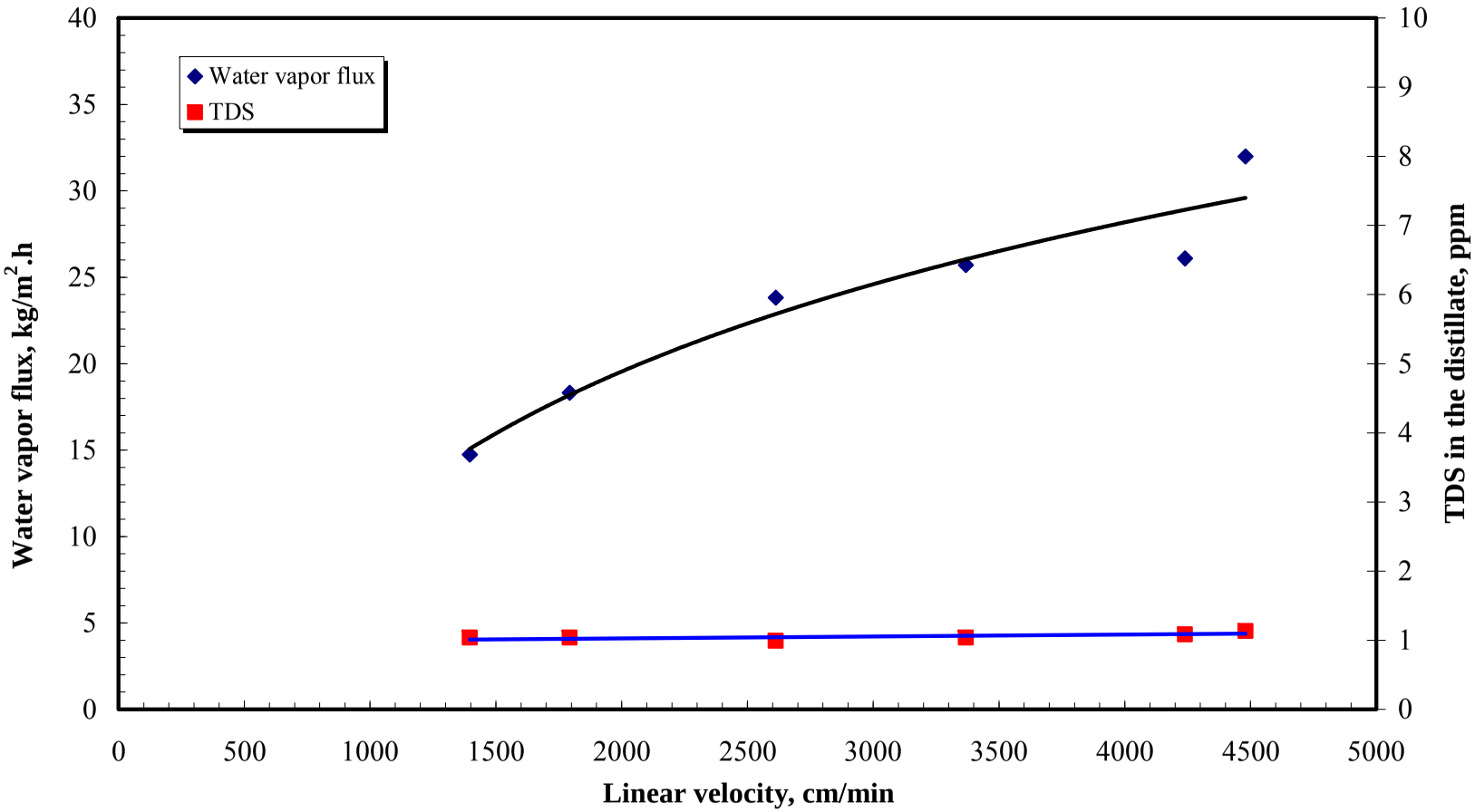

Figure 11. Variation of water vapor flux of module S/N 1006 with linear velocity of DI water flowing on the tube side (shell side: 3.6% brine at 609 cm/min of interstitial velocity at an inlet temperature 80–83 °C; tube side: inlet temperature 28–46 °C, outlet temperature 70–82 °C).

Figure 12a. Photograph of the DCMD pilot-scale demo setup.

Figure 12b. Photograph of the DCMD pilot-scale demo setup (view from a distance).

Figure 12c. Photograph of the membrane module assembled in DCMD pilot-scale demo system.

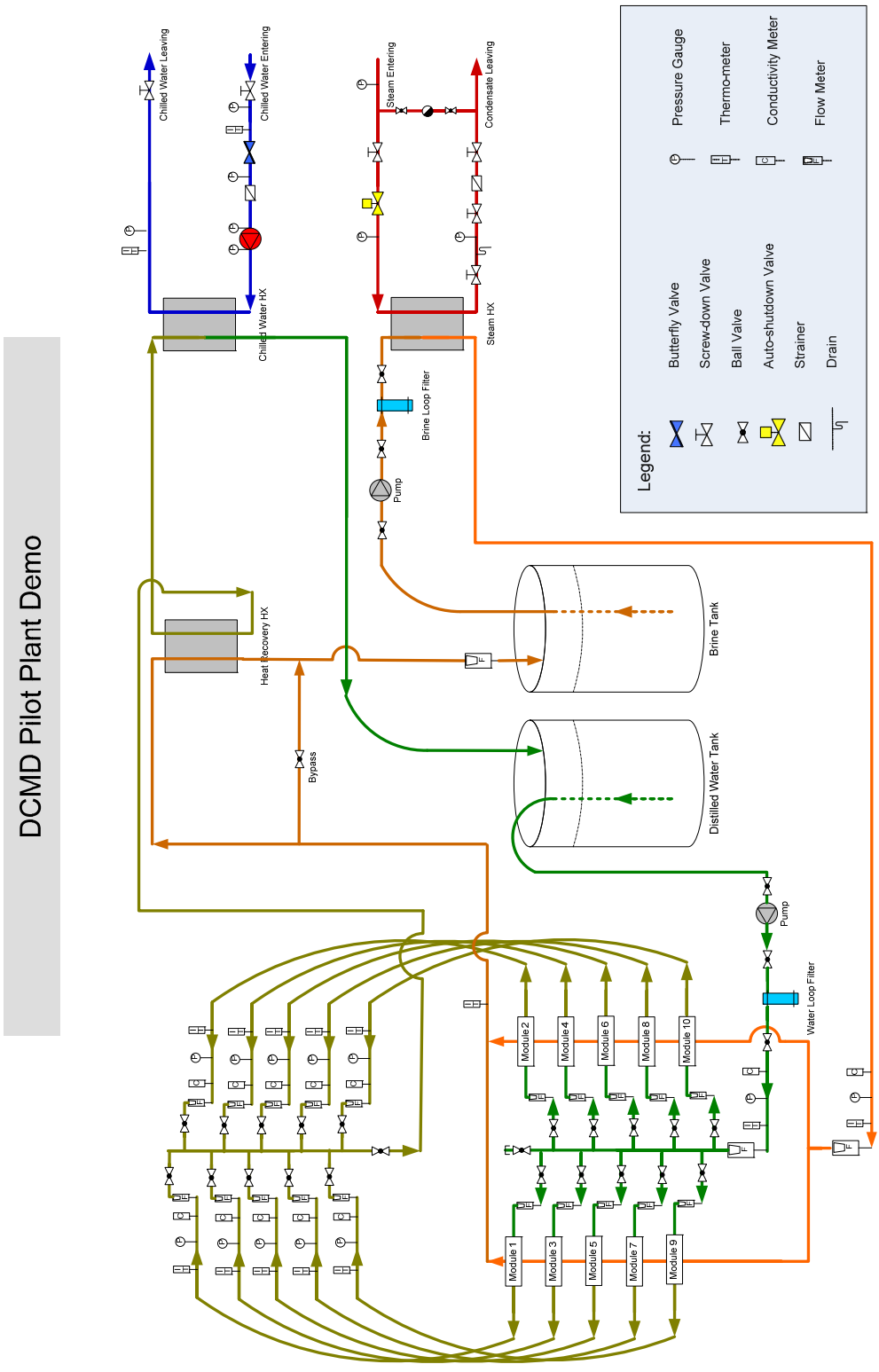

Figure 13. Schematic of DCMD pilot plant.

The brine from the brine tank is pumped by a centrifugal pump and a microfilter (1 μm, Cole Parmer) into a steam heat exchanger where house steam is used to heat the brine up to the desired temperature (less than or equal to 91 °C). The hot brine is then sent (after monitoring its temperature, pressure, conductivity, and flow rate) into the module bank. Usually, the brine is split into two streams each of which is introduced into each module bank. After the spent brine streams are cooled down, they are combined and sent to the heat recovery heat exchanger after measuring the temperature. The brine heated up somewhat by the hot distillate is next sent to the brine tank.

Figure 14 illustrates that the top of the assembly, where two rectangular modules, each having an area of 0.66 m^2, are stacked one on top of the other for testing. This was the most common testing configuration used in the pilot plant studies. We have identified them as a single-pair unit. Single modules were also being tested. Figure 15 shows a pipe coming out of the distillate tank—this represents overflow from the tank and allows measurement of the water vapor flux.

4.5 Task 5: Develop Pilot Plant Test Procedures

The pilot plant was tested for operability in the months of January 2006 and early February 2006. No major problems were found. Small leakages were observed on the brine side of some of the modules through the gaskets between the cover plate and the picture frame. During experiments, they were collected as drops on a flat plate over which the modules were kept. No leakages were observed at the tube sheet; brine did not leak into the distillate or vice versa. Brine side flow rate could be varied between 22 and 66 L/min (5.81–17.4 gpm). The distillate side flow rate could be varied between 22 and 67 L/min. The distillate temperature could be varied between 20 and 50 °C. The maximum brine temperature achieved was 93 °C. The centrifugal pumps, the heat exchangers, and the microfiltration units operated satisfactorily. The readings from each flow meter, solution conductivity measuring unit, pressure gauge, and thermometer were digitally displayed; from the displays, the data were manually recorded in individual data sheets. Generally, runs were going to be made on a daily basis. No flow loop and other cleaning activity were to be undertaken after shutdown. However, the modules were to be visually inspected after runs as often as possible.

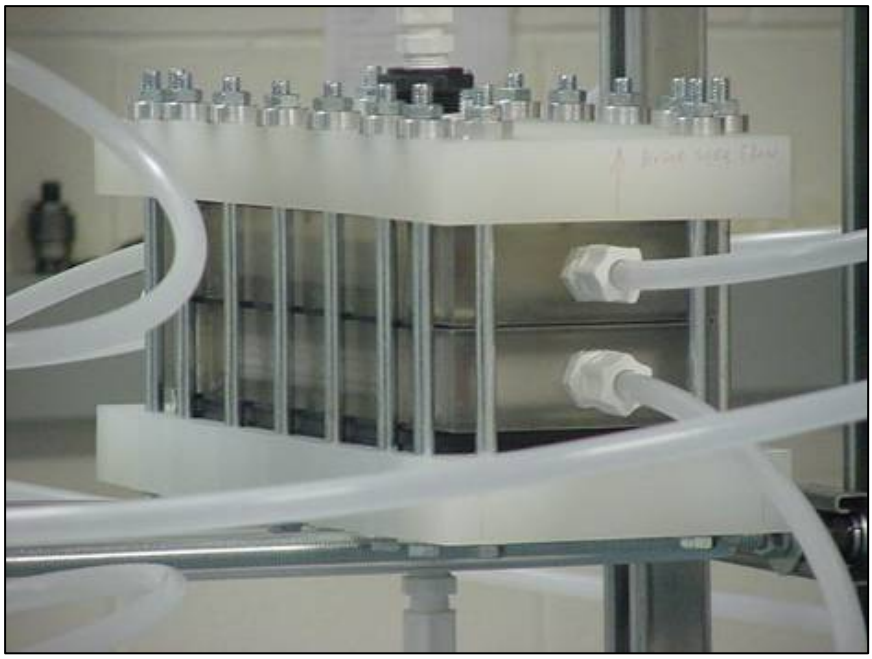

Figure 14. Photo of connections of DCMD modules.

Figure 15. Photo of water vapor flux measurement.

The pilot plant was going to be run every day using different combinations of modules. The variables to be studied were brine velocity, distillate velocity, brine feed temperature, and distillate feed temperature. In all experiments, the brine concentration was to be kept constant by adding the produced distillate back to the brine tank unless otherwise mentioned. The general experimental procedure was to measure the temp eratures as a function of time (→); if three consecutive measurements over a period of 15 minutes do not change by more than 0.1 °C, then steady state may be assumed and water vapor flux measurements made.

4.6 Task 6: Gather Test Data and Analyze Pilot Plant Performance

Before we describe in detail the different module configurations studied and the desalination results obtained, we would like to report first some observations about the membrane modules and hollow fibers. Data gathering began in the middle of February 2006. Out of the ten modules prepared and supplied by AMT Inc., nine modules had functioned well. A few fibers in one of the modules were found to be degrading. The nature of the degradation coincided with the possibility of potential damage from the plasma polymerization process variations (as indicated by AMT Inc., Minnetonka, Minnesota. The fibers in all other modules showed remarkable endurance/performance. After a day's run was over, the cover plates of the modules were removed periodically, and the fibers were visually inspected. We observed that there were slight tendencies of fiber bunching leading to limited channeling possibilities on the brine side as shown in figure 16. This could have been avoided if a hollow fiber mat was used to develop the modules.

A variety of module assembly configurations was used. Figure 17 illustrates two DCMD modules in series with the hot brine leaving one module and entering the next located immediately and physically downstream without any cover plate, face plate, etc. The two variations in this configuration are that distillate can enter in a parallel direction or in a countercurrent direction. If the brine leaving the hollow fibers in the first module immediately enters the hollow fiber bed in the second module without any lateral mixing, the countercurrent mode would be advantageous. That, however, is not valid here since there is a substantial gap between the two fiber beds leading to brine mixing. Figure 18 shows two single-pair units in series putting four DCMD modules in series. This figure also shows six DCMD modules in series via three single-pair units in series. Figure 19a displays eight DCMD modules with two sets of two single-pair units (in series) connected in parallel. The arrangement employed on the distillate side consists of parallel entry of the distillate into two parallel two single-pair units with countercurrent entry of the distillate in parallel into the second module of the two

Figure 16. Photo of fiber bunching leading to fluid channeling on the DCMD module shell side.

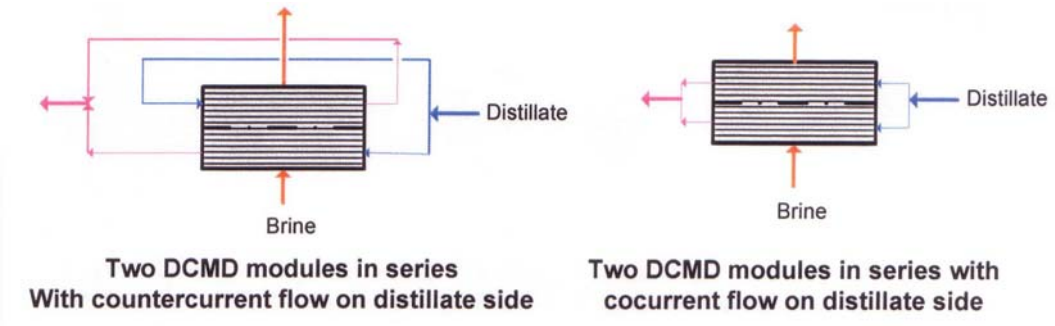

Figure 17. Schematic of fluid flow directions for a single-pair DCMD unit test.

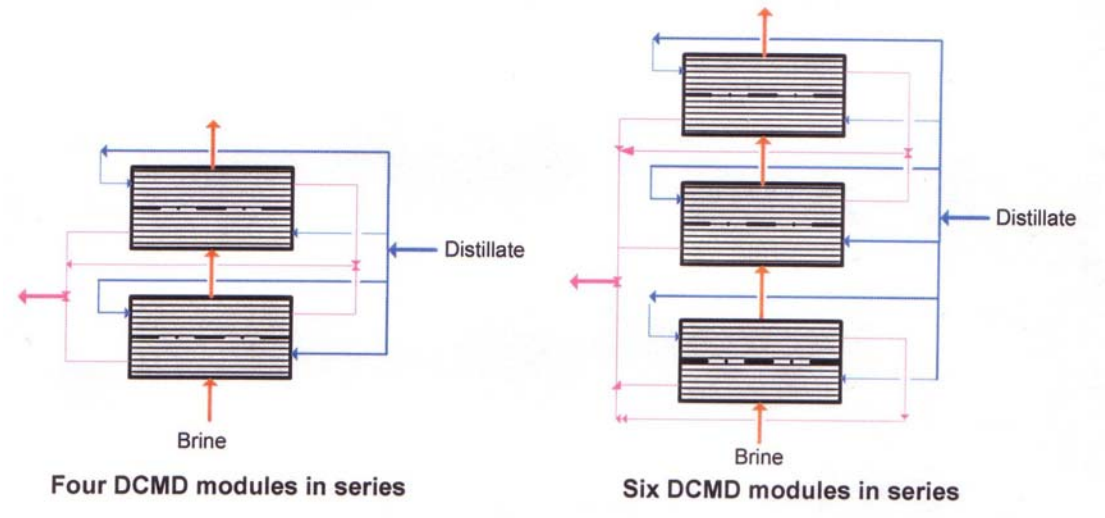

Figure 18. Schematic of fluid flow directions for tests of different fiber layer depths on the DCMD shell side.

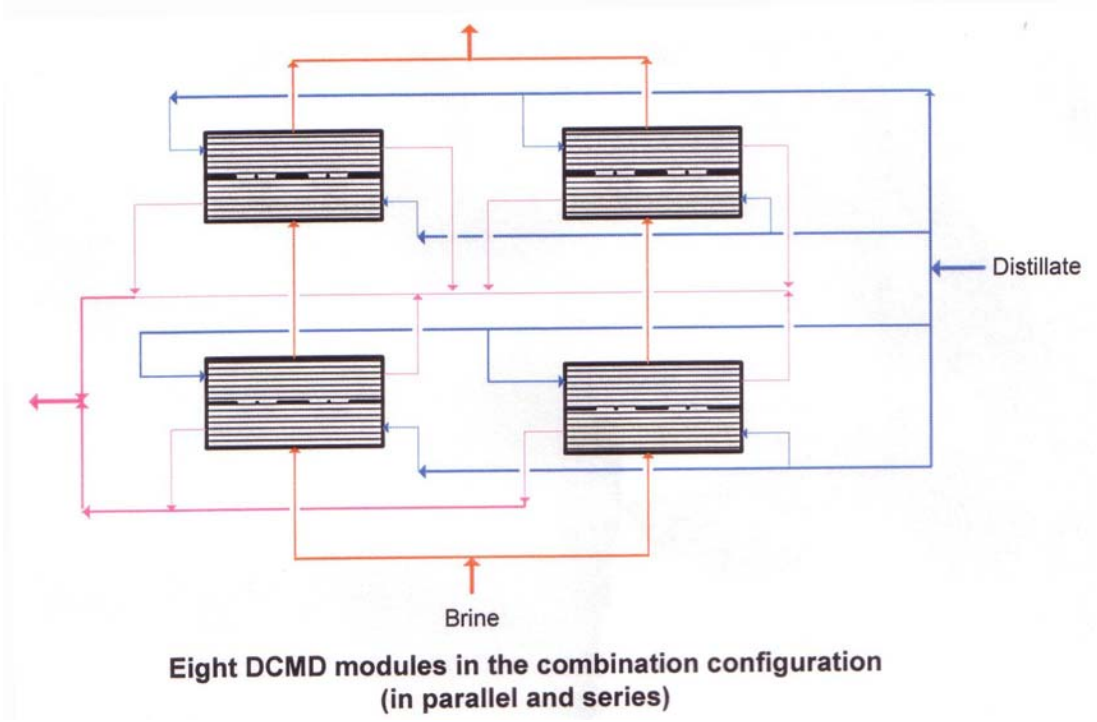

Figure 19a. Schematic of fluid flow directions for tests with eight DCMD modules in the combination configuration (in parallel and series).

parallel two single-pair units. Figure 19b follows the same scheme where there are two parallel legs of the cascade with each leg having five modules in series with two sets of two single-pair units and a single module. The distillate flow arrangement is similar to that in figure 19a between the two parallel two single-pair units.

Figures 20a, 20b, 20c, and 20d illustrate pilot plant configurations where different numbers of single-pair units are connected in parallel vis-à-vis the hot brine flow. Figure 20a has two such units in parallel, whereas figure 20b has three such units in parallel. Figure 20c has four units in parallel, and figure 20d has five units in parallel. These configurations were designed to expose as much of the membrane surface area as possible to the highest possible temperature, namely, the hot brine feed to achieve the highest flux. Of course, the brine flow rate decreases leading to lower heat transfer coefficient in each pair unit. Figure 21 is similar to figure 19a except that, in each leg of the set up, the distillate entering the lowest module (fourth module) in the cascade exits and enters the second module higher up in the cascade. The same strategy is followed with the third and the first modules in the cascade. This means that distillate in the modules exposed to a higher brine temperature are at a higher temperature. One would like to know if there is a substantial water vapor flux loss as a result.

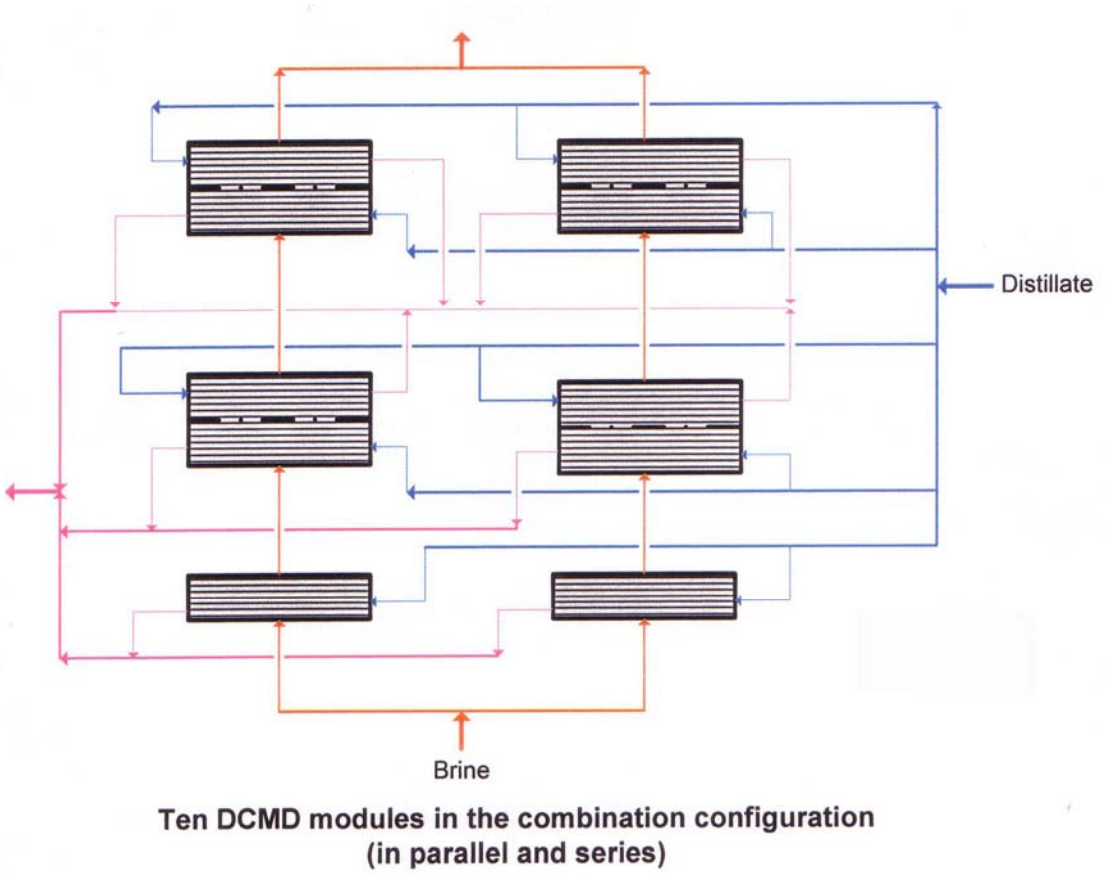

Figure 19b. Schematic of fluid flow directions for tests with 10 DCMD modules in the combination configuration (in parallel and series).

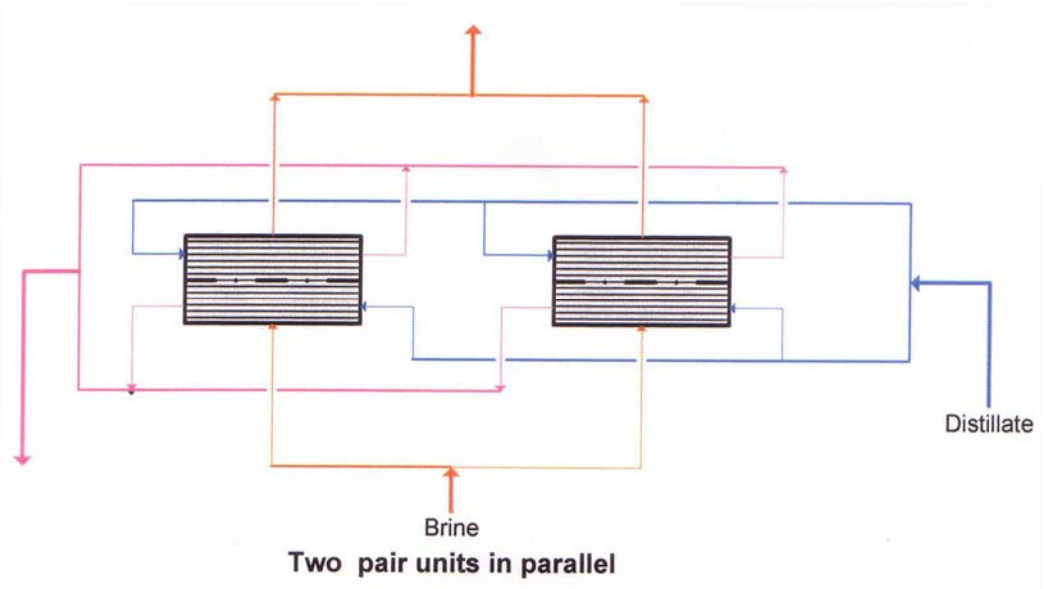

Figure 20a. Schematic of fluid flow directions for tests with two single-pair DCMD units in parallel.

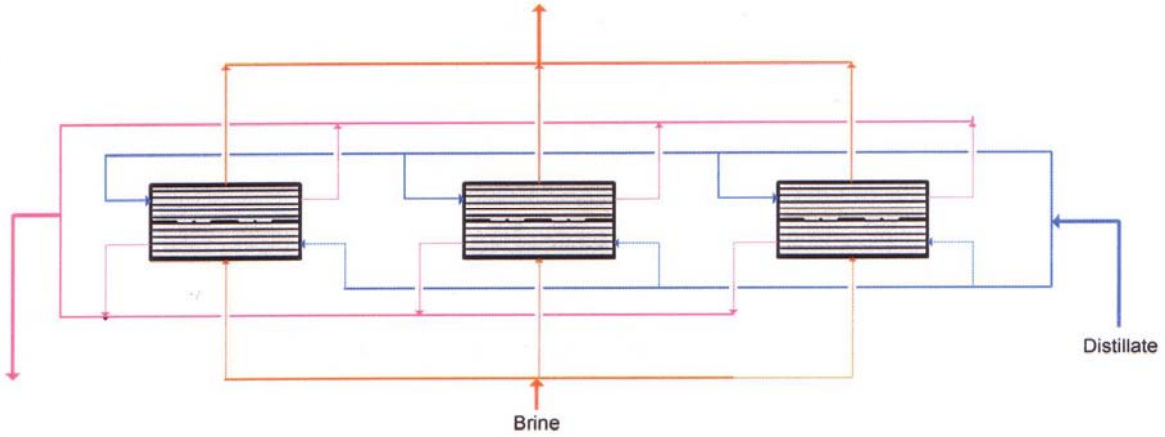

Figure 20b. Schematic of fluid flow directions for tests with three single-pair DCMD units in parallel.

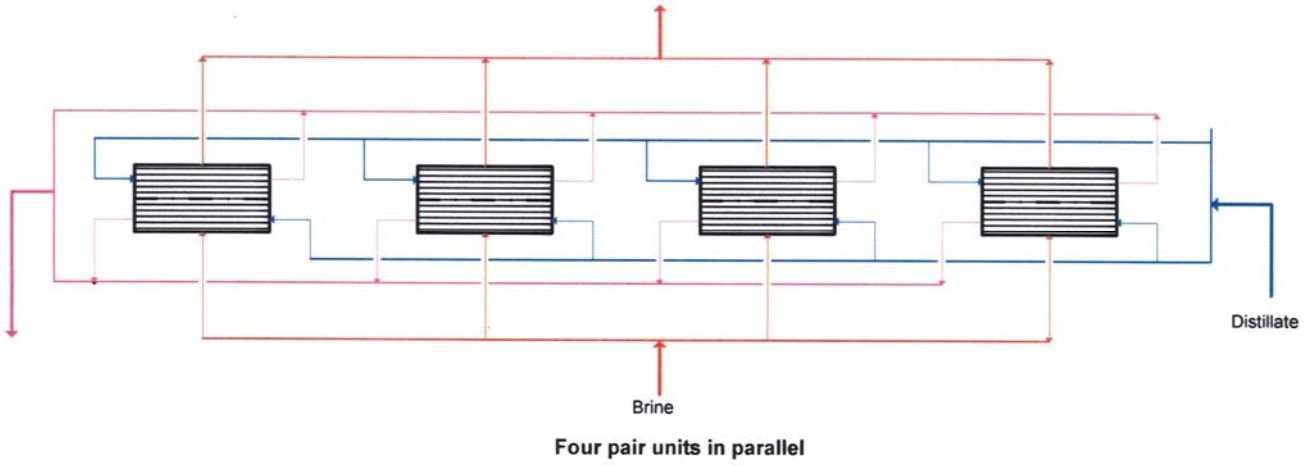

Figure 20c. Schematic of fluid flow directions for tests with four single-pair DCMD units in parallel.

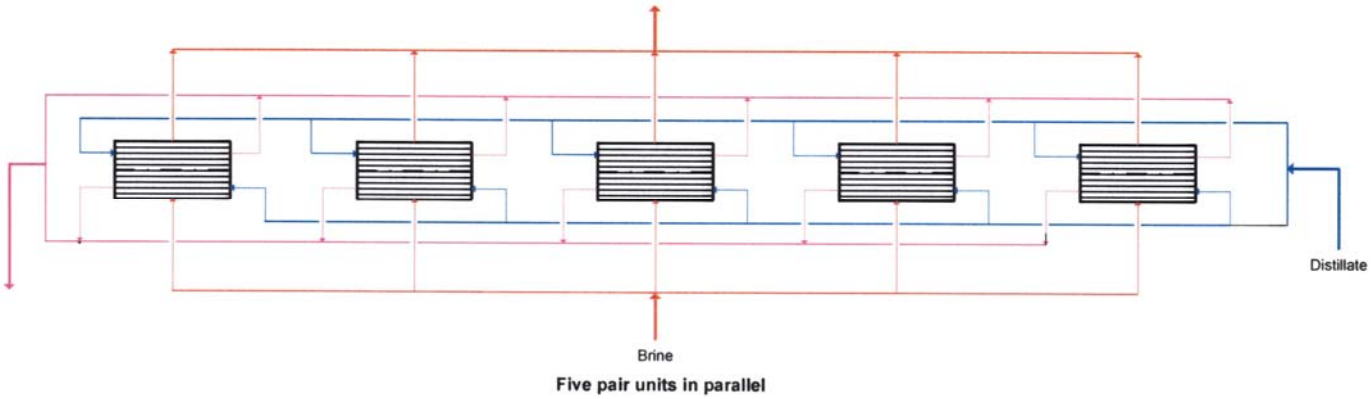

Figure 20d. Schematic of fluid flow directions for tests with five single-pair DCMD units in parallel.

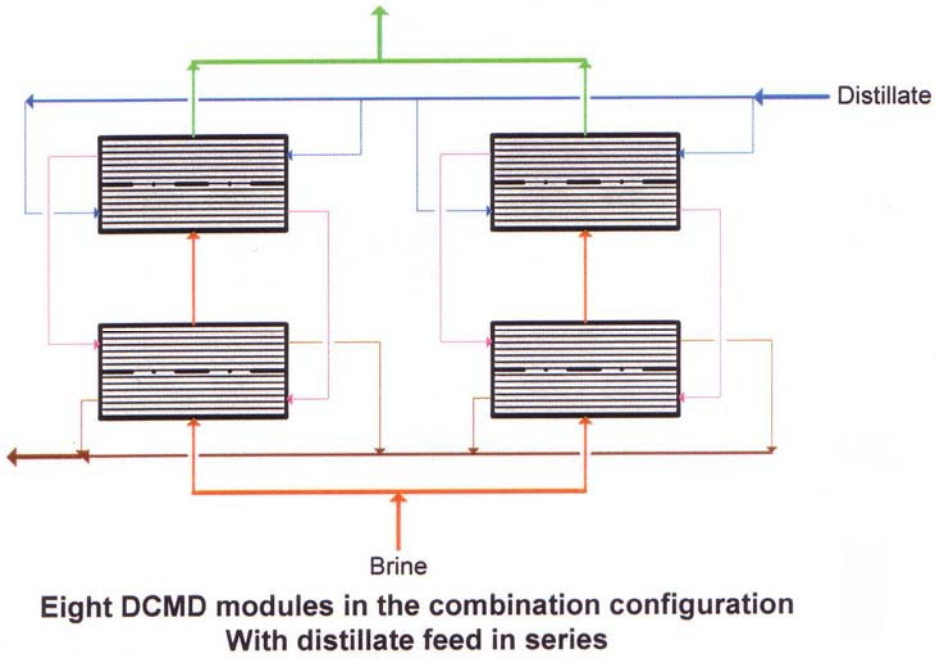

Figure 21. Schematic of fluid flow directions for tests with four-pair DCMD units in the combination configuration on the shell side (in parallel and series) and distillate feed in series on the fiber bore side.

Two types of feed brines were used in the experiments: (1) city water with or without added salt and (2) seawater trucked in from Long Island Sound, Connecticut.

We will first report results obtained **primarily with city water with or without added salt**. The city water analysis provided to us indicated that the total dissolved solids were 34 ppm; the conductivity of this water was 55 microsiemens (μS) at 21°C (69.8 °F). Later in the report, the results from tests with seawater from Long Island Sound will be provided along with an analysis of the seawater.

4.6.1 The City Water-Based DCMD Results

Considerable amount of data was gathered involving primarily variations in the flow rates of the hot brine or the distillate for any given configuration and feed solution. Further, a few studies were carried out with salt (NaCl) concentration varying between 3.5 to 10 weight percent (wt%). First, we will illustrate the data from just one DCMD module (S/N 1011) having a membrane surface area of 0.663 m^2 (figure 22). As the shell side velocity of 90-91°C brine was increased, a flux of 50 $kg/m^2/h$ (29.5 gfd) was achieved. In this figure, we also show a line which represents the results of our model simulations for this module using a k_m value of 0.0015 $kg/m^2/h/Pa$. This aspect will be considered later when we describe the model and results. An item of considerable interest here is that quite

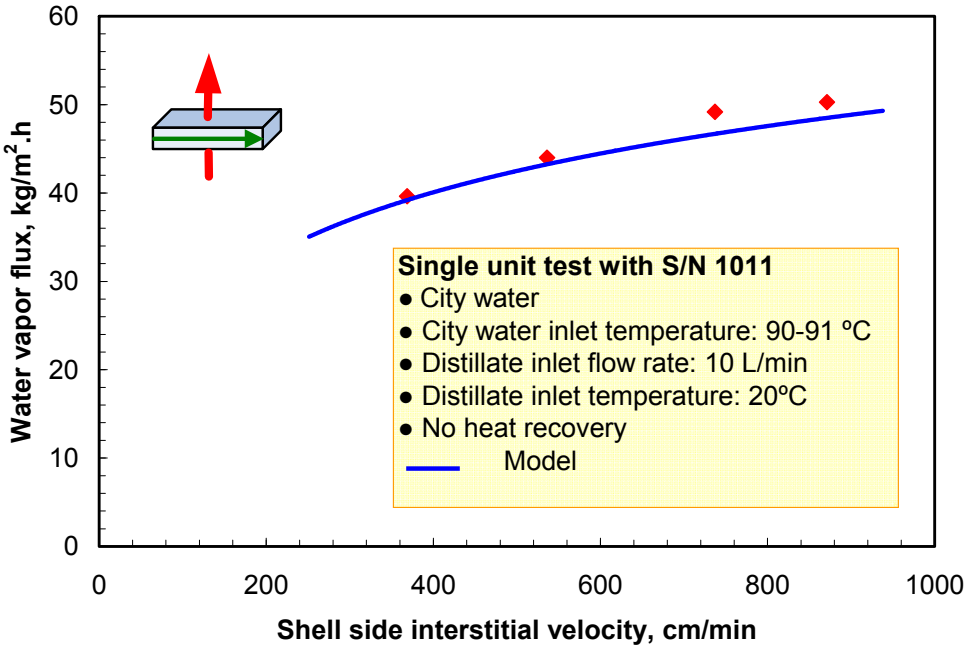

Figure 22. DCMD water vapor flux changed with variation of shell side interstitial velocity of city water for a single module (SN1011, distillate linear velocity, 4,852 cm/min).

a high flux level was being achieved at high brine velocities. Further, the model developed and described later in the report appears to describe the observed flux well.

Figure 23 illustrates the data obtained with a single-pair unit subjected to city water as the brine at an inlet temperature which was varied between 64 and 90 °C. The water vapor flux increased from a low value of 20 kg/m^2/h to almost 50 kg/m^2/h at the highest temperature. The distillate inlet temperature during this study was held at 22 °C. The results obtained when the distillate inlet temperature was increased from 22 °C to 44 °C are illustrated in figure 24. We notice that even if the distillate temperature is a high 44 °C, the water vapor flux is reduced from about 48 kg/m^2/h to about 38 kg/m^2/h. The fact that heat recovery is going on in a heat exchanger is not relevant since the water vapor flux is determined by the temperatures and flow conditions of the two streams on two sides of the membrane.

The tests in figures 23 and 24 were carried out at fixed flow rates of the hot brine and the cold distillate and city water as the source of the hot brine. The effects of a variation in the velocity of the hot brine and added salt concentration in the city water are shown in figure 25 for a single-pair unit. As the shell side brine velocity increases, the water vapor flux increases substantially (almost linearly). Further, increasing the salt concentration from very little (in city water) to 3.5%, 6.0% and 10.0% NaCl appears to decrease the water vapor flux to only a small

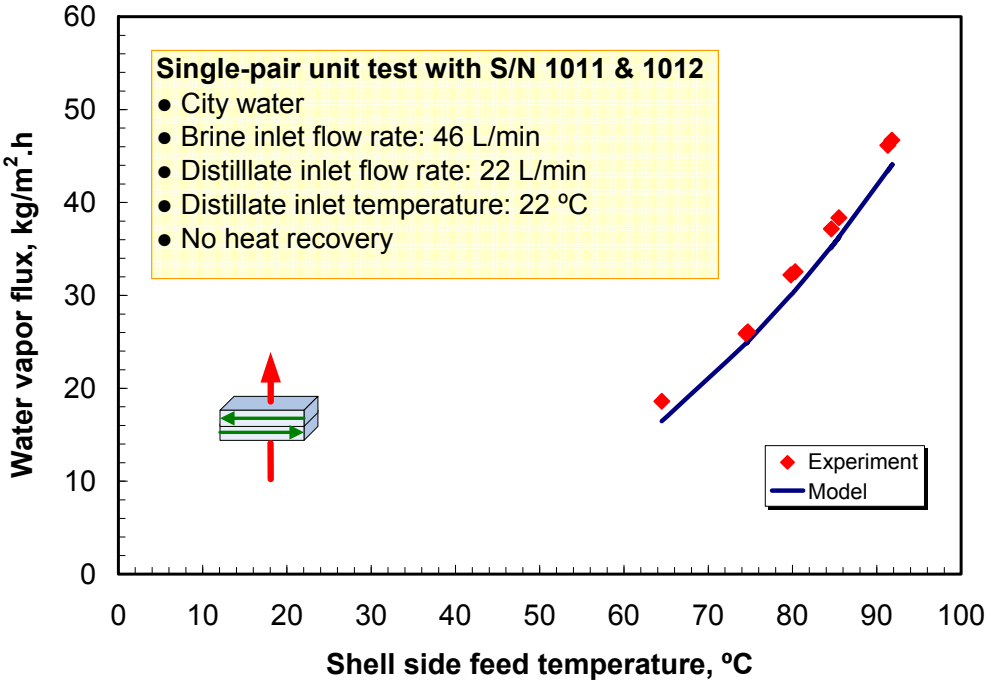

Figure 23. DCMD water vapor flux change with variation of shell side feed temperature for a single-pair unit (shell side interstitial velocity, 770 cm/min; distillate side linear velocity, 4,760–4,960 cm/min).

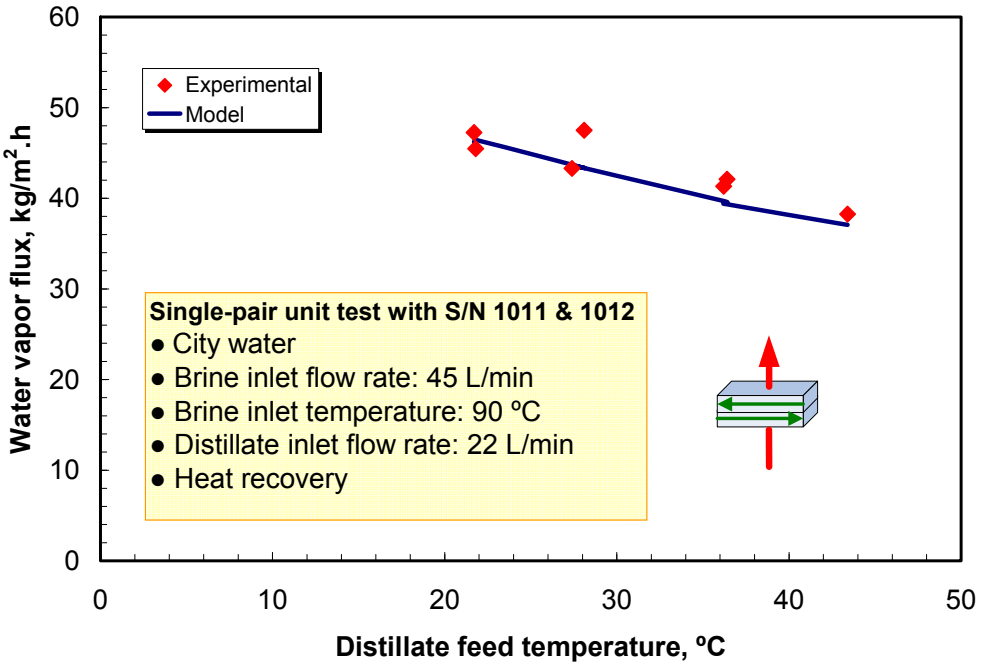

Figure 24. DCMD water vapor flux change with variation of distillate feed temperature for a single-pair unit (shell side interstitial velocity, 754–762 cm/min; shell side temperature, 90 ºC; distillate linear velocity, 4,850–5,250 cm/min).

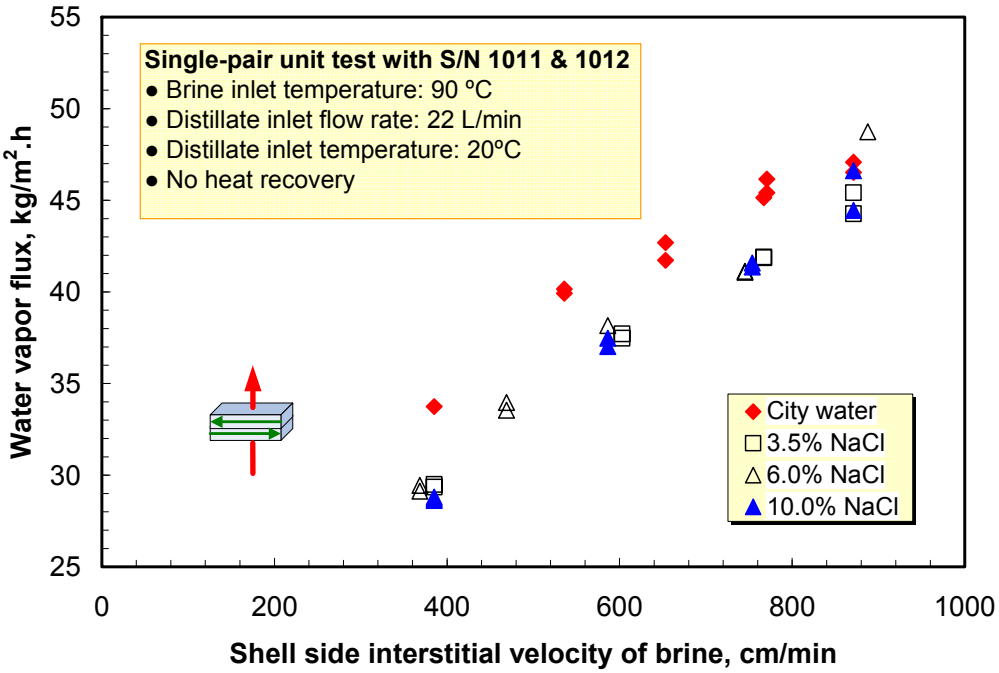

Figure 25. DCMD water vapor flux change with variation of shell side interstitial velocity as well as salt concentration for a single-pair unit (distillate linear velocity, 4,850 cm/min).

extent, around 10–15%. The effect of the distillate velocity is explored in figure 26 for a single-pair unit. As the distillate velocity was increased, the distillate temperature was reduced leading to an increased vapor pressure driving force and therefore an increased water vapor flux.

In these studies with the single-pair unit discussed so far, the distillate stream was introduced in the countercurrent pattern as identified in figure 25. Figure 27 appears to suggest that if there is an effect of the distillate introduction pattern between the first and the second module in the single-pair unit in terms of cocurrent versus countercurrent configuration, it is minor. We believe this because there is substantial mixing of different sections of the brine flow exiting the first module and entering the second one due to the empty space at the back of the fiber pack in the first module.

Following is a report of the results obtained with four-pair units whose test configuration is shown in figure 19a. There were a total of eight modules in this test whose results are given in figure 28 in terms of water vapor flux versus the shell side hot brine velocity. The data illustrate results for 10% NaCl in city water as well as 6% NaCl in city water; for the latter, three different inlet temperatures of the hot brine—70 °C, 80 °C, and 90 °C—were studied. At the highest brine velocity and brine inlet temperature at 90°C, these eight modules were producing

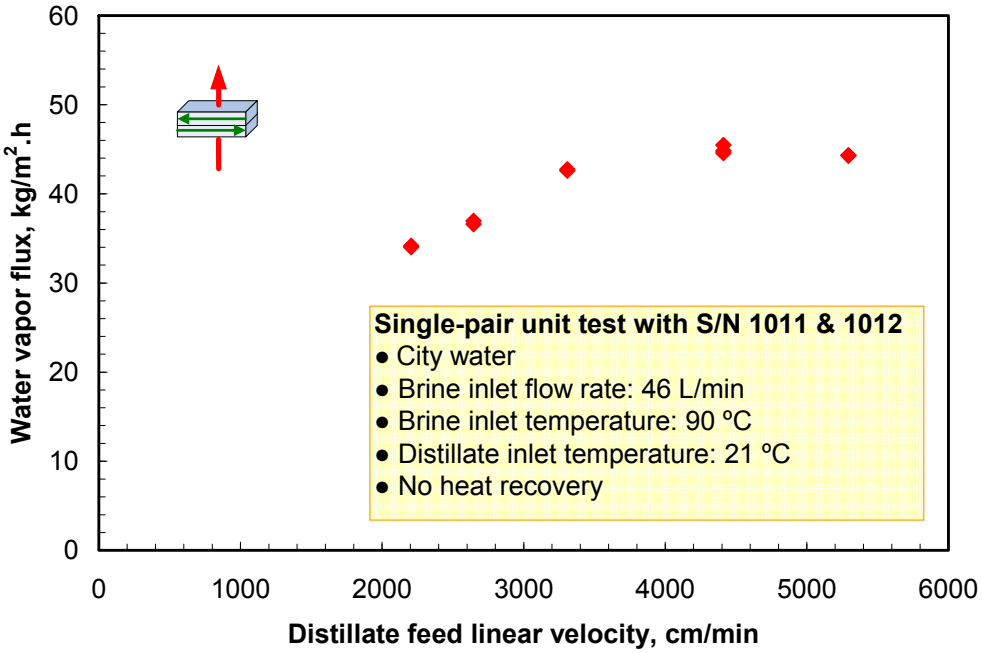

Figure 26. DCMD water vapor flux change with variation of distillate linear velocity for a single-pair unit (shell side interstitial velocity, 770 cm/min).

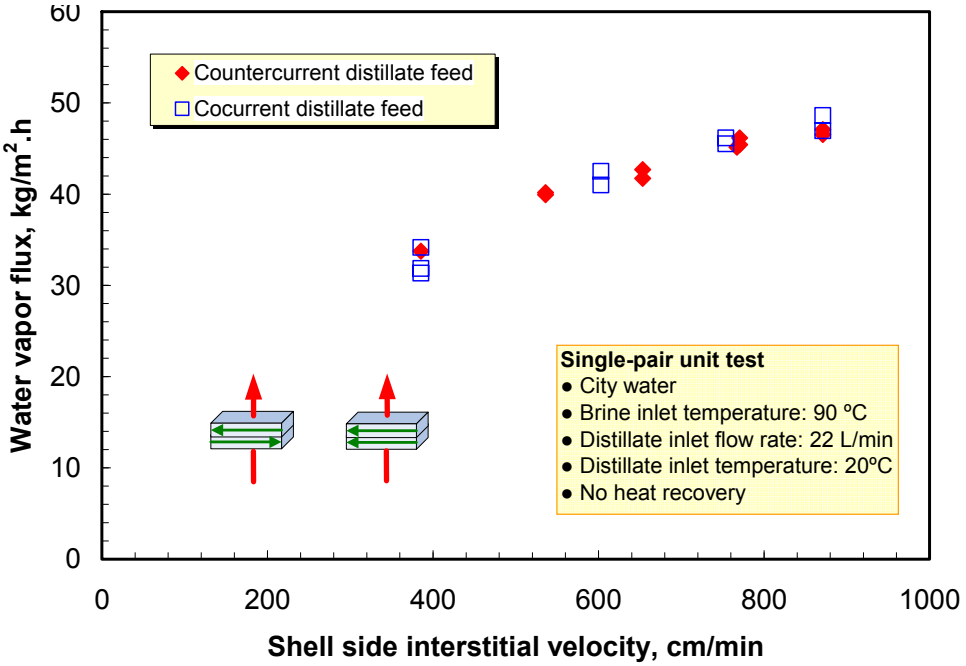

Figure 27. DCMD water vapor flux change with variation of shell side interstitial velocity for countercurrent and cocurrent distillate feed for a single-pair unit (distillate linear velocity, 4,850 cm/min).

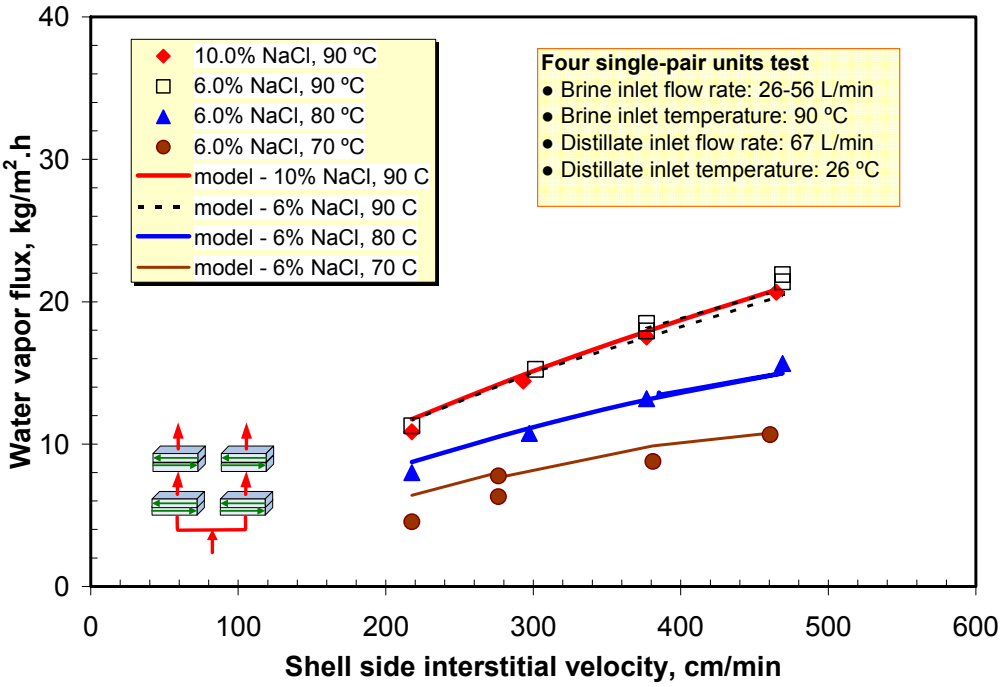

Figure 28. DCMD water vapor flux change with variation of shell side interstitial velocity for four single-pair DCMD units in the combination configuration (in parallel and series) on the shell side (distillate linear velocity, 3,700 cm/min).

around 0.53 gpm. Note that each module was being fed the cold distillate at the same temperature. Addition of two more modules would have increased the overall production rate to around 0.65 gpm. However, reaching 1 gpm was difficult because of the following reasons.

1. We designed the plant based on an estimated 40-kg/m^2/h (23.6-gfd) average flux. At the time of our design, we had limited data available for lower brine temperatures. Neither did we have any model equation available to predict the fluxes at lower brine temperatures down the cascade as the hot brine was cooled from one module to the next module.

2. When the full proposal was submitted by us to Reclamation, our expectation was that the modules would be supplied by AMT Inc.; they had submitted a proposal for $85,000 to Reclamation. Both of these proposals were based on two separate preproposals to Reclamation. However, it was our misunderstanding since Reclamation could fund only one pilot plant project. Consequently, in the revised budget submitted prior to award, NJIT had to provide for the modules at the level of $30,000 causing a severe constraint in the availability of funds for extra modules.

3. By having two legs of hot brine flow in the loop, the brine flow velocity in any leg was reduced. In figure 28, the maximum brine velocity was around 470 cm/min (15.4 ft/min) on the shell side. In figure 26, we observe that the highest hot brine velocity could be as much as 900 cm/min. Therefore, if we could increase the total brine flow rate to double the value in figure 28, we could have obtained potentially as much as 30% higher flux; such an increase would have brought us quite close to the design goal of 1 gpm. Unfortunately, the load available to us at UTRC from the chiller side was limited. Therefore, we were unable to increase the brine flow rate very much in our pilot plant.

Figure 29 illustrates the four-pair unit configuration of figure 21, where the distillate feed streams are in series (i.e., cold distillate fed into the second bank of two modules gets heated up a bit and then sent to the first bank of two modules). As a result, the driving force is reduced in the first bank of two modules, and we end up with overall flux values somewhat lower than that in figure 28 where the distillate feed streams were in parallel.

Figure 30 illustrates the basic phenomena of salt concentration change in the distillate tank in the overall pilot plant configuration employed. The distillate tank had city water to start with. As distilled water from the modules was introduced into the distillate tank—if, in fact, we were producing distilled water from the modules—the conductivity of the water in the distilled water tank would have been reduced. That was exactly what we observed in figure 30 with the water conductivity slowly decreasing with time. By using equations (4a), (4b), and (4c), the salt concentration in the distilled water product was estimated to be less than 1 ppm if the distillate tank in figure 31 is assumed to be like a continuous stirred tank reactor (CSTR). For this figure, D_n represents the dilution number which is the ratio of the distillate production rate divided by the volume of the distilled water in the tank.

Mass Balance: $$\frac{dC_t}{dt} = \frac{P}{V}(C_t - C_p) = D_n(C_t - C_p) \quad (4a)$$

Initial condition: at t=0, $C_t = C_0$ (4b)

Integrating equation (4a), $$C_p = \frac{\exp(D_n t)C_0 - C_t}{\exp(D_n t) - 1} \quad (4c)$$

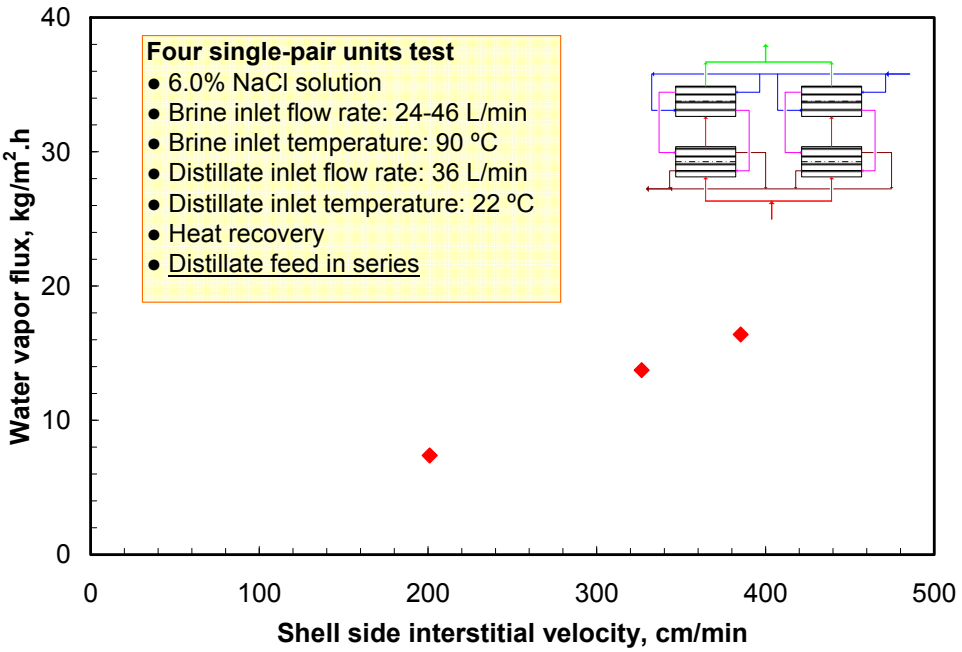

Figure 29. DCMD water vapor flux change with variation of shell side interstitial velocity for four single-pair DCMD units in the combination configuration (in parallel and series) on the shell side and distillate feed in series on the fiber bore side (distillate linear velocity, 4,040 cm/min).

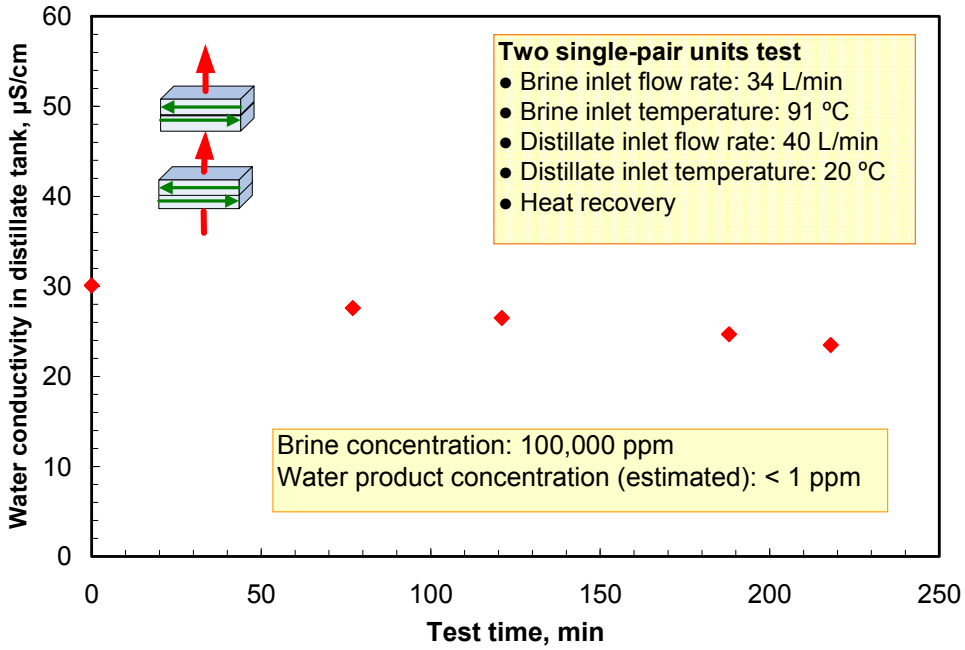

Figure 30. DCMD water vapor flux obtained at steady state 10% NaCl solution desalination test for two single-pair DCMD units in parallel on the shell side (distillate linear velocity, 4,410 cm/min).

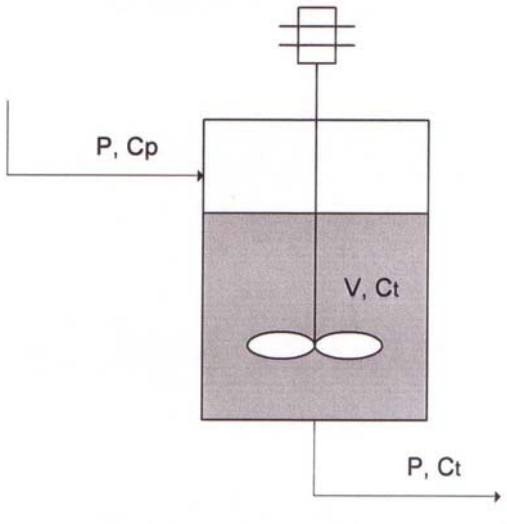

Figure 31. Schematic of CSTR model.

A few other pieces of information are useful.

1. When we conducted the four-pair units test (as in figures 28 and 29), the hot brine inlet temperature of 90 °C (194 °F) was reduced to around 54 °C at the outlet. One may wish to reduce it still further by adding another module downstream in each leg. However, at least one module was kept in reserve to compare its performance near the end of the tests with others being constantly tested.

2. The exposed fiber length in each module was 26 cm (0.85 ft). This length of the fiber was totally unsupported. From the translucent picture frame windows, we could clearly see that the fibers underwent significant oscillation. Although such an oscillation is highly beneficial toward achieving a higher heat transfer coefficient on the brine side, it would be desirable to have intermediate supports to reduce the fiber stress at the two tube-sheet locations at the two ends.

3. There was substantial dead volume in each module at the end of the fiber bed. Its elimination, along with countercurrent distillate introduction between the two modules mounted back-to-back in one unit pair, introduces higher volumetric efficiency and potentially higher flux.

So far, we have provided a significant amount of performance data for a number of module configurations: single module, single-pair unit, four-pair units, three-pair units, two-pair units. **Most of the data, however, were for a single-pair unit which consisted of two DCMD modules in series back-to-back without any cover plate and face plate in between and providing a surface area (in general) of 2 x 6,634 cm^2 = 1.32 m^2**. We will now provide the results from a variety of configurations employing multiple single-pair units.

Figure 32 shows the performance of three-pair units in parallel as a function of brine temperature yielding at a brine temperature of 92 °C (196.7 °F), a flux of as much as 33 kg/m^2/h. Let us put this result in perspective. The total water production rate from this configuration was:

$$33\,\frac{\text{kg}}{\text{m}^2-\text{h}}\ \text{x}\ 1.32\quad\frac{\text{m}^2}{\text{unit pair}}\ \text{x}\ 3\ \text{unit pairs} \cong 130\,\frac{\text{kg}}{\text{h}}$$

If we had five unit pairs with this flux level, we would have produced $130\,\text{x}\,\frac{5}{3} = 217.8\,\frac{\text{kg}}{\text{h}} = 0.95\,\text{gpm}$ of distilled water. If instead of the parallel configuration, these modules were in series (figure 33) at a lower distillate velocity, we also would have achieved a flux of around 30 kg/m^2/h (17.67 gfd). Note, however, that the shell side interstitial velocity in figure 33 was more than twice that in figure 32; the fractional recovery was higher in figure 33, but the flux was somewhat lower.

Figure 34 illustrates a configuration where four-pair units were in parallel. Since the total flow rate available in the test facility was not sufficient (shell side interstitial velocity of 268 cm/min), the flux obtained was low around 15–16 kg/m^2/h. The performance obviously was significantly less than those from the configurations of figures 32 and 33. On the other hand, the configuration of figure 35 with four-pair units in two parallel flow lines using 6% NaCl solution yielded a flux of 20 kg/m^2/h. The shell side interstitial velocity was around 460 cm/min, considerably lower than those in figures 32 and 33. Obviously, the performance here was considerably better than that in figure 34 since the shell side interstitial velocity was almost twice. This figure (figure 35) is also useful in that it shows that, even with a distillate feed temperature 55 °C, we can get a decent flux level of 16 kg/m^2/h.

Figure 36 illustrates a configuration of five-pair units in parallel with a rather low shell side interstitial velocity of 218 cm/min yielding a flux level of 15 kg/m^2/h (8.8 gfd) for a brine feed at 90 °C (194 °F). Figure 37 shows10 modules in two parallel flow loops; when the shell side interstitial velocity was higher, around 470 cm/min, an overall flux level of approximately 21 kg/m^2/h was achieved. The overall production rate from these modules was 140 kilograms per hour (kg/h) (i.e., approximately 0.62 gpm). We needed a higher brine flow rate and a higher brine interstitial velocity to achieve the goal of 1-gpm distillate production capacity. Unfortunately, the design capabilities of cooling side (chiller) at the UTRC facility inhibited higher pumping rates needed. As we have seen earlier (in figure 32) and here (in figure 37), the highest value of the total distilled water production rate achieved was 140 kg/h (i.e., 0.62 gpm which is about 893 gallons per day [gpd]).

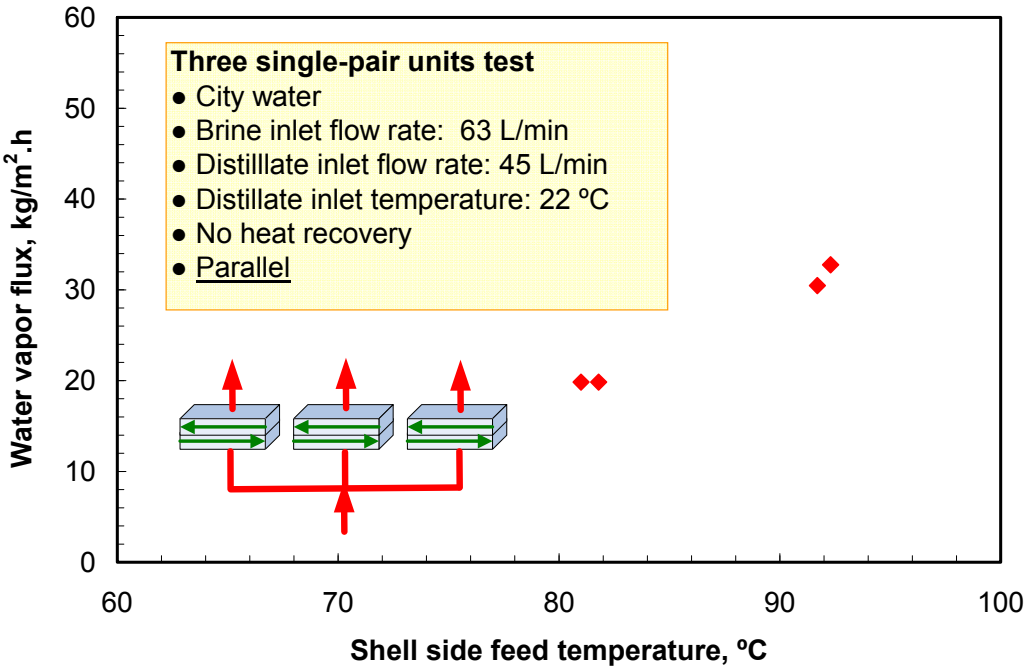

Figure 32. DCMD water vapor flux change with variation of shell side feed temperature of city water for three single-pair units in parallel (shell side interstitial velocity, 351 cm/min; distillate side linear velocity, 3,230–3,310 cm/min).

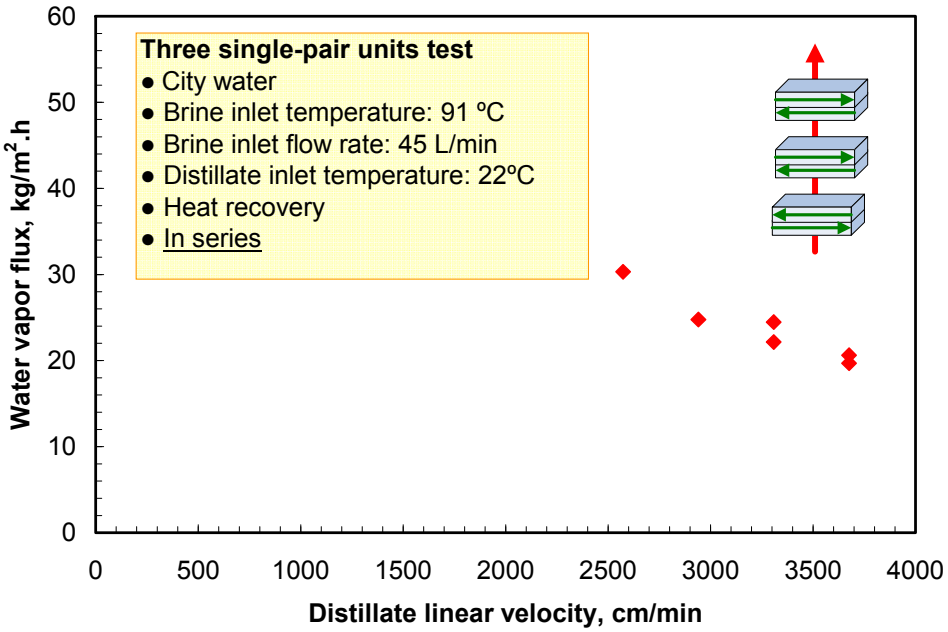

Figure 33. DCMD water vapor flux change with variation of distillate linear velocity of city water for three single-pair units in series (shell side interstitial velocity, 754 cm/min).

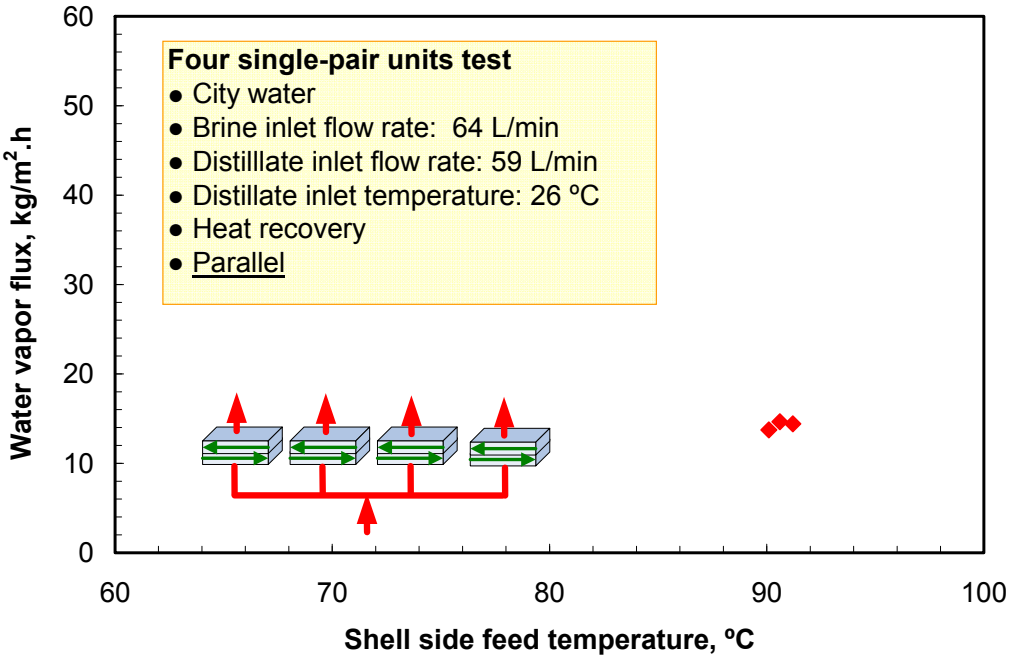

Figure 34. DCMD water vapor flux change with variation of shell side feed temperature of city water for four single-pair units in parallel (shell side interstitial velocity, 268 cm/min; distillate side linear velocity, 3,250 cm/min).

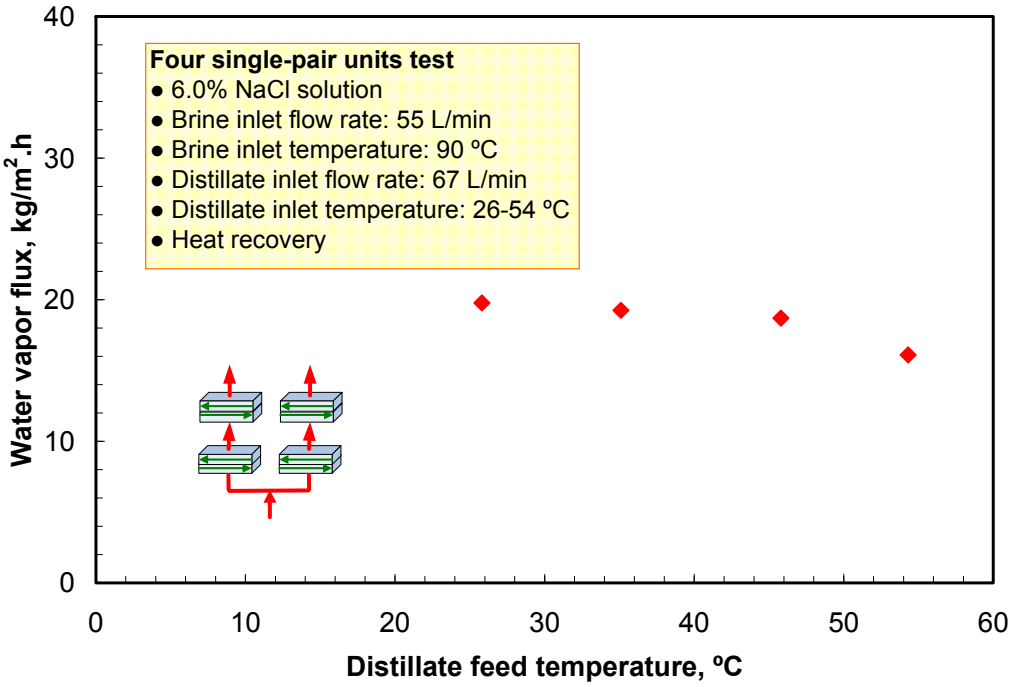

Figure 35. DCMD water vapor flux change with variation of distillate feed temperature for four single-pair units in two parallel flow loops of 6% NaCl solution (shell side interstitial velocity, 460 cm/min; distillate linear velocity, 3,760–3,930 cm/min).

4.6.2 DCMD Results with Seawater

Seawater was brought to UTRC in a 5,600-gallon tanker truck from Long Island Sound, Connecticut. Figure 38 shows a picture of the tanker truck being loaded with seawater. Detailed data on the seawater composition are provided in table 5.

Figure 38. Tanker truck being filled with seawater at Long Island Sound, Connecticut.

Table 5. Major Elements of Seawater

Ions	Concentration (ppm)	
	Fresh Seawater Sample	Double Concentrated Seawater Sample
Chloride (Cl^-)	14,300	29,250
Sulfate (SO_4^{2-})	1,790	3,890
Sodium (Na^+)	7,820	17,850
Calcium (Ca^{2+})	3,220	6,960
Magnesium (Mg^{2+})	920	1,910
Total TDS	28,050	59,860

4.6.2.1 Seawater Analysis

The ion concentrations of sodium (Na^+), calcium (Ca^{2+}), and magnesium (Mg^{2+}) were analyzed using a Spectro ICPMS instrument (UTRC, East Hartford, Connecticut). The samples were diluted 50 times in a 100-mL glass flask. Two mL of each sample was pipetted into the glass flask. Five mL of nitric acid (HNO_3) was added to the flask, and then the flask was filled to the 100-mL line with deionized water (DI H_2O). The instrument was calibrated using a blank solution and three standard solutions, each containing about 200 ppm of a single compound (Ca, Na, or Mg). The blank solution was prepared by adding 5 mL of HNO_3 into a 100-mL glass flask and filling to the 100-mL line with DI H_2O. The calcium and sodium calibration solutions were prepared volumetrically by

pipetting 2 mL of the standard solution into a 100-mL flask. Added to the flask were 5 mL of HNO_3, and then the flask was filled with DI H_2O to the 100-mL line. The National Institute of Standards and Technology (NIST) traceable standards' concentrations were 10 milligrams per milliliter (mg/mL). The magnesium calibration solution was prepared gravimetrically using a 9.9-mg/mL NIST traceable solution. Added to a plastic container were 1.9 grams (g) of the solution. Added to the container were 5 mL of HNO_3, and then DI H_2O was added to reach a weight of 100.0 g. The solution prepared had a concentration of 188 ppm. Each measurement (blank, calibration standards, and samples) was repeated three times, and each set of results was averaged. The anion concentrations of chloride (Cl^-) and sulfate (SO_4^{2-}) were analyzed using an ion chromatography system of the Otto H. York Center for Environmental Science and Engineering (NJIT, Newark, New Jersey).

The running conditions were as follows:

IC instrument: Dionex ICS 1500 Ion Chromatography System
Column: Dionex IonPac AS18, Analytical (250 x 4 mm)
Mobile phase: 32.0 millimolars (mM) NaOH
Flow Rate: 1.5 mL/min
Temperature: 35 ^oC (95 °F)
Detection: Suppressed conductivity
Injection: 50 microliters (µL)
Data: EzChrom Chromatography Data System

The seawater samples were diluted before injection by mixing 50 µL of seawater sample with 50 mL of Milli-Q water (dilution factor = 1,001).

4.6.2.2 Performance with Seawater

Figure 39 illustrates data on water vapor flux for seawater with three single-pair units (per figure 20b) in parallel. Note that the brine velocity through each single-pair unit was one-third of the maximum value in figure 25. Therefore, the average flux of 25 kg/m^2/h (14.7 gfd) is understandable. This figure merely shows that there was no change during the 300 minutes that the run was conducted for the first time.

Figures 40 and 41 provide further data obtained with the seawater trucked in from Long Island Sound as brine feed. Figure 40 illustrates the performance of four-pair units in two parallel flow loops at a shell side interstitial velocity of 460 cm/min (15.1 ft/min). The flux data have been illustrated over a period of 220 minutes. It was stable. The overall production rate was approximately 112 kg/h (247 pounds mass per hour [lbm/hr]). The flux level was around 21–22 kg/m^2/h and was very close to the data obtained at a distillate temperature

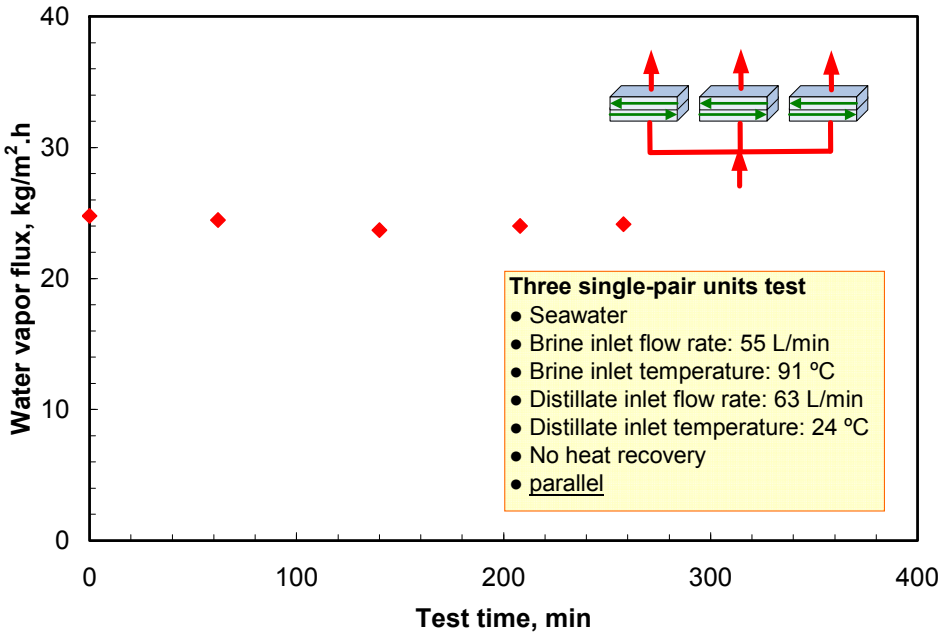

Figure 39. DCMD water vapor flux obtained at steady state for seawater desalination test using three single-pair DCMD units in parallel on the shell side (distillate linear velocity, 4,040 cm/min).

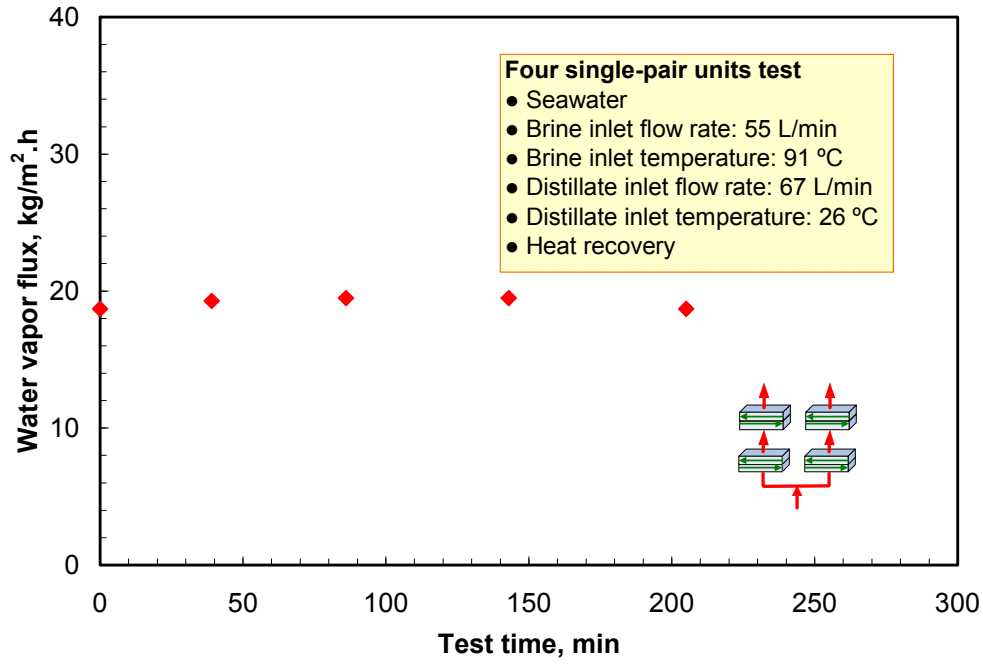

Figure 40. DCMD water vapor flux obtained at steady state seawater desalination test for four single-pair DCMD units in two parallel flow loops on the shell side (shell side interstitial velocity 460 cm/min; distillate linear velocity, 3,690 cm/min).

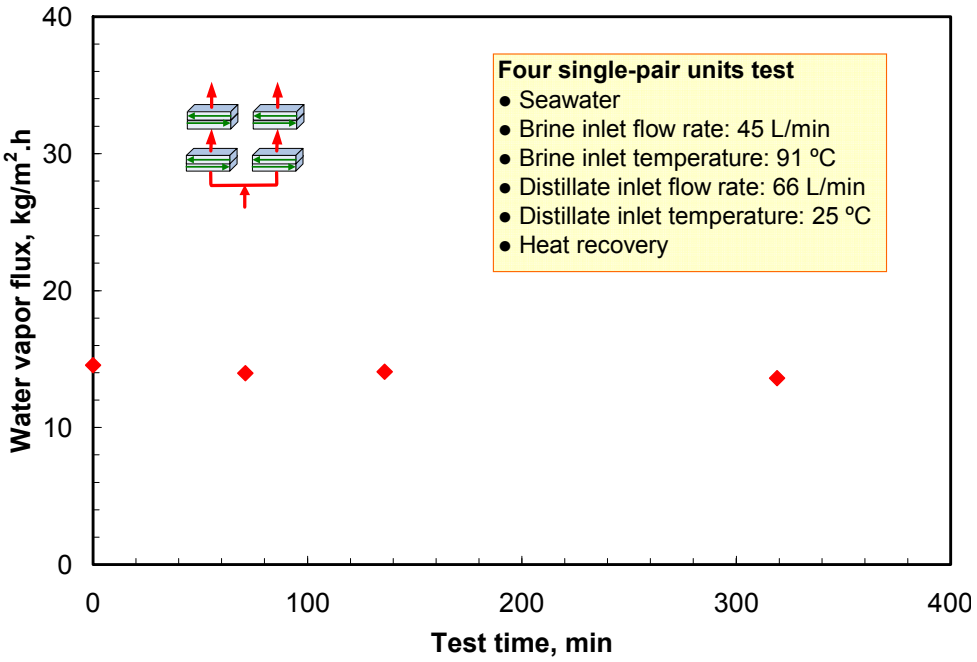

Figure 41. DCMD water vapor flux obtained at steady state seawater desalination test for four single-pair DCMD units in two parallel flow loops on the shell side (shell side interstitial velocity, 377 cm/min; distillate linear velocity, 3,640 cm/min).

of 26 °C with 6% synthetic NaCl solution as shown earlier in figure 28. Figure 41 illustrates the performance of an identical system for seawater when the shell side interstitial velocity was reduced to 377 cm/min. One can see that the water vapor flux is immediately reduced to the level of 16 kg/m^2/h. Thus, hot brine velocity is very important in achieving a high flux level other conditions remaining unchanged.

Additional runs were conducted with seawater including those where the seawater was concentrated several times. The composition of the trucked-in seawater (from Long Island Sound) employed, as far as the cations are concerned (table 5), (according to UTRC Analytical Group) are given below:

Na^+	Ca^{++}	Mg^{++}
7,820 ppm	3,220 ppm	920 ppm

The calcium levels were found to be unusually high in this seawater. This seawater was obtained downstream of Haddam Neck Nuclear powerplant. Potentially, the descaling from the powerplant led to the spike in Ca^{++} concentration. The higher calcium levels, however, did provide a much more severe test on the scaling problem. This is shown in figure 42 where water vapor flux has been plotted against the percent of water recovered. In this experiment, the brine was continuously concentrated. After it had reached around 18% salt,

we observed suddenly a very large amount of scaling particulate matter deposit throughout the system. This is because the calcium concentration had probably reached around 18,000 ppm. The operation was shut down. All of the modules were cleaned with just a water wash. The modules were put back on, and the performance was observed to be essentially identical (figure 43).

This experimental run (figure 42) lasted for 19.5 hours over 4 days. It demonstrated the robustness of the present membrane system. It suggests that at normal seawater scaling salt levels (Ca^{2+} 300–400 ppm), the present DCMD system could potentially concentrate seawater by as much as six times or higher.

4.6.3 Modeling the Performances of Individual DCMD Modules and the Pilot Plant Module Assembly[1]

Figure 5b shows the photos of the DCMD modules of Phase II and Phase III research without the cover plates at two scales. Details of these modules' dimensions from Phase II and Phase III studies (Sirkar and Li, 2003, 2005) are provided in table 6. Hot brine flows perpendicular to the fibers in the picture frame as the cold distillate is introduced to the bore of the fibers at one end and exits as the heated distillate at the other end of the fibers. An approximate schematic of the staggered fiber arrangement vis-à-vis the hot brine flow is shown in figure 44a for the larger module S/N 1004 (having 16 consecutive layers of fibers compared with 10 layers in the much smaller module MXFR #3 (Li and Sirkar, 2004). If we consider now any fiber layer (e.g., *j*th layer, j = 1, 2, …, m), on the distillate side, the distillate volume flow rate coming in is $V_{p0,\,j}$ at a temperature $T_{p0,\,j}$; the corresponding values at the exit of the fiber length L are $V_{p1,\,j}$ and $T_{p1,\,}$j (figure 44b). However, we have a more complex situation on the brine side. The local hot brine velocity and temperature depend on the location along the fiber length since water evaporation rate depends on the location.

Therefore, we will now define the variables used in our model to describe the local brine flow conditions (velocity and temperature).

The length coordinate along the distillate flow direction is x. Define now $V'_{f0,\,j}(x)$, $T_{f0,\,j}(x)$ and $V'_{f1,\,j}(x)$, $T_{f1,\,j}(x)$ as the local brine inlet volumetric flow rate per unit fiber length and temperature, and local brine outlet volumetric flow rate per unit fiber length and temperature respectively for the fibers in the *j*th layer. Over a small length, Δx of the fibers in the *j*th layer, the local values of $V_{p1,\,j}$, $T_{p1,\,j}$, namely, $V_{p1,\,j}(x)$ and $T_{p1,\,j}(x)$ change to $V_{p1,\,j}(x+\Delta x)$ and $T_{p1,\,j}(x+\Delta x)$ (figure 44c); correspondingly, $V'_{f0,\,j}(x)$ and $T_{f0,\,j}(x)$ are changed beyond the *j*th layer to $V'_{f1,}$

[1] Most of the material on this subject appeared in a paper, entitled, "Direct Contact Membrane Distillation-based Desalination: Novel Membranes, Devices, Larger-scale Studies and a Model," in *I&EC Research*, 46, 2307-2323, 2007.

Table 6. Details of Larger Hollow Fibers and Membrane Modules for Phase II and Phase III Research

Particulars	MXFR #3	S/N 1004	S/N 1005
Support membrane type	PP 150/330		
Fiber I.D. (μm)	330		
Wall thickness (μm)	150		
Maximum pore size (μm)	0.65		
Membrane porosity	approximately 0.6–0.8		
Coating [1]	Silicone fluoropolymer [2]		
Arrangement of fibers	Staggered		
Number of fibers (number of layers x fibers/layer)	10 x 18 = 180	16 x 68 = 1,088	
Effective membrane surface area (cm^2) [3]	119	2,864	
Effective cross-sectional area for shell side liquid flow (cm^2) [4]	8.74	108.9	
Rectangular module frame (internal dimensions)	L: 6.4 cm; W: 2.5 cm; H: 1.8 cm	L: 25.4 cm; W: 8.6 cm; H: 4.45 cm	
Packing fraction of fibers	0.12	0.22	
Shell side flow mode	10 x 18 = 180	16 x 68 = 1,088	
Support membrane type	Crossflow		

[1] All coatings were applied on the outside diameter of the support fibers by AMT Inc., Minnetonka, Minnesota, using their proprietary plasmapolymerization technology.

[2] Phase II research (Sirkar and Li, 2003).

[3] Based on fiber internal diameter.

[4] Based on open area for flow = frame cross-sectional area—fiber projected area (number of fibers in one layer x fiber O.D. x length of fiber cm^2).

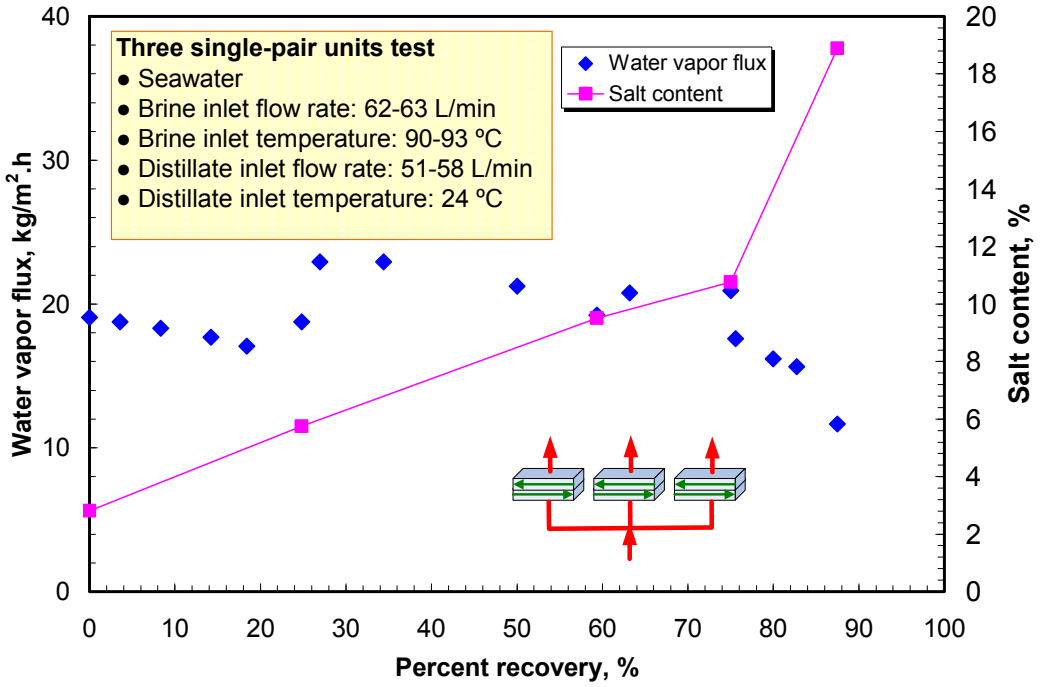

Figure 42. DCMD water vapor flux change with percent recovery of water from seawater for three single-pair units.

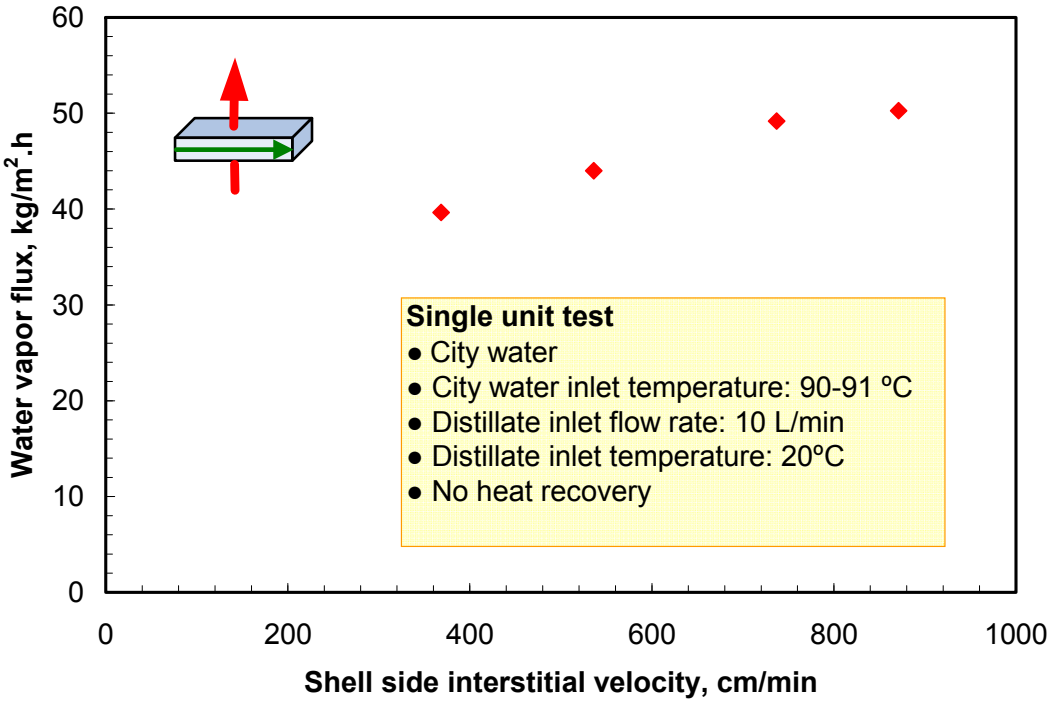

Figure 43. DCMD performance of a single module after cleaning.

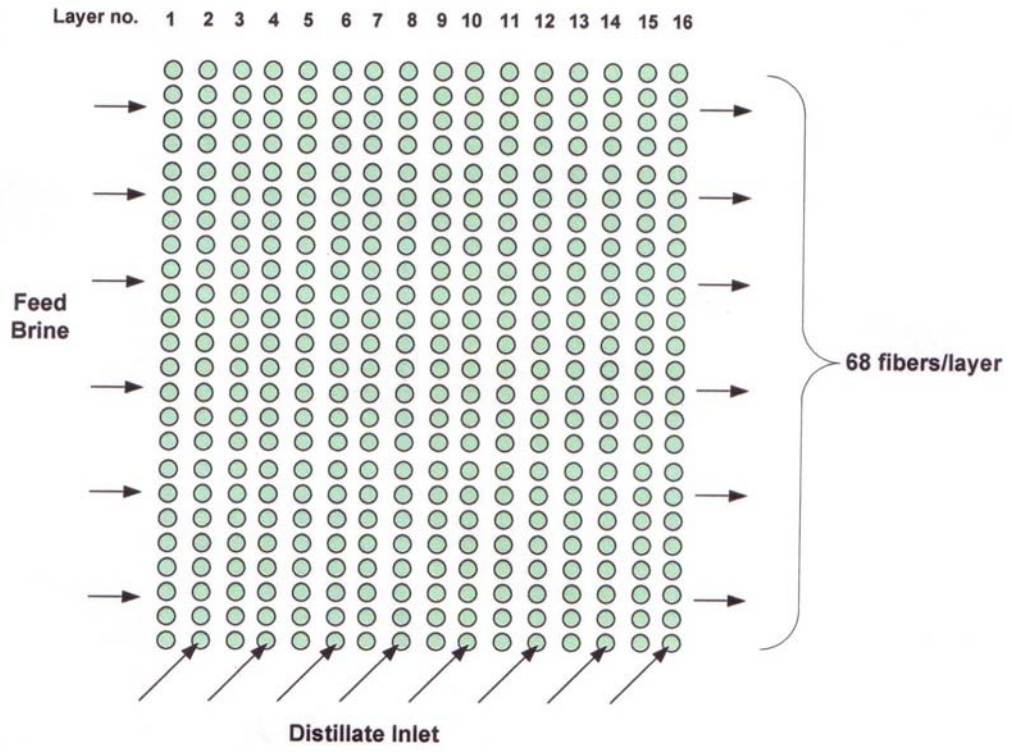

Figure 44a. Arrangement of fibers in a DCMD module.

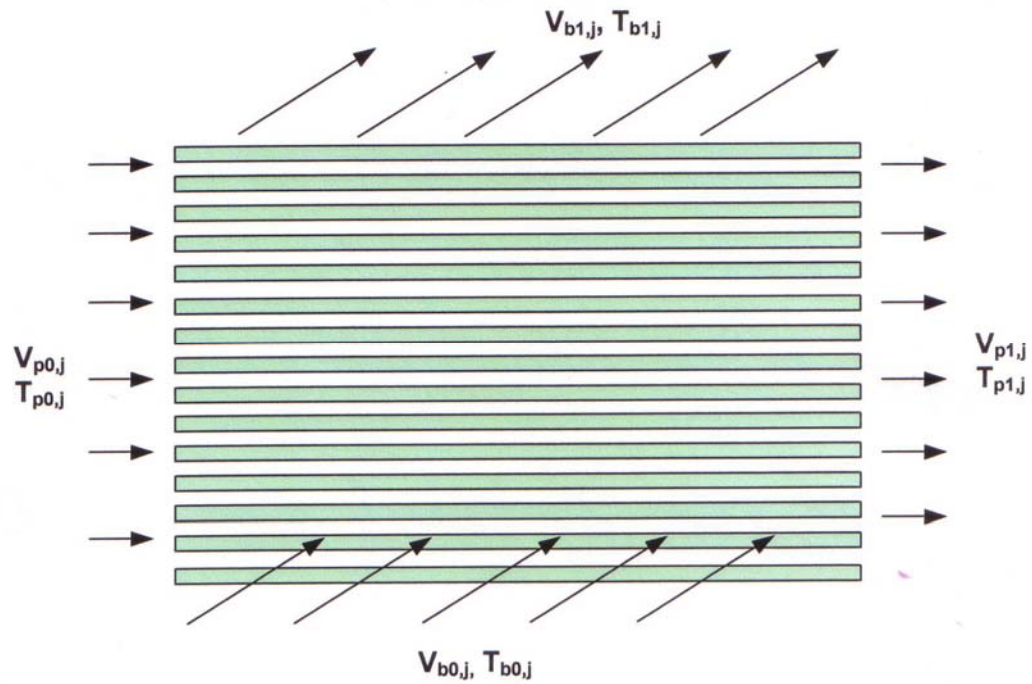

Figure 44b. jth fiber layer in the DCMD module.

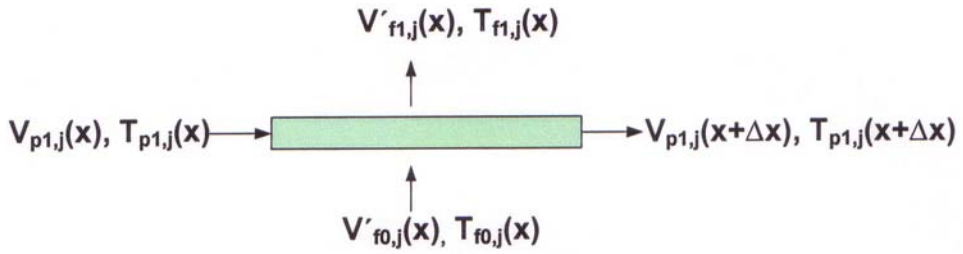

Figure 44c. Mass and energy balance for the length of Δx in the distillate flow direction.

$_j$(x), $T_{f1,j}$(x). The inlet and outlet brine volumetric flow rates for the *j*th layer $V_{b0,j}$, $V_{b1,j}$, can be calculated by integrating $V'_{f0,j}$(x) and $V'_{f1,j}$(x) over the fiber length from x=0 to x=L, respectively (figure 44b). The inlet and outlet brine temperatures $T_{b0,j}$, $T_{b1,j}$ are the cup-mixing values of $T_{f0,j}$ (x) and $T_{f1,j}$(x) over the fiber length based on energy balance. For the first fiber layer (j = 1), $V_{b0,j}$ and $T_{b0,j}$ are known from the brine feed conditions. Correspondingly, for j =1, $V'_{f0,j}$(x) (=$V_{b0,j}$/L), and $T_{f0,j}$ (x) (=$T_{b0,j}$) are constant from x=0 to x=L. At the distillate entrance location (x = 0), the water vapor flux is highest and, therefore, the temperature drop in the hot brine, e.g., ($T_{f0,j}$(x) – $T_{f1,j}$(x)), will be highest; so will be the hot brine velocity reduction (which, however, is of a very small magnitude). At any location x, the bulk brine temperature T_f drops to T_{fm} at the membrane surface (figure 1b); the corresponding quantities for numerical calculations are $T_{f0,j}$ (x) and $T_{fm,j}$ (x). On the distillate side, the temperature T_{pm} at the membrane surface drops to the bulk distillate temperature T_p with corresponding notational changes to $T_{pm,j}$ (x) and $T_{p1,j}$(x).

In the next layer of fibers (*(j+1)*th layer), we made a basic assumption, namely, **that there was no lateral mixing in the x-direction of the hot brine between two consecutive fiber layers.**[2] Therefore, the hot brine velocity and temperature being imposed on the *(j+1)*th layer of fibers depend on the fiber length coordinate x and are obtained as output from the calculations for the previous layer of fibers (*j*th layer). This process is continued till the last layer of fibers in a given module. Consequently, our computational scheme proceeds from fiber layer to layer for a given hot brine input at the first fiber layer and a constant flow rate and temperature input into all fibers in all layers on the distillate side. Ideally, there may be minor variations in distillate side flow rate with the layer number, since as the brine temperature decreases with increasing layer number, the temperature decreases in brine leads to a lower temperature rise in the distillate; therefore, an increasing viscosity and consequently a lower flow rate since the pressures at the fiber inlet and outlet on the distillate side are essentially same regardless of the layer number. For given distillate feed conditions (i.e., inlet volumetric flow rate

[2] In the next section, we experimentally verified this assumption.

V_{d0} and temperature T_{d0}), for each fiber layer $V_{p0,j}$ (=V_{d0}/m, where m is the number of fiber layers) and $T_{p0,j}$ (=T_{d0}) are constant. Correspondingly, the distillate outlet volumetric flow rate V_{d1} is the sum of $V_{p1,j}$ for all fiber layers, and the distillate outlet temperature T_{d1} is the flow weighted average of $T_{p1,j}$ for all fiber layers based on energy balance.

Following are the local equations for heat transfer in brine for the *j*th fiber layer containing n fibers of internal diameter d_i and outer diameter d_o over a length dx of the fiber at location x. The expression below is the heat transfer rate per unit length.

4.6.3.1 Shell Side Hot Brine: Heat Transfer

$$\left.\frac{dQ(x)}{dx}\right|_j = h_f A_{rf} \alpha (T_{f0,j}(x) - T_{fm,j}(x)) \tag{5}$$

where $$A_{rf} = (\frac{d_o}{d_i}),\ \alpha = n\pi d_i \tag{6}$$

In our VMD paper (Li and Sirkar, 2005), we observed that Zukauskas' equation (Žukauskas, 1987) (7a, 7b)

$$Nu_f = \frac{h_f d_o}{k_o} = 1.04 \mathrm{Re}_o^{0.4} \mathrm{Pr}_o^{0.36} (\frac{\mathrm{Pr}_o}{\mathrm{Pr}_w})^{0.25} F_c \qquad (\mathrm{Re_o} < 40) \tag{7a}$$

$$Nu_f = \frac{h_f d_o}{k_o} = 0.71 \mathrm{Re}_o^{0.5} \mathrm{Pr}_o^{0.36} (\frac{\mathrm{Pr}_o}{\mathrm{Pr}_w})^{0.25} F_c \qquad (\mathrm{Re_o} > 40) \tag{7b}$$

appeared to describe the observed variation of water vapor flux with brine flow velocity quite well. Therefore, we used this equation to calculate the heat transfer coefficient h_f on the brine side for given values of the Reynolds number Re_o and Pr_o:

$$\mathrm{Re}_o = \frac{d_o u_o \rho_o}{\mu_o},\ \mathrm{Pr}_o = \frac{C_{po}\mu_o}{k_o},\ \mathrm{Pr}_w = \frac{C_{pw}\mu_w}{k_w} \tag{8}$$

4.6.3.2 Tube Side Distillate: Heat Transfer

The equation corresponding to equation (5) for the tube side distillate is:

$$\left.\frac{dQ(x)}{dx}\right|_j = h_p A_{rp} \alpha (T_{pm,j}(x) - T_{p1,j}(x)) \tag{9}$$

$$A_{rp} = \frac{d_i}{d_i} (=1) \tag{10}$$

The heat transfer coefficient h_p in the permeate (i.e., distillate) side may be described in a number of ways. One of them is based on the Sieder-Tate equation (Sieder and Tate, 1936):

$$Nu_p = \frac{h_p d_i}{k_i} = 1.86 (\frac{d_i}{L})^{0.33} (\mathrm{Re}_i \, \mathrm{Pr}_i)^{0.33} (\frac{\mu_i}{\mu_{wi}})^{0.14} \tag{11a}$$

$$\mathrm{Re}_i = \frac{d_i u_i \rho_i}{\mu_i} \; ; \quad \mathrm{Pr}_i = \frac{C_{pi} \mu_i}{k_i} \tag{11b}$$

4.6.3.3 Heat Transfer Across the Porous Membrane

Heat is transferred from the hot brine-membrane interface to the distillate-membrane interface in two ways. Water vapor flux convection creates an enthalpy flux, and there is conductive flux through the solid matrix as well as the porous gas space (porosity of the membrane, ε_m) (Guijt et al., 2005):

$$\left. \frac{dQ(x)}{dx} \right|_j = h_m A_{r\ln} \alpha (T_{fm,j}(x) - T_{pm,j}(x)) + N_{v,j}(x) \alpha (\Delta H_v (T_{pm,j}(x)) + C_{pm,j} T_{pm,j}(x)) \tag{12}$$

$$h_m = \varepsilon_m h_{mg} + (1 - \varepsilon_m) h_{ms} \tag{13}$$

The second term on the right hand side of equation (12) involves expressing the enthalpy of the water vapor as it is added to the distillate at the distillate-membrane interface; here, the basis of enthalpy calculations is liquid water at a temperature of 0 ºC. The quantity $N_{v,j}(x)$ is the water vapor mass flux in the *j*th fiber layer at any x. The area ratios relevant are:

$$A_{r\ln} = \frac{d_{lm}}{d_i} \; ; \quad d_{lm} = \frac{d_o - d_i}{\ln(\frac{d_o}{d_i})} \; ; \qquad A_{rp} = 1 = \frac{d_i}{d_i} \tag{14}$$

The heat transfer coefficient for the solid polymeric matrix h_{ms} is defined by:

$$h_{ms} = \frac{2 k_{ms}}{(d_o - d_i)} \tag{15a}$$

where k_{ms} is the thermal conductivity of the matrix material. The corresponding quantity for the gas phase is:

$$h_{mg} = \frac{2k_{mg}}{(d_o - d_i)} \tag{15b}$$

Both of these quantities are defined with respect to the total surface area of the fibers; their individual area effects are taken into account via ε_m in equation (13).

4.6.3.4 Heat Transferred by the Hot Brine

The heat lost by the hot brine per unit fiber length from the *j*th fiber layer at any location x is:

$$\left.\frac{dQ(x)}{dx}\right|_j = \rho_{f0,j}(x)V'_{f0,j}(x)C_{pf0,j}(x)T_{f0,j}(x) - \rho_{f1,j}(x)V'_{f1,j}(x)C_{pf1,j}(x)T_{f1,j}(x)) \tag{16}$$

Here, $V'_{f0,j}(x)$ and $V'_{f1,j}(x)$ are defined above as the local brine inlet and outlet volumetric brine flow rates per unit fiber length for the *j*th layer. For the first fiber layer, $V'_{f0,1}(x)$ (= $V_{b0,1}/L$) and $T_{f0,1}(x)$ (=$T_{b0,1}$) are constant for a given brine feed flow rate $V_{b0,1}$ and feed temperature $T_{b0,1}$. The rate of thermal energy gain by the distillate flow from the fiber entrance (x = 0) to axial location x is obtained by integrating equation (9) along x and equating it to the rate of enthalpy gain by the distillate:

$$Q(x)\Big|_j = \int_0^x dQ(x)\Big|_j = \int_0^x h_p A_{rp}\alpha(T_{pm,j}(x) - T_{p1,j}(x))dx \tag{17a}$$

$$Q(x)\Big|_j = \rho_{p1,j}(x)V_{p1,j}(x)C_{p1,j}(x)T_{p1,j}(x) - \rho_{p0,j}V_{p0,j}C_{p0,j}T_{p0,j} \tag{17b}$$

4.6.3.5 Water Vapor Flux in a Fiber Layer at Any x

As is generally practiced in the literature, the water vapor mass flux is to be described using a membrane mass transfer coefficient k_m (here, $N_{v,j}(x)$ is defined based on I.D.).

$$N_{v,j}(x) = k_m A_{r\ln}(p_{fm,j}(x) - p_{pm,j}(x)) \tag{18}$$

Integration of this expression along the length of the fiber for n fibers in a given layer for the *j*th layer yields:

$$\int_0^L N_{v,j}(x)\alpha dx = \rho_{b0,j}V_{b0,j} - \rho_{b1,j}V_{b1,j} \tag{19}$$

A corresponding result on the permeate side from x = 0 to x leads to:

$$\int_0^x N_{v,j}(x)\alpha dx = \rho_{p1,j}(x)V_{p1,j}(x) - \rho_{p0,j}V_{p0,j} \tag{20}$$

The driving partial pressure of water at location x in the hot brine in *j*th fiber layer, namely, $p_{fm,j}(x)$, may be estimated from Antoine equation (Smith et al., 2001) by assuming vapor—liquid equilibrium, and an activity coefficient of water equal to 1:

$$p_{fm,j}(x) \cong p^0_{fm,j}(x) = 10^3 \exp(16.260 - \frac{3799.89}{T_{fm,j}(x) + 273.15 - 46.8}) \tag{21a}$$

The corresponding partial pressure of water vapor on the permeate side is:

$$p_{pm,j}(x) \cong p^0_{pm,j}(x) = 10^3 \exp(16.260 - \frac{3799.89}{T_{pm,j}(x) + 273.15 - 46.8}) \tag{21b}$$

To be exact, these expressions are actually the vapor pressure of water $p^0_{fm,j}(x)$ and $p^0_{pm,j}(x)$ on the feed interface and the distillate interface, respectively. The actual water vapor partial pressures are related to these two values via:

$$p_{fm,j}(x) = x_{fm}\gamma_{fm}p^0_{fm,j}(x)\ ; \quad p_{pm,j}(x) = x_{pm}\gamma_{pm}p^0_{pm,j}(x) \tag{22a}$$

where γ_{fm} and γ_{pm} are the activity coefficients of water at those locations and x_{fm} and x_{pm} are the corresponding water mole fractions. The activity coefficient of water γ_{water} has been related to the salt mole fraction x_{NaCl} via (Lawson and Lloyd, 1997):

$$\gamma_{water} = 1 - 0.5x_{NaCl} - 10x^2_{NaCl} \tag{22b}$$

In this analysis, the dependent variables for the *j*th layer that are unknown are as follows: $Q(x)|_j$, $T_{fm,j}(x)$, $T_{pm,j}(x)$, $T_{p1,j}(x)$, $p_{fm,j}(x)$, $p_{pm,j}(x)$, $N_{v,j}(x)$, $V'_{f1,j}(x)$, $T_{f1,j}(x)$, $V_{p1,j}(x)$. Of these, $p_{fm,j}(x)$, $p_{pm}(x)$, $T_{f1,j}(x)$, $Q(x)|_j$, $V'_{f1,j}(x)$ depend on the other five primary variables. We have correspondingly the following equations:

$$\begin{aligned} Q(x)\big|_j &= \int_0^x h_p A_{rp}\alpha(T_{pm,j}(x) - T_{p,j}(x))dx \\ &= \rho_{p1,j}(x)V_{p1,j}(x)C_{p1,j}(x)T_{p1,j}(x) - \rho_{0,j}V_{p0,j}C_{p0,j}T_{p0,j} \end{aligned} \tag{17a, b}$$

$$N_{v,j}(x) = k_m A_{r\ln}(p_{fm,j}(x) - p_{pm,j}(x)) \tag{18}$$

$$\int_0^x N_{v,j}(x)\alpha dx = \rho_{p1,j}(x)V_{p1,j}(x) - \rho_{p0,j}V_{p0,j} \tag{20}$$

$$\left.\frac{dQ(x)}{dx}\right|_j = h_f A_{rf}\alpha(T_{f0,j}(x) - T_{fm,j}(x)) = h_p A_{rp}\alpha(T_{pm,j}(x) - T_{p1,j}(x)) \quad (23a)$$

$$\left.\frac{dQ(x)}{dx}\right|_j = h_p A_{rp}\alpha(T_{pm,j}(x) - T_{p1,j}(x))$$
$$= h_m A_{r\ln}\alpha(T_{fm,j}(x) - T_{pm,j}(x)) + N_{v,j}(x)\alpha(\Delta H_v(T_{pm,j}(x)) + C_{pm,j}T_{pm,j}(x)) \quad (23b)$$

Given the feed conditions of brine and distillate in the *j*th layer at x (i.e., flow rate and temperature), the values of $T_{fm,j}(x)$, $T_{pm,j}(x)$, $T_{p1,j}(x)$, $N_{v,j}(x)$, and $V_{p1,j}(x)$ can be calculated from the set of five equations above, along with the boundary condition $Q(0)|_j = 0$. These equations were solved using the Newton-Raphson Method for n×n systems (Maron and Lopez, 1991). The values of other variables can be calculated correspondingly using appropriate relations.

4.6.3.6 Modeling Results

The order of presentation of DCMD modeling results are as follows:

1. DCMD performances obtained using the two larger modules S/N 1004 and S/N 1005 of Phase III research (Sirkar and Li, 2005)
2. The utility of the model using not only the data from the larger MD modules of Phase III study but also the much smaller module MXFR #3 of the Phase II study (Sirkar and Li, 2004)
3. Predicting pilot plant results

Two rectangular cross flow membrane modules of Phase III—namely, S/N 1004 and S/N 1005—are described in table 6. Solution of the five equations 17a, 17b, 18, 20, 23a, and 23b were carried out using the input values V_{b0}, T_{b0}, V_{d0}, T_{d0}, and details of the module geometry and fiber dimensions and properties. Of the latter, the values of the thermal conductivities, k_{mg} and k_{ms}, are 0.03 W/m-K (Kreith and Bohn, 2001) and 0.17 W/m-K (Mark, 1999), respectively. However, the value of the membrane water vapor mass transfer coefficient k_m is an unknown. Li and Sirkar (2005) had developed an estimate of k_m for the module MXFR #3 from VMD measurements. The conditions for DCMD measurement, especially the presence of air in the pores and different temperature profiles along the pore length, suggest that k_m in DCMD will be somewhat different. We have, therefore, used k_m as the only adjustable parameter here. The values assumed were:

S/N 1004 and S/N 1005 $\longrightarrow$ $k_m = 0.0022$ kg/m^2/h/Pa
MXFR #3 $\longrightarrow$ $k_m = 0.0018$ kg/m^2/h/Pa
SN 1006 $\longrightarrow$ $k_m = 0.0028$ kg/m^2/h/Pa

Note that Li and Sirkar (2005) found a value of k_m not too far from these values.

The results of simulations for the water vapor flux obtained in the two larger modules S/N 1004 and S/N 1005 are shown in figure 45 as solid lines. It appears that the model predictions are reasonably close to the observed variation of the water vapor flux with the distillate flow velocity variation. The predictions of the distillate outlet temperature as a function of the distillate velocity variation also appear to describe the observed data well. The simulations for the water vapor flux for three different salt concentrations in the larger module S/N 1004 as a function of brine feed temperature (figure 46) illustrate (as does the experimental data) that the increased salt concentration has a very minor effect on the observed/predicted water vapor flux, a distinct strength of DCMD/VMD processes.

The same behavior, namely, very limited effect of the salt concentration (3% and 10%) on the observed water vapor flux as a function of the distillate linear velocity is predicted in figure 47.

The increase of the distillate inlet temperature had a strong effect on the reduction of water vapor flux and the rise in the distillate outlet temperature; this was predicted by the model for the module S/N 1004 as shown in figure 48. We know that as the feed brine temperature was increased, the water vapor flux was increased due to higher water vapor pressure. This was shown in figure 46 for module S/N 1004 and in figure 49 for smaller module MXFR #3 at two different brine velocities. The model predicted such a behavior reasonably well, which was also shown in those figures.

In the next three figures (figures 50–52), the predictive ability of the model for the extensive data collected with both modules S/N 1004 and MXFR #3 are tested. Figure 50 tests this vis-à-vis the experimentally observed shell side outlet temperature. We note that generally the model is able to predict these values well over a temperature range varying between 30–90 °C (86–194 °F). There is some scatter, especially with the data from the smaller module. Figure 51 shows that the model can predict the values of the tube side distillate outlet temperature over a wide range, 30–90 ºC. However, the scatter appears to be somewhat larger. There is an overprediction at lower temperatures and underpredicton at higher temperature. This suggests that, perhaps among other strategies, we need to test other heat transfer coefficient correlations for the tube side. The scatter as shown in figure 52 for the water vapor flux values is larger. However, the range of water vapor flux covered here is broad: 4–5 to 60 kg/m^2/h (2.4–35.3 gfd). The question of whether one k_m can be used over a wide range of temperature for such predictions is crucial here.

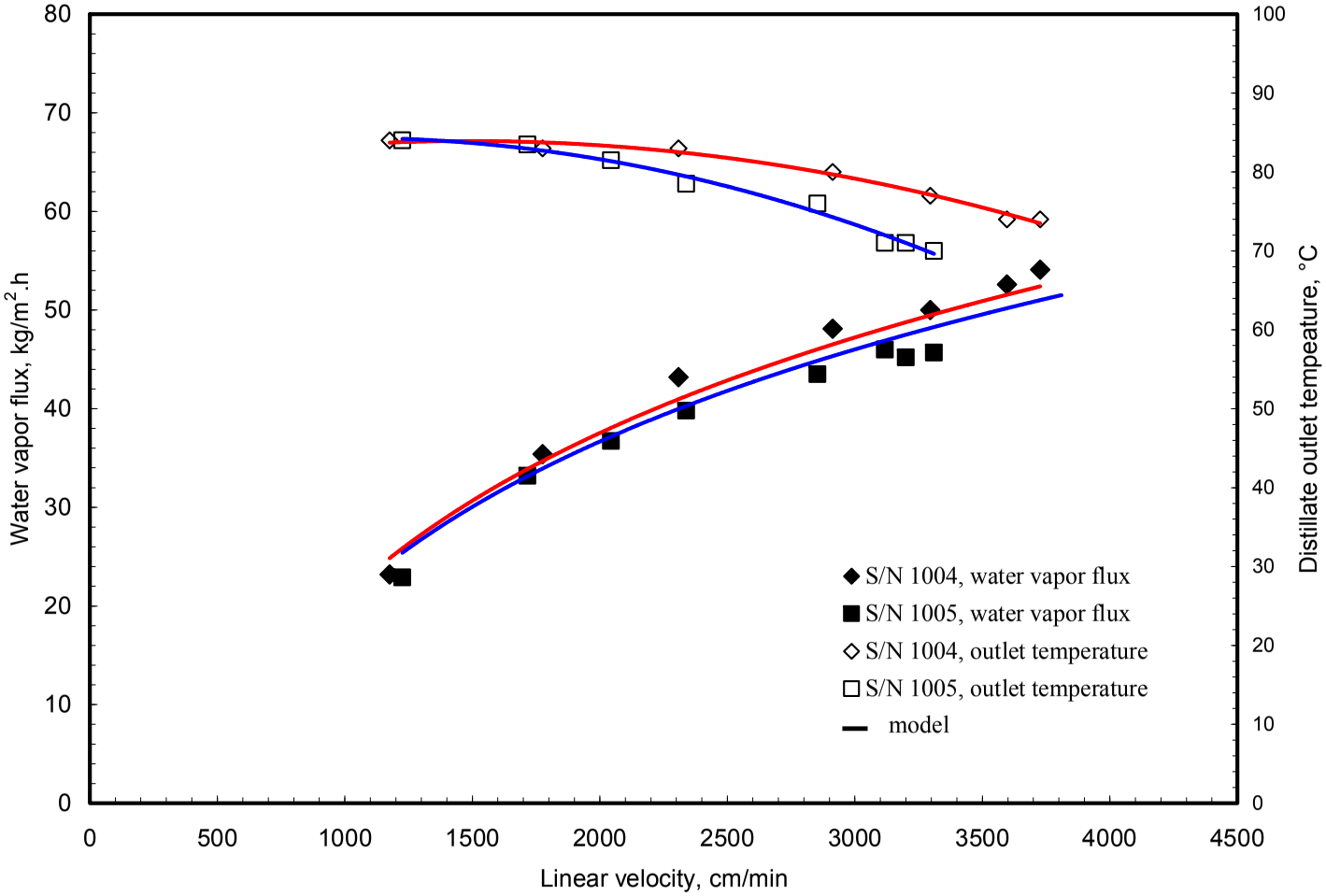

Figure 45. Comparison of DCMD performances of modules S/N 1004 and S/N 1005: variation of water vapor flux with inlet linear velocity and outlet temperature of distillate flowing through the tube side at inlet temperatures of 16–24 ºC and 3% brine at 85 ºC flowing on the shell side at 25 L/min (interstitial velocity of 230 cm/min).

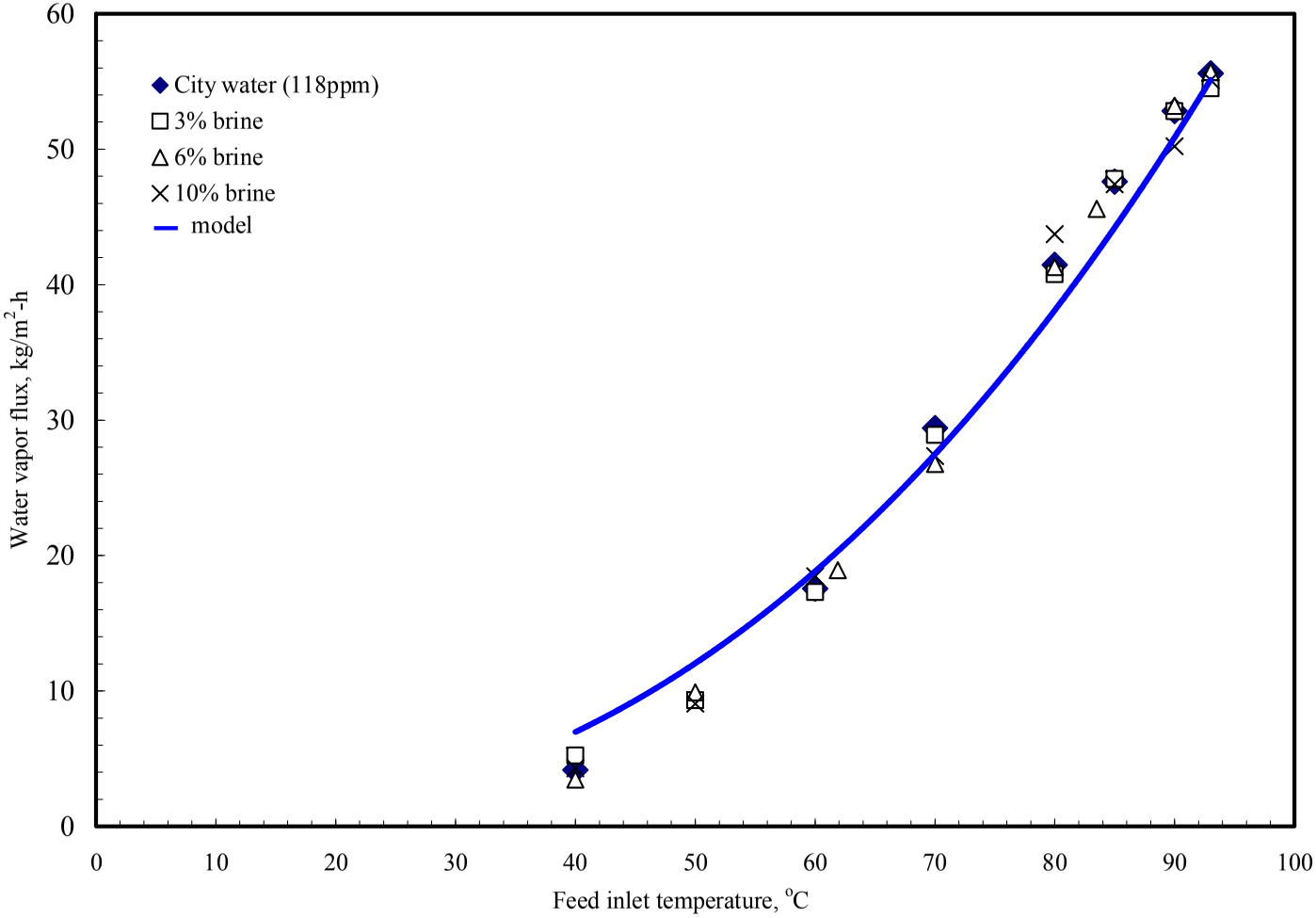

Figure 46. DCMD performance of module S/N 1004 with city water, 3% brine, 6% brine, and 10% brine as feed solutions: variation of water vapor flux with feed inlet temperature (shell side: brine solution at 230 cm/min of interstitial velocity; tube side: distillate at 2,850 cm/min of average linear velocity at 25–35 ºC of the inlet temperature).

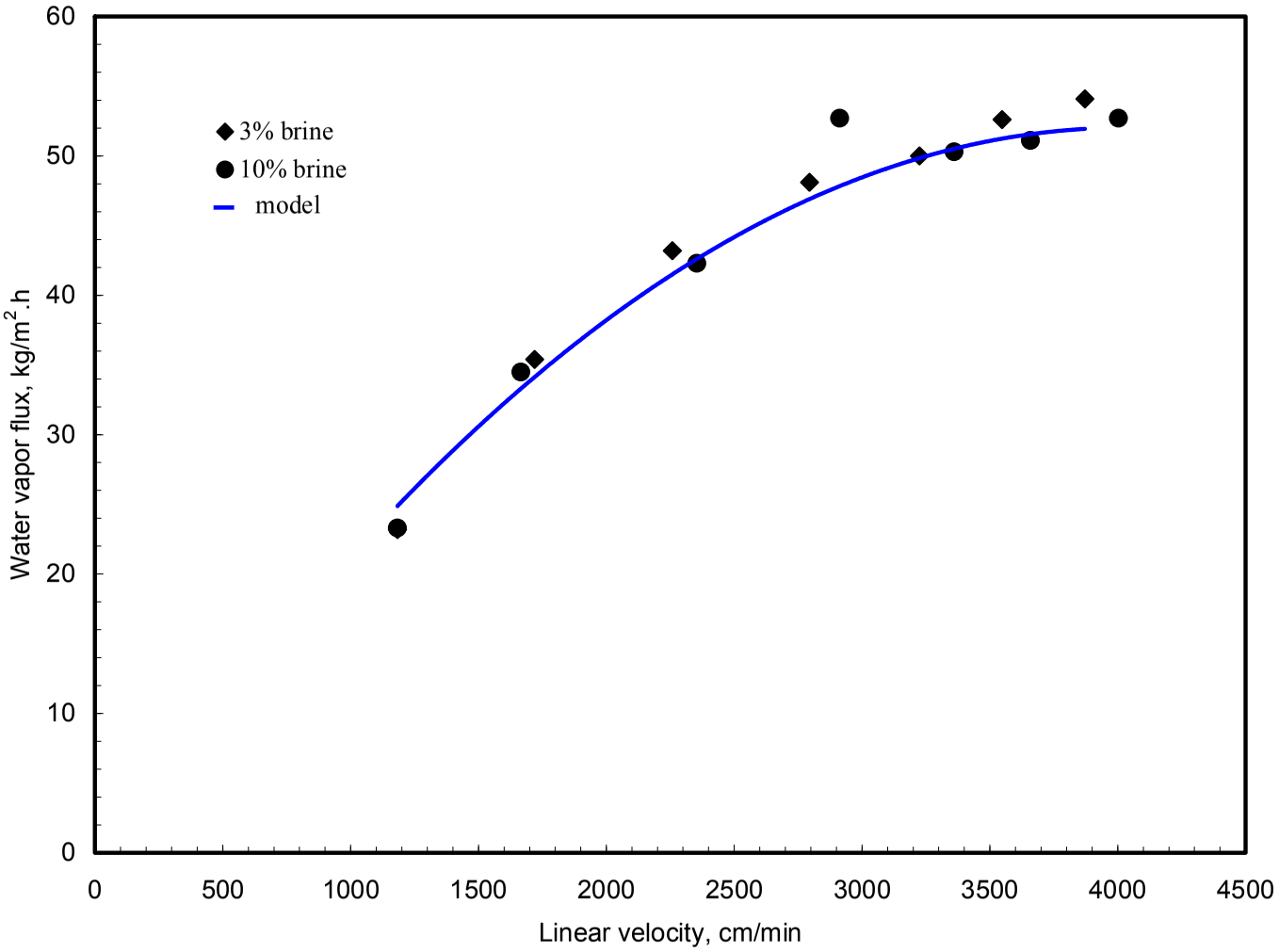

Figure 47. DCMD performance of module S/N 1004 (membrane surface area: 2,864 cm^2) with 3% brine and 10% brine as feed solutions: variation of water vapor flux with linear velocity of distillate flowing through tube side at inlet temperatures of 18–26 ºC and hot brine flowing on shell side with 25 L/min (interstitial velocity of 230 cm/min) at a temperature of 85–88 ºC.

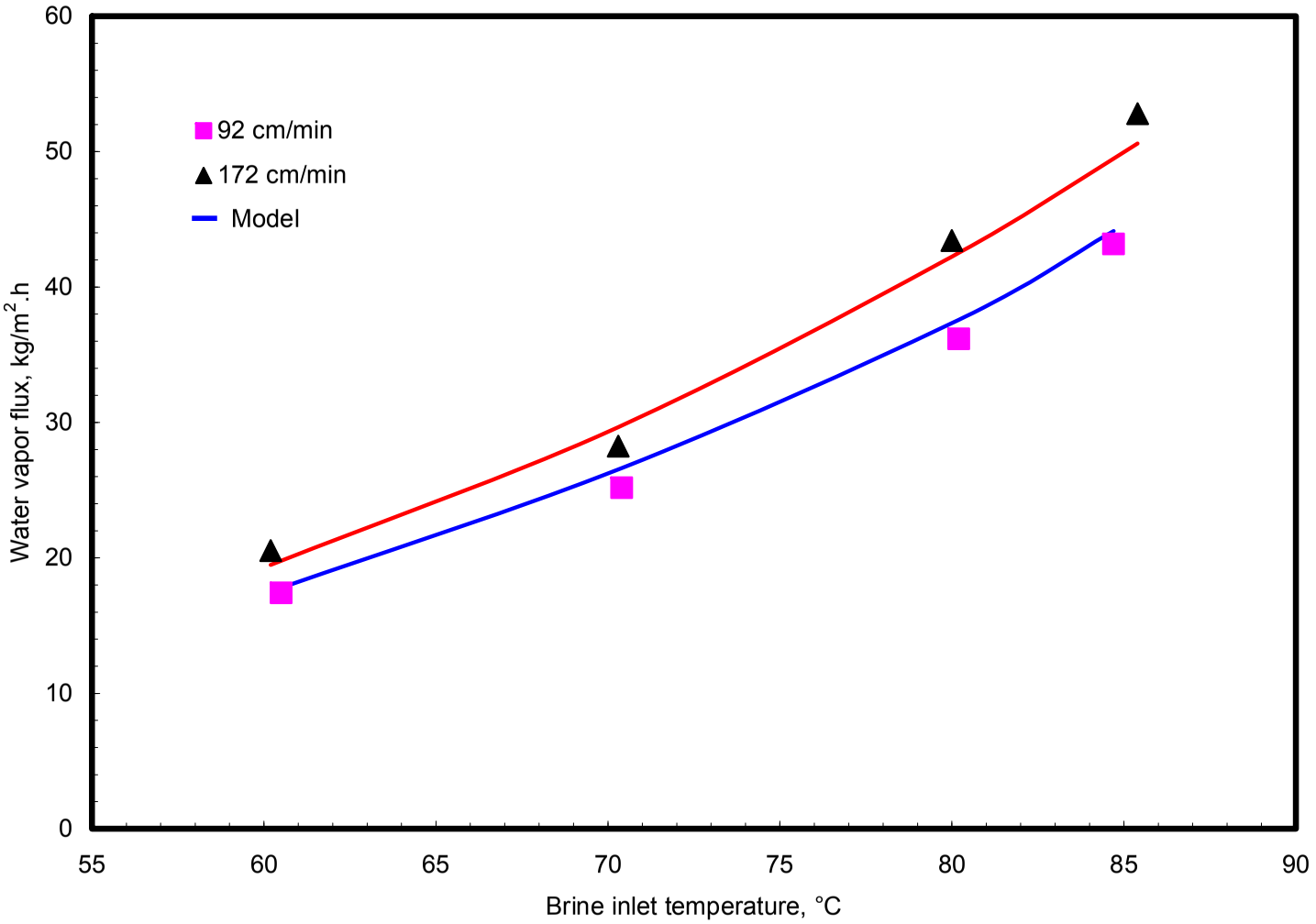

Figure 48. DCMD performance of module S/N 1004 (membrane surface area: 2,864 cm^2): variation of water vapor flux with distillate inlet temperature (shell side: 3% brine at 230 cm/min of interstitial velocity at a temperature of 91–93 ºC; tube side: distillate at 2,950 cm/min of linear velocity); variation of distillate outlet temperature with the distillate inlet temperature also shown.

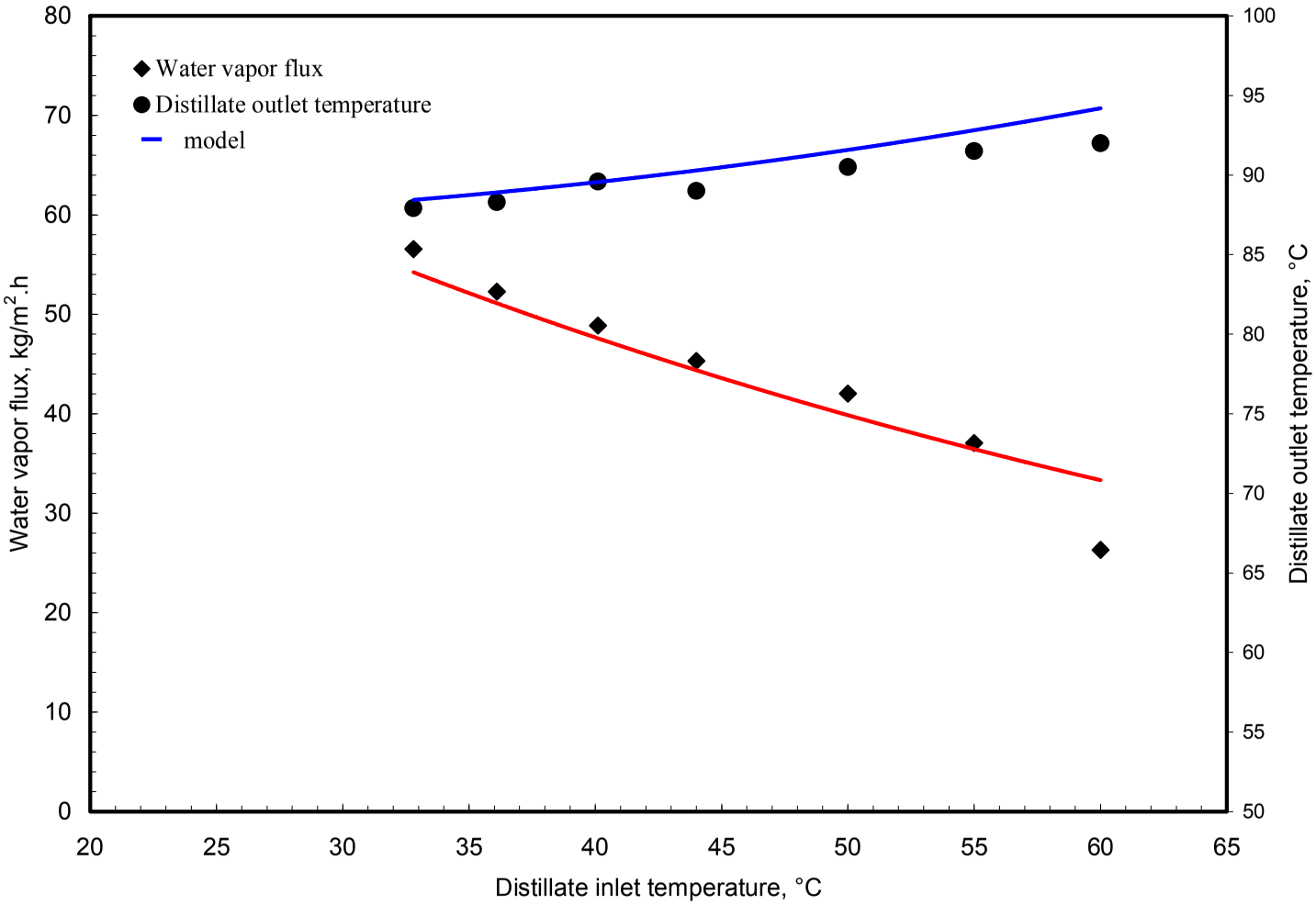

Figure 49. DCMD performance of module MXFR #3 (membrane surface area: 190 cm^2): variation of water vapor flux with inlet temperature of hot brine (1% NaCl) as feed flowing on the shell side (crossflow) at various interstitial velocities (tube side, 15–17 ºC DI water, linear velocity 1,660 cm/min).

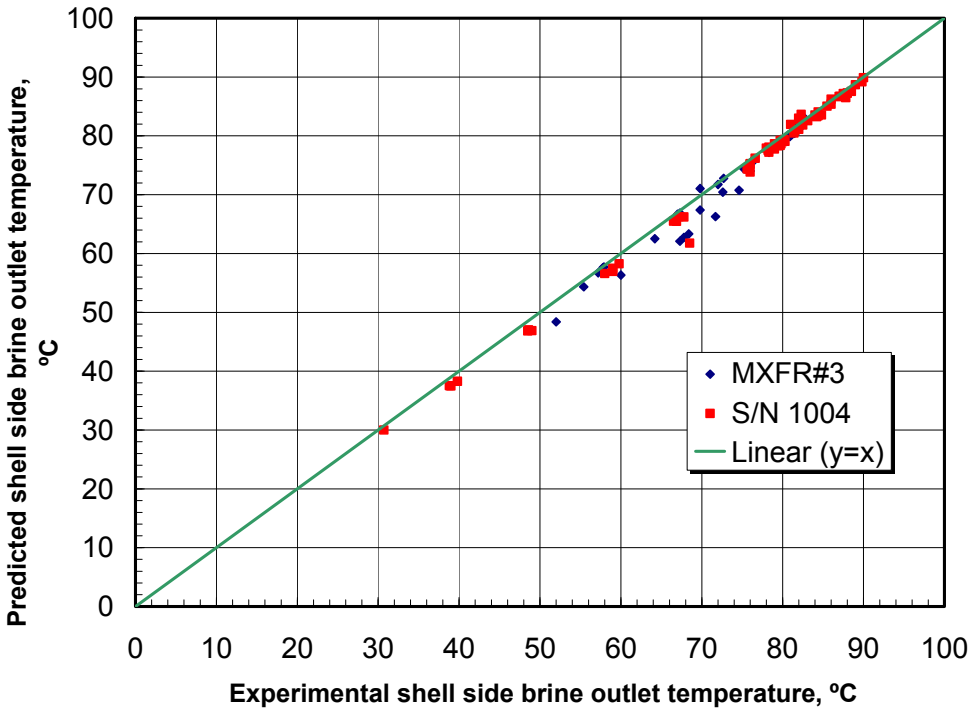

Figure 50. Comparison of predicted shell side brine outlet temperatures with DCMD experimental data for modules MXFR #3 and S/N 1004 (running conditions: for MXFR #3, 1% NaCl solution, shell side brine feed rate 200–2,280 mL/min (interstitial velocity 23–260 cm/min) , brine feed temperature 30.8 ~ 93.8 ºC, tube side distillate (deionized water) feed rate 112–600 mL/min (linear velocity 727–3,900 cm/min), distillate feed temperature 12.5–22.4 ºC; for S/N 1004, city water or 3–10% NaCl solution, shell side brine feed rate 5,000–33,000 mL/min (interstitial velocity 46–300 cm/min), brine feed temperature 30.8–93.8 ºC, tube side distillate feed rate 1,100–4,090 mL/min (linear velocity 1,264–4,400 cm/min), distillate feed temperature 18.3–60 ºC) (data from Sirkar and Li, 2003; Sirkar and Li, 2005).

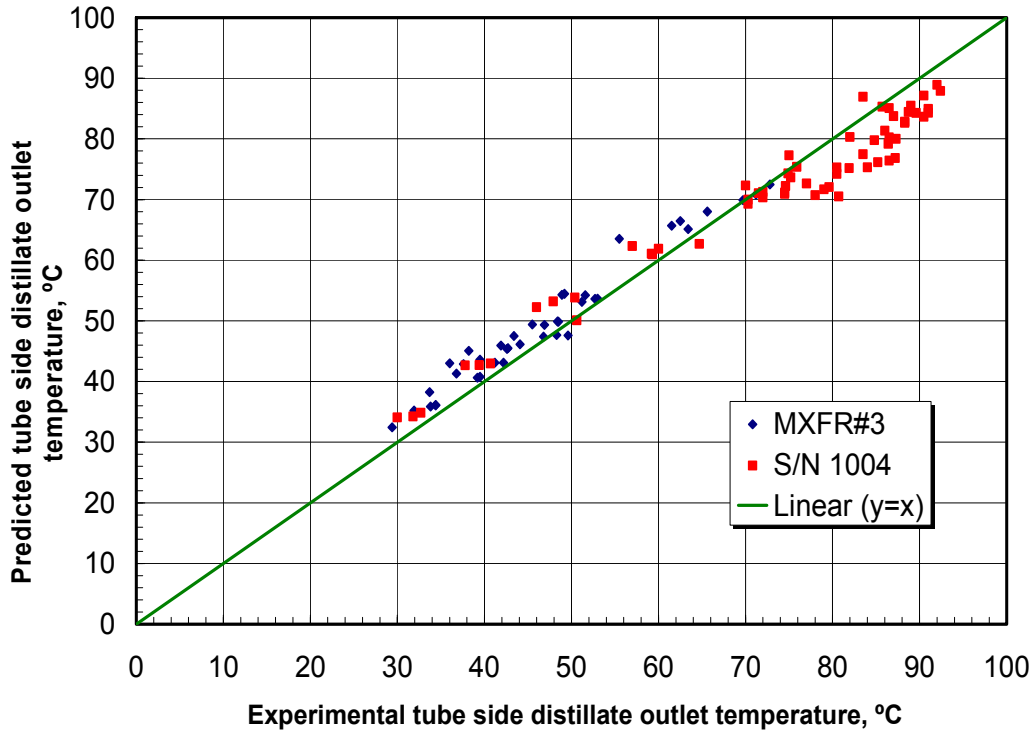

Figure 51. Comparison of predicted tube side distillate outlet temperatures with DCMD experimental data for modules MXFR #3 and S/N 1004 (running conditions: for MXFR #3, 1% NaCl solution, shell side brine feed rate 200–2,280 mL/min (interstitial velocity 23–260 cm/min) , brine feed temperature 30.8 ~ 93.8 ºC, tube side distillate (deionized water) feed rate 112–600 mL/min (linear velocity 727–3,900 cm/min), distillate feed temperature 12.5–22.4 ºC; for S/N 1004, city water or 3–10% NaCl solution, shell side brine feed rate 5,000–33,000 mL/min (interstitial velocity 46–300 cm/min), brine feed temperature 30.8–93.8 ºC, tube side distillate feed rate 1,100–4,090 mL/min (linear velocity 1,264–4,400 cm/min), distillate feed temperature 18.3–60 ºC) (data from Sirkar and Li, 2003; Sirkar and Li, 2005).

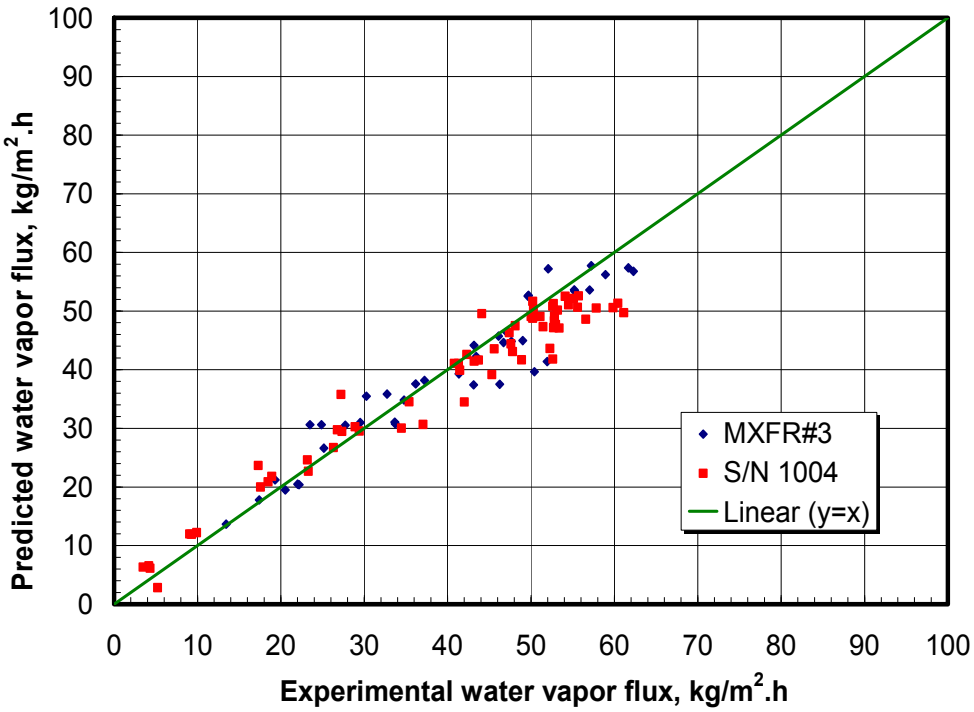

Figure 52. Comparison of predicted water vapor flux with DCMD experimental data for modules MXFR #3 and S/N 1004. Running conditions for MXFR #3, 1% NaCl solution; shell side brine feed rate 200–2,280 mL/min (interstitial velocity 23–260 cm/min); brine feed temperature 30.8 ~ 93.8 ºC; tube side distillate (deionized water) feed rate 112–600 mL/min (linear velocity 727–3,900 cm/min); distillate feed temperature 12.5–22.4 ºC. Running conditions for S/N 1004, city water or 3–10% NaCl solution; shell side brine feed rate 5,000– 33,000 mL/min (interstitial velocity 46–300 cm/min); brine feed temperature 30.8–93.8 ºC; tube side distillate feed rate 1,100–4,090 mL/min (linear velocity 1,264–4,400 cm/min); distillate feed temperature 18.3–60 ºC) (data from Sirkar and Li, 2003; Sirkar and Li, 2005).

The remaining figures on modeling results (figures 53–56) focus on model predictions regarding the performance variation along the fiber length, the module depth as well as the temperature polarization for the module MXFR #3. Figure 53 points out that as the hot feed brine hits the first layer of fibers, the distillate starts getting heated up; as a result, the water vapor flux is reduced along the fiber length; the brine is cooled down to a lesser extent. Correspondingly as we go down the fiber bed, we observe that the feed brine near the exit of the distillate stream is considerably warmer than that near the distillate stream entrance. This is a direct result of the assumption of no lateral brine side mixing in our model. Figure 54 is focused on temperature polarization in the feed brine region as well as in the distillate fiber bore for the first layer of fibers. As expected, the extent of temperature polarization on the brine side with efficient crossflow-based heat transfer is considerably less than that in the distillate tube side. We observe a similar temperature polarization behavior in figure 55 for the 10^{th} layer of fibers in module MXFR #3.

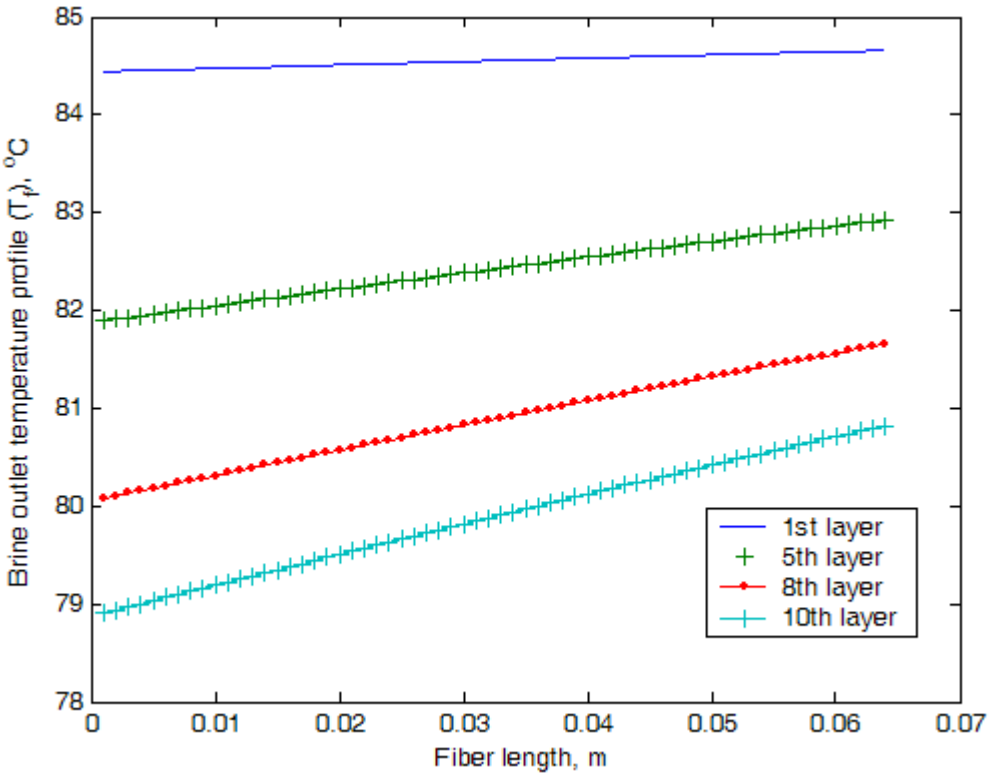

Figure 53. Variation of local temperature profiles of brine bulk temperature along the fiber length for different fiber layers in DCMD module MXFR #3 (shell side flow rate 2,000 mL/min, interstitial velocity 229 cm/min, inlet temperature 85.1 ºC; tube side flow rate 400 mL/min, linear velocity 2,600 cm/min, inlet temperature 19.8 ºC).

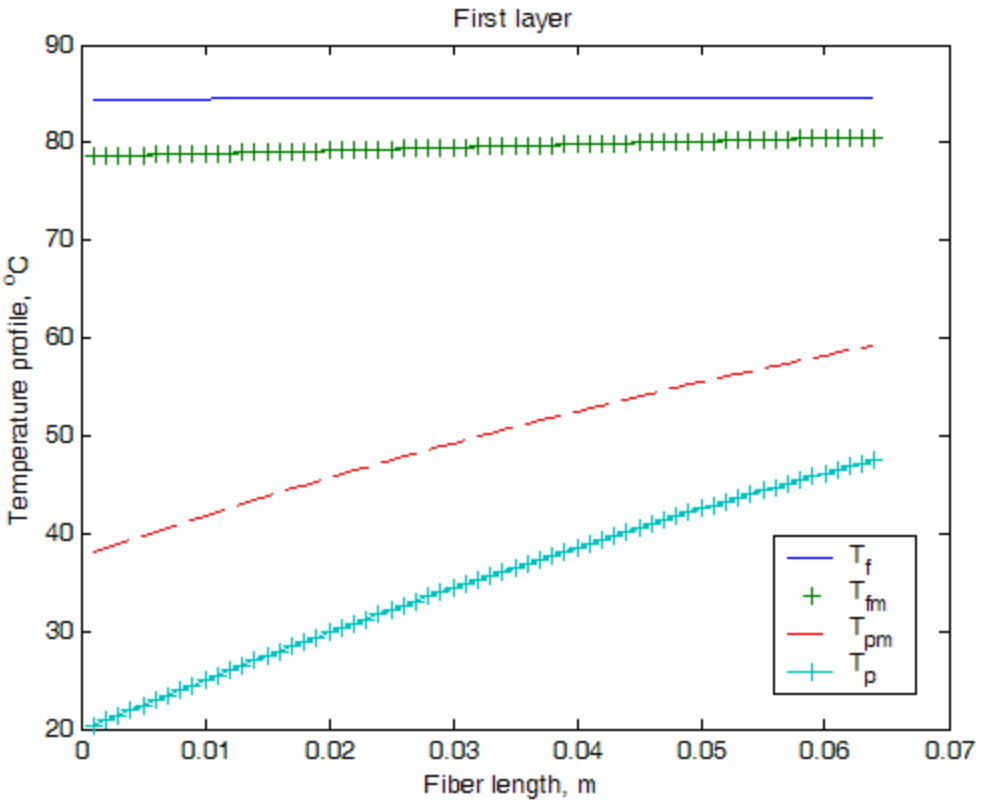

Figure 54. Variation of local temperature profiles of brine bulk temperature, wall temperature on the fiber outside surface, wall temperature on the fiber inside surface and distillate bulk temperature along the fiber length for the first fiber layer in DCMD module MXFR #3 (shell side flow rate 2,000 mL/min, interstitial velocity 229 cm/min, inlet temperature 85.1 ºC; tube side flow rate 400 mL/min, linear velocity 2,600 cm/min, inlet temperature 19.8 ºC).

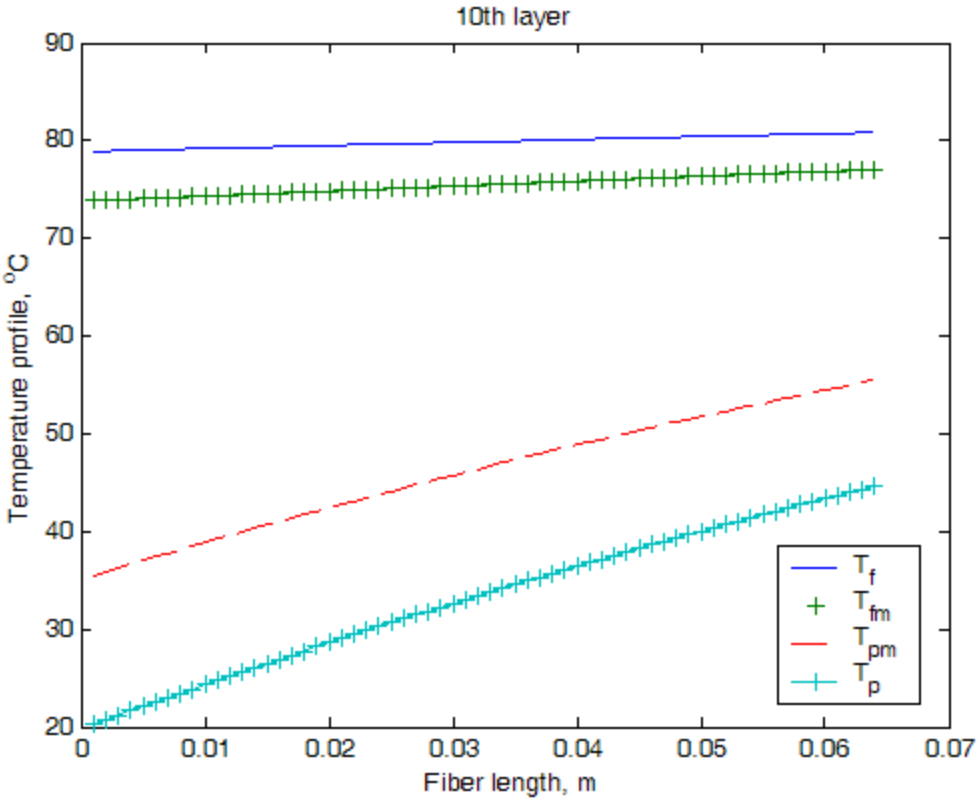

Figure 55. Variation of local temperature profiles of brine bulk temperature, wall temperature on the fiber outside surface, wall temperature on the fiber inside surface and distillate bulk temperature along the fiber length for the 10th fiber layer in DCMD module MXFR #3 (shell side flow rate 2,000 mL/min, interstitial velocity 229 cm/min, inlet temperature 85.1 ºC; tube side flow rate 400 mL/min, linear velocity 2,600 cm/min, inlet temperature 19.8 ºC).

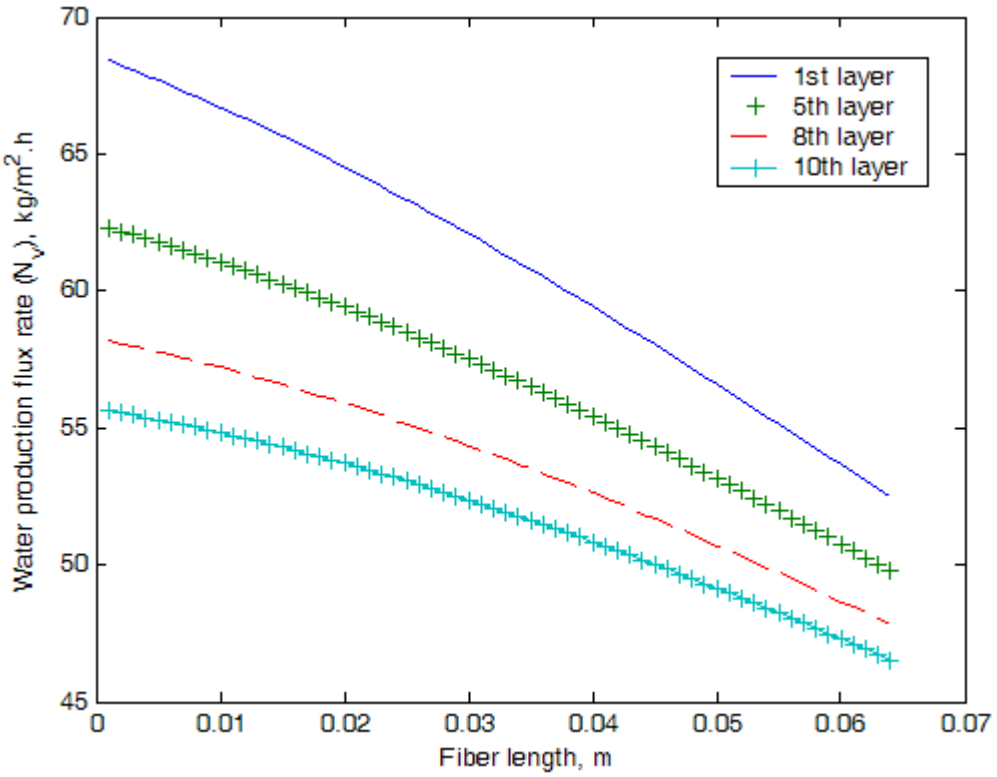

Figure 56. Variation of local water vapor flux along the fiber length for the 10th fiber layer in DCMD module MXFR #3 (shell side flow rate 2,000 mL/min, interstitial velocity 229 cm/min, inlet temperature 85.1 ºC; tube side flow rate 400 mL/min, linear velocity 2,600 cm/min, inlet temperature 19.8 ºC).

The result of a significant rise in distillate temperature along the fiber length will lead to a reduction in the local water vapor flux. This strong reduction in local water vapor flux with fiber length along distillate flow direction is illustrated in figure 56 for four layers of fibers in the small module MXFR #3. Such a flux reduction will reduce the brine temperature drop with fiber length leading to hotter brine near the distillate outlet as we have observed earlier in figure 53. These modeling results suggest that additional considerations are needed to exploit such observed behavior to beneficial ends in multimodule cascades for the DCMD pilot plant.

The previous discussion demonstrated that the model developed could describe the performances of modules S/N 1004, S/N 1005, as well as MXFR #3. Following are the results of using the model to describe the pilot plant module performances. Figure 57 illustrates, for a four-pair unit test, the water vapor flux production rate as a function of the shell side interstitial velocity of brine coming in at either 10% NaCl or 6% NaCl in tap water. For 6% NaCl solution, three hot brine temperatures were utilized, 90 ºC, 80 ºC, and 70 ºC. For the 10% NaCl solution, only 90 ºC was utilized. Modeling calculations were carried out for the

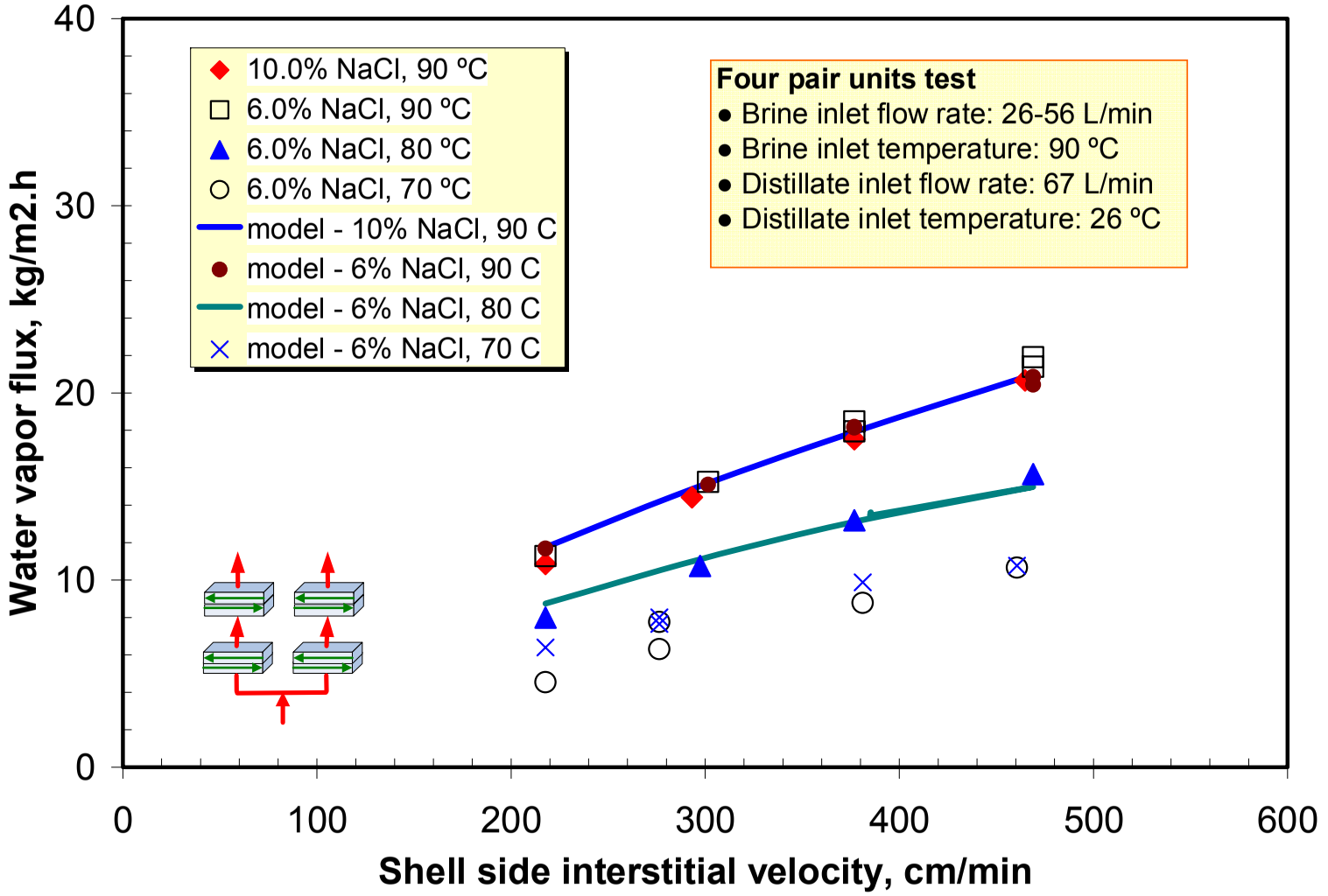

Figure 57. DCMD water vapor flux change with variation of shell side interstitial velocity for four single-pair DCMD units in the combination configuration (in parallel and series) on the shell side (distillate linear velocity 3,694 cm/min).

10% solution as well as the 6% solution. It appears that the model is able to predict the behavior of water vapor flux production quite well. Some of the experimental data (6% NaCl, 90 ºC brine feed) were illustrated earlier in figure 28. The total water production rate at the highest brine velocity was 20 kg/m^2/h x 1.32 x 4 = 105.6 kg/h, which works out to about 0.46 gpm.

4.6.4 Verification of No Lateral Flow Mixing in a DCMD Module

We have assumed in our model that there is no lateral mixing in the hot brine as it moves through the fiber bed. Figure 58 shows schematically the locations of eight temperature probes on a frame at the exit end of the brine flow in module S/N 1014. The actual photo of the setup implemented at NJIT is provided in figure 59. The intent was to measure the hot brine temperature as it exits the fiber bed and find out whether the temperature variation predicted in the model along the distillate flow path based on the assumption of no lateral mixing was valid or not. The probes were put in two layers of four each as shown in figure 58. Figures 60, 61, and 62 illustrate the measured temperatures in the hot brine exiting the 29th fiber layer at three hot brine velocities. These figures also have solid lines obtained from the model. It appears that, in general, the model predicts a somewhat higher exit brine temperature than the experimental values as the distillate flow length increases. This suggests that there is some degree of lateral mixing in the hot brine which we have to take into account in modeling to improve our predictive capabilities.

4.6.5 Contact Angle Measurements

A Cahn DCA315 (Thermo Fisher Scientific, Inc., Waltham, Maryland) balance was used to characterize dynamic contact angle of water on hollow fiber membrane surfaces. The measurements may help understand the effects of various parameters such as temperature, source and concentration of contaminants, thermal cycle, etc., on the hydrophobicity of the membrane surfaces. Cahn DCA 315 employing Wilhelmy technique (Adam, 1968) measures advancing (dry surface) contact angle as well as receding (wet surface) contact angle by monitoring the wetting forces during advancing and receding of water interacting with samples. The samples were treated under controlled environment and tested using the DCA. Before the contact angle measurement, the equipment was calibrated with distilled water. Figures 63a–63f show the slippage of the force-distance data for fibers taken from a variety of modules used earlier as well as in this research. The results are summarized in table 7. Virtually all samples appear to be hydrophobic. Those that have been exposed to salt solutions appear to be somewhat less hydrophobic than fibers obtained from modules S/N 1002 and MXFR #4 of Phase III and Phase II studies.

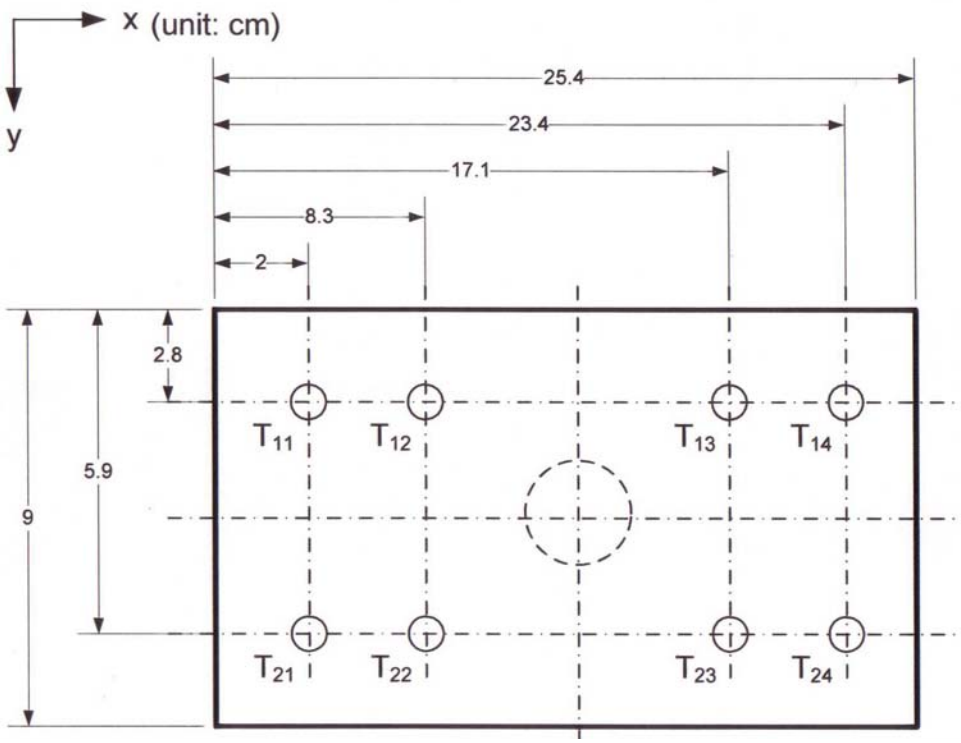

Figure 58. Inside frame dimensions of the face plate for DCMD modules (SN series) and the positions of eight temperature probes for temperature profile measurement of hot brine on the shell side.

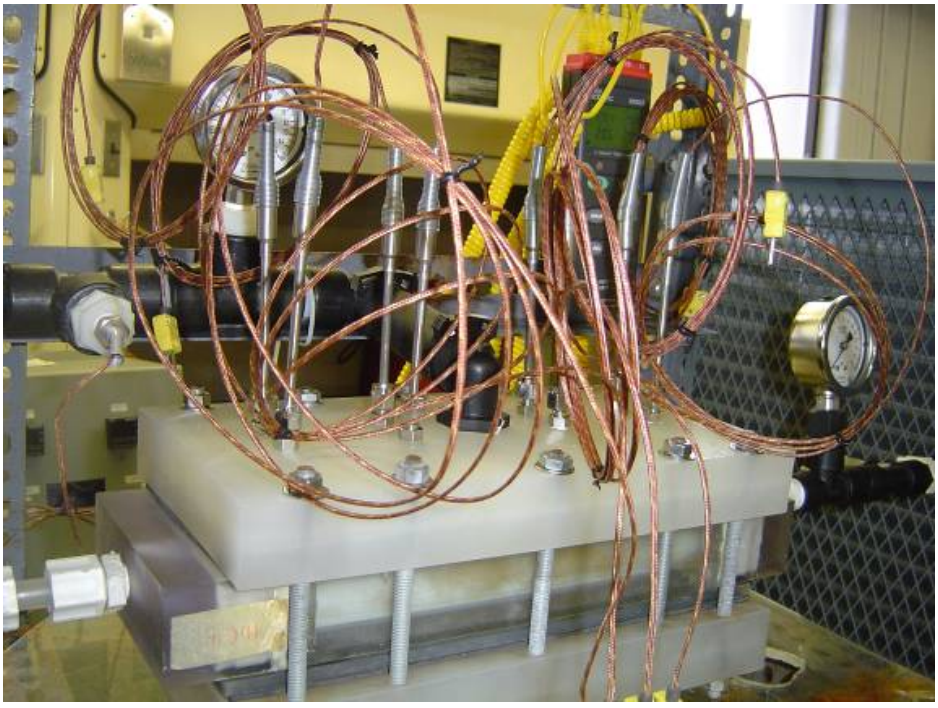

Figure 59. Photo of assembling of temperature probes in S/N 1004 DCMD module for measuring local brine temperature profile on the shell side.

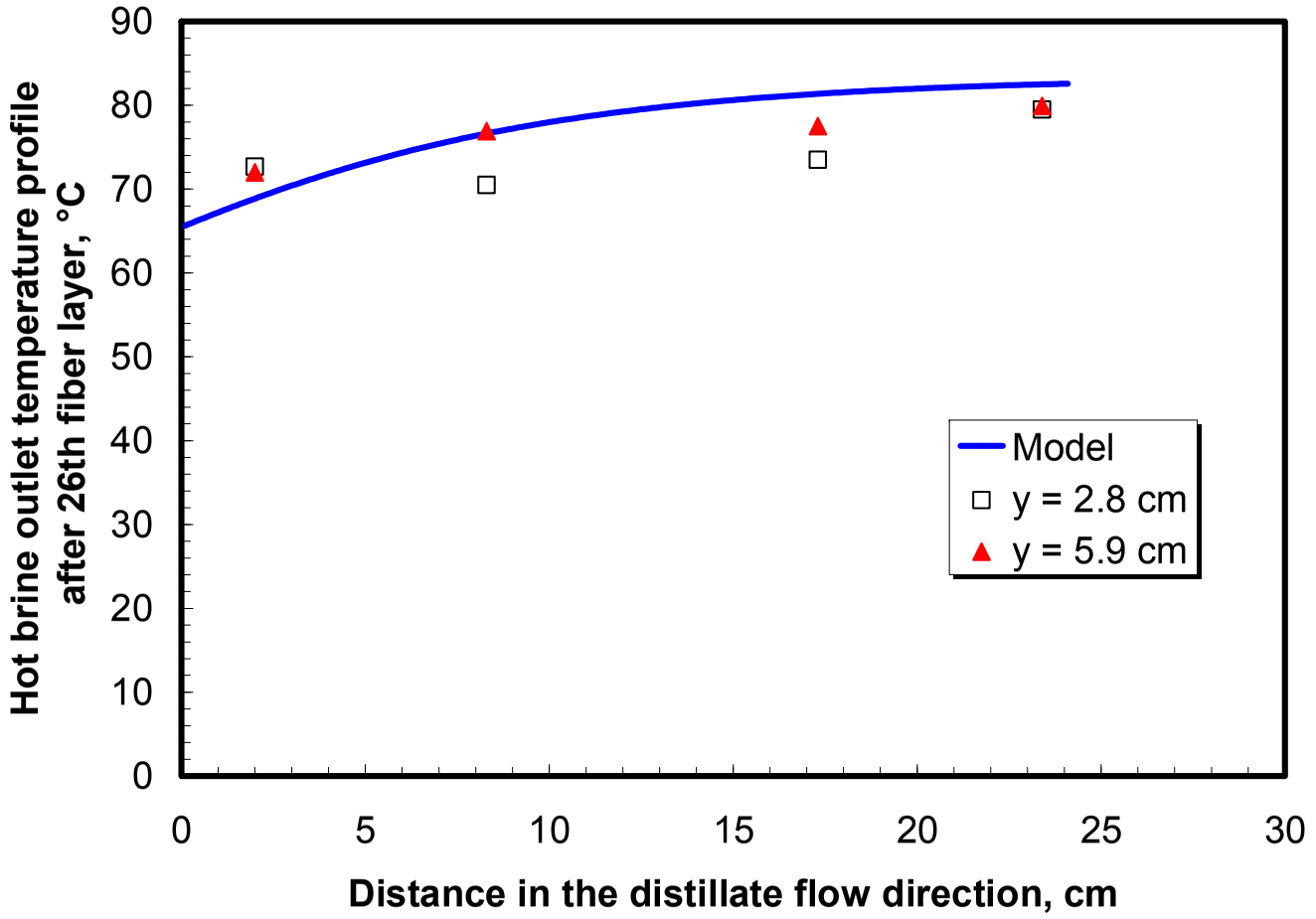

Figure 60. Variation of hot brine outlet temperature profile of module S/N 1014 for DCMD with the distance in the distillate flow direction after the hot brine passed the 26th fiber layer (crossflow) on the shell side (hot brine feed rate 23,500 mL/min [interstitial velocity 521 cm/min] and feed temperature 83.3 °C; distillate [DI water] feed rate 2,300 mL/min [linear velocity 1,034 cm/min] and feed temperature 25.7 °C).

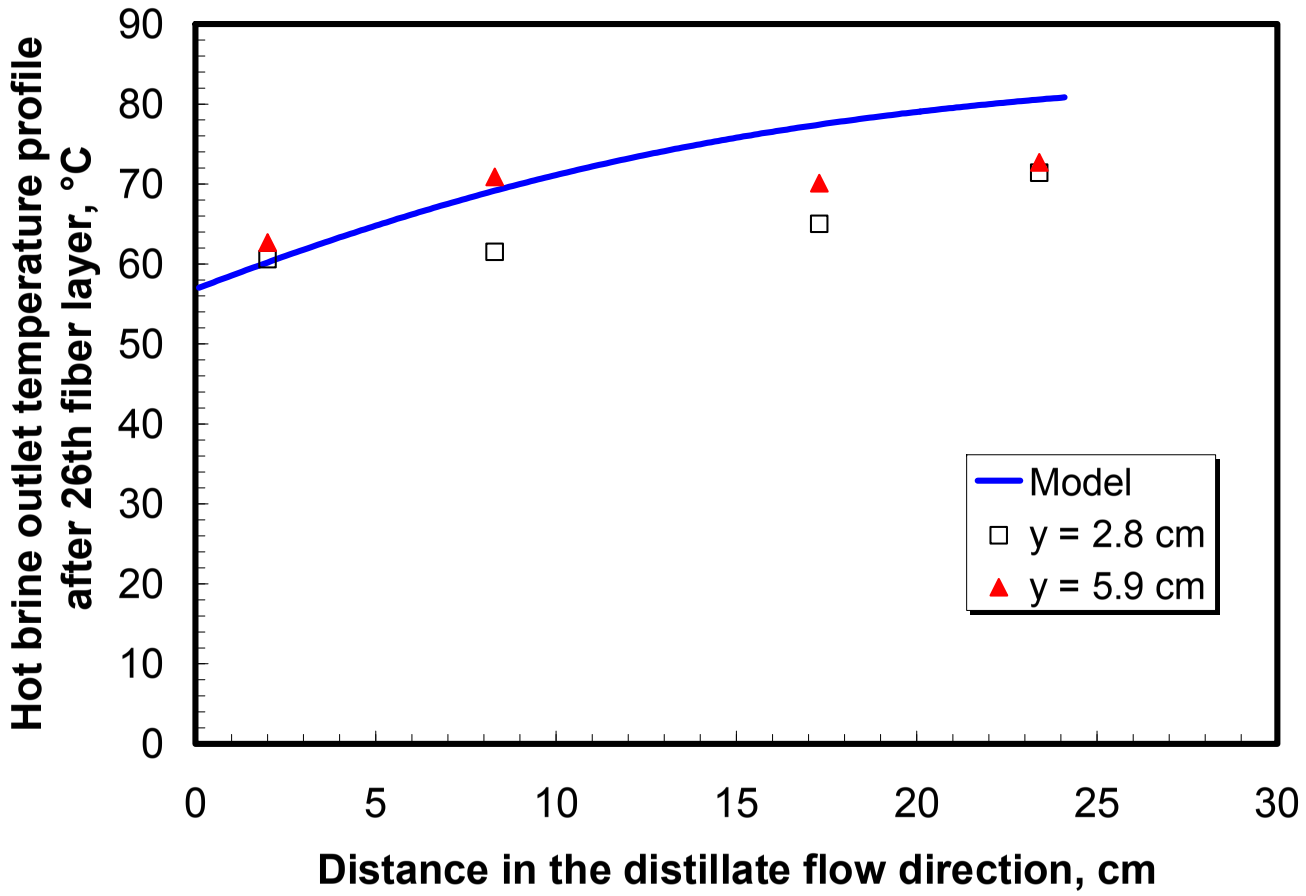

Figure 61. Variation of hot brine outlet temperature profile of module S/N 1014 for DCMD with the distance in the distillate flow direction after the hot brine passed the 26th fiber layer (crossflow) on the shell side (hot brine feed rate 13,700 mL/min (interstitial velocity 303 cm/min) and feed temperature 84.8 °C; distillate (DI water) feed rate 3,200 mL/min (linear velocity 1,430 cm/min) and feed temperature 25.4 °C).

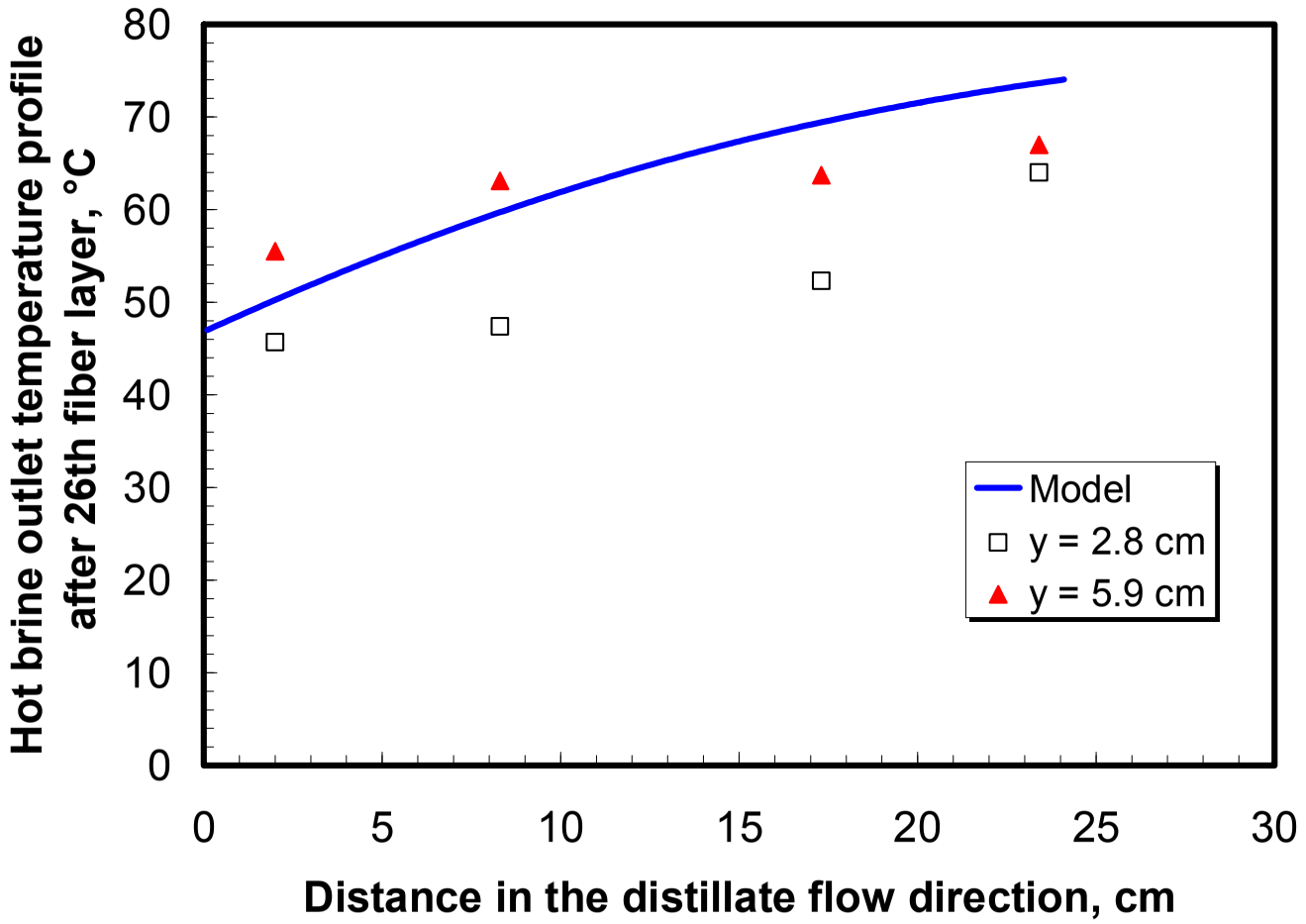

Figure 62. Variation of hot brine outlet temperature profile of module S/N 1014 for DCMD with the distance in the distillate flow direction after the hot brine passed the 26th fiber layer (crossflow) on the shell side (hot brine feed rate 8,700 mL/min [interstitial velocity 192 cm/min] and feed temperature 80.8 °C; distillate [DI water] feed rate 3,100 mL/min [linear velocity 1,380 cm/min] and feed temperature 25.1 °C).

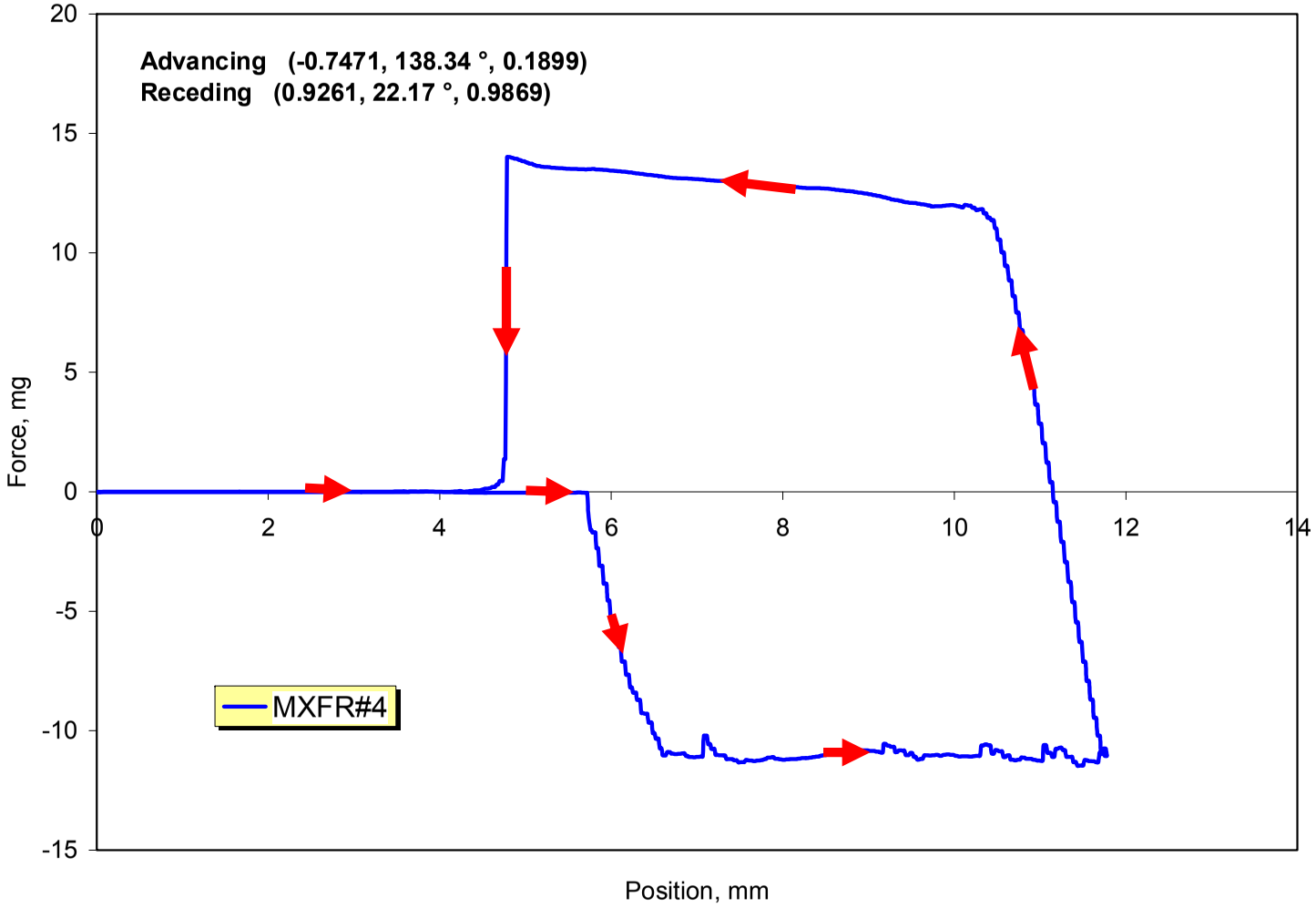

Figure 63a. Slippage of contact line in a dynamic contact angle measurement (coated PP 150/330 hollow fiber sample from MXFR #4 [Sirkar and Li, 2003]).

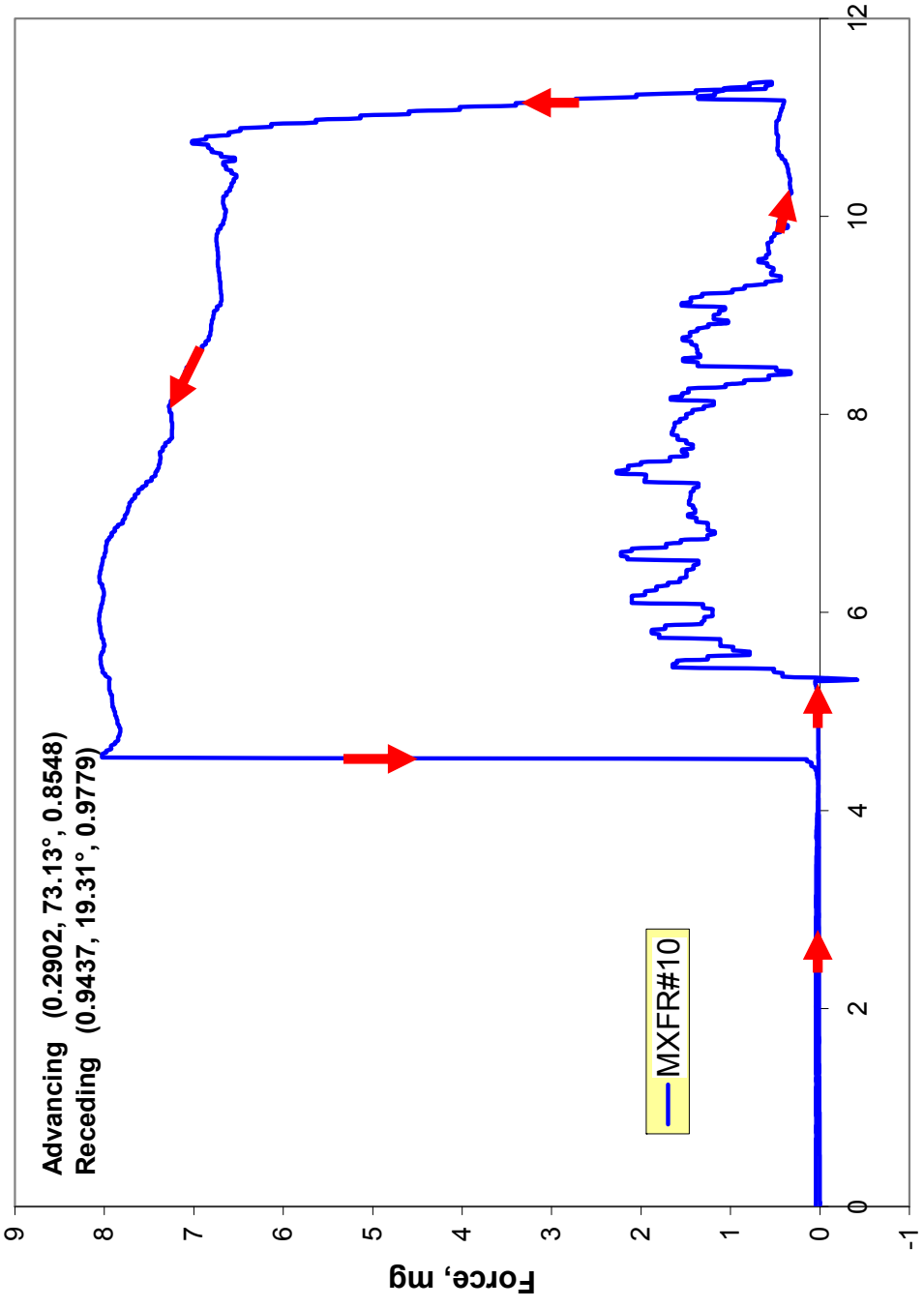

Figure 63b. Slippage of contact line in a dynamic contact angle measurement (coated PP 50/280 hollow fiber sample from MXFR #10 [Sirkar and Li, 2003]).

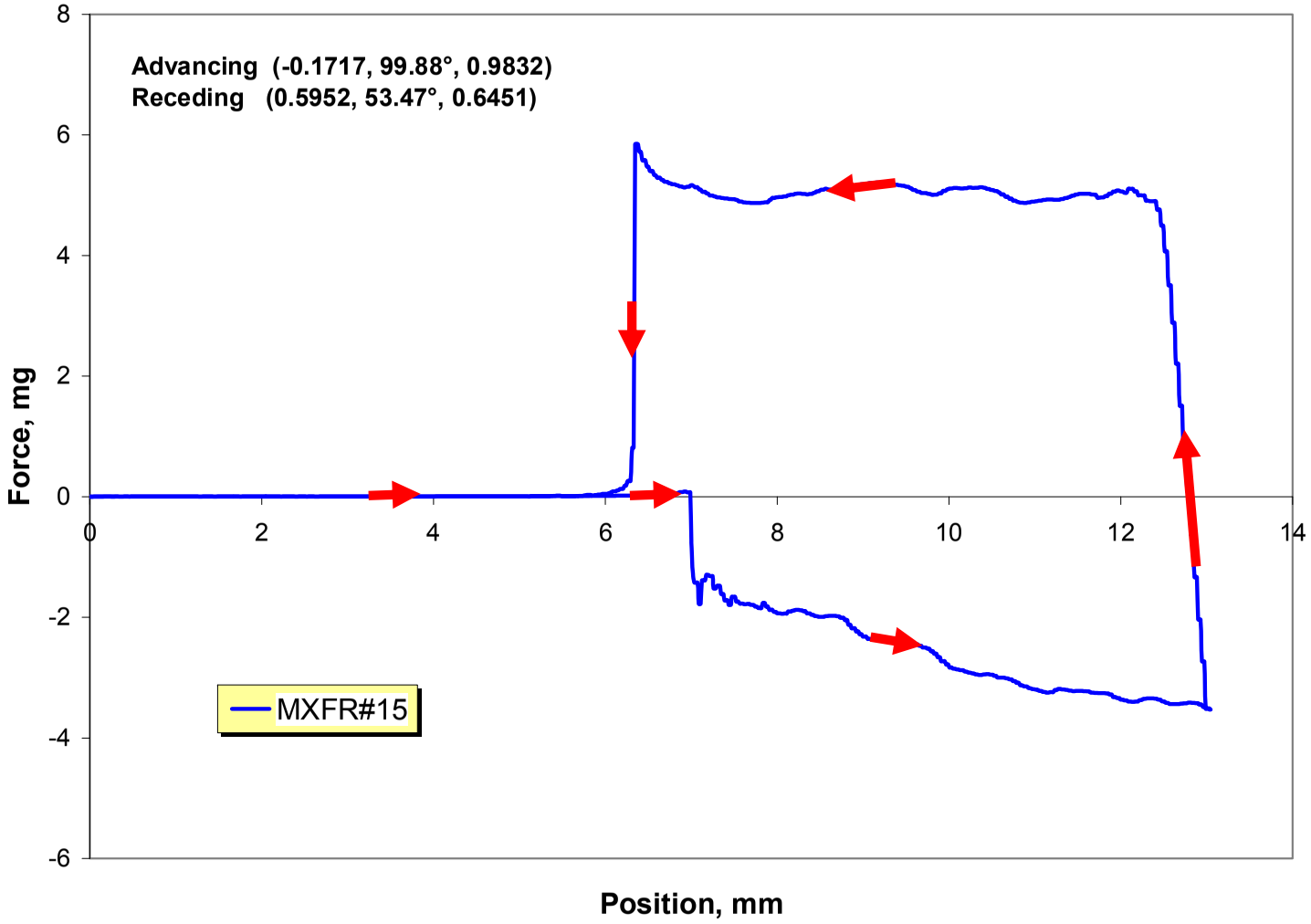

Figure 63c. Slippage of contact line in a dynamic contact angle measurement (uncoated PP 50/280 hollow fiber sample from MXFR #15 [Sirkar and Li, 2003]).

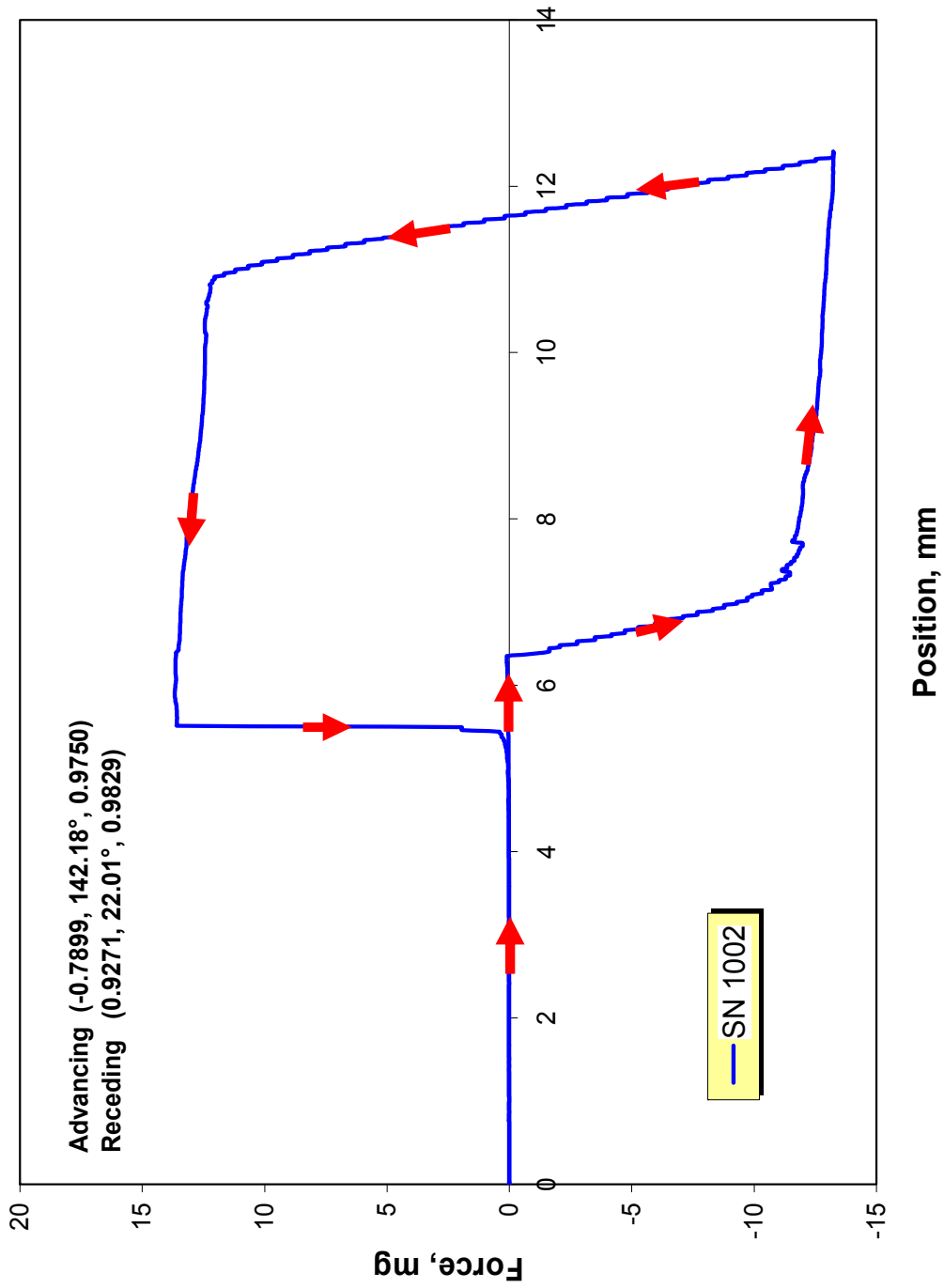

Figure 63d. Slippage of contact line in a dynamic contact angle measurement (coated PP 150/330 hollow fiber sample from S/N 1002 and Li, 2005).

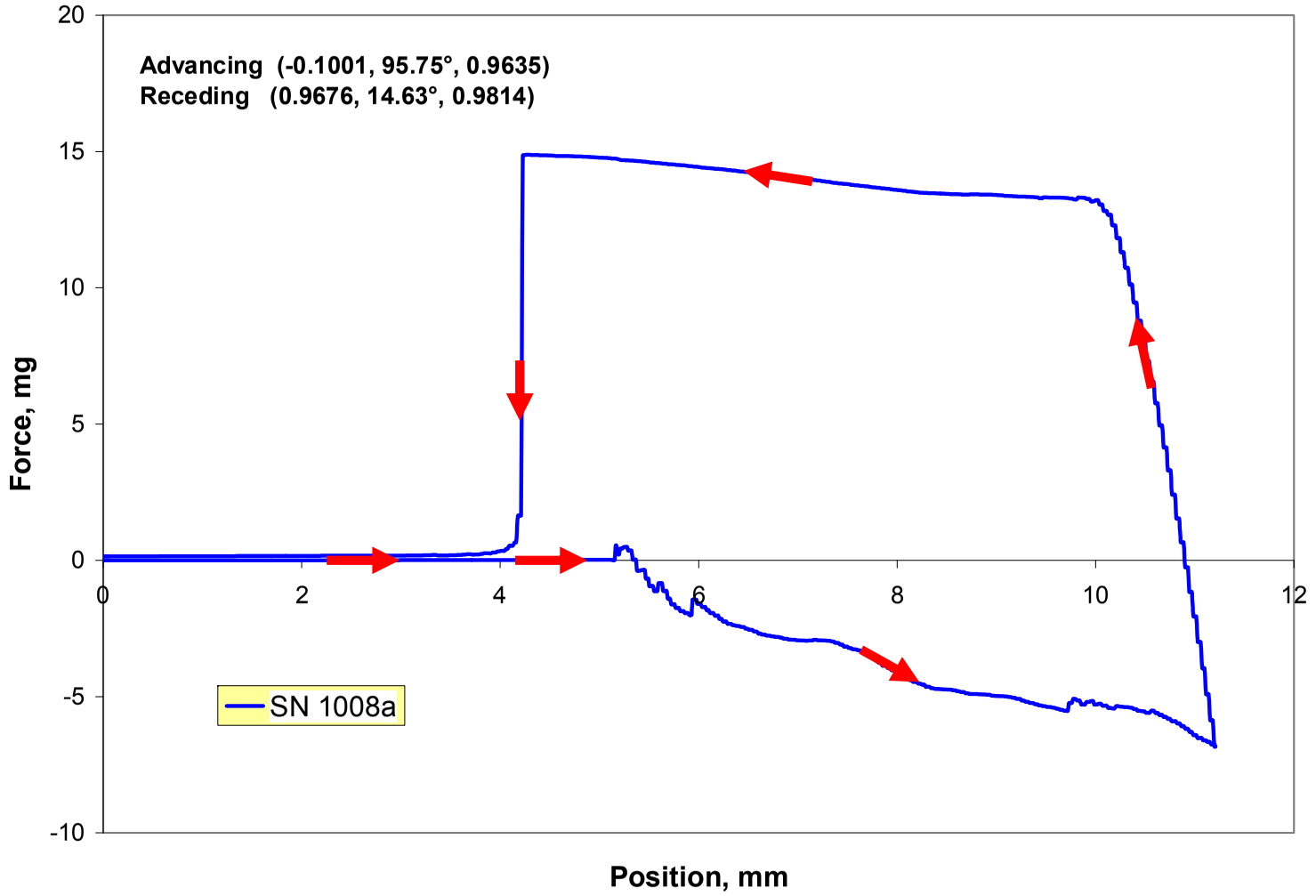

Figure 63e. Slippage of contact line in a dynamic contact angle measurement (coated PP 150/330 hollow fiber sample from S/N 1008).

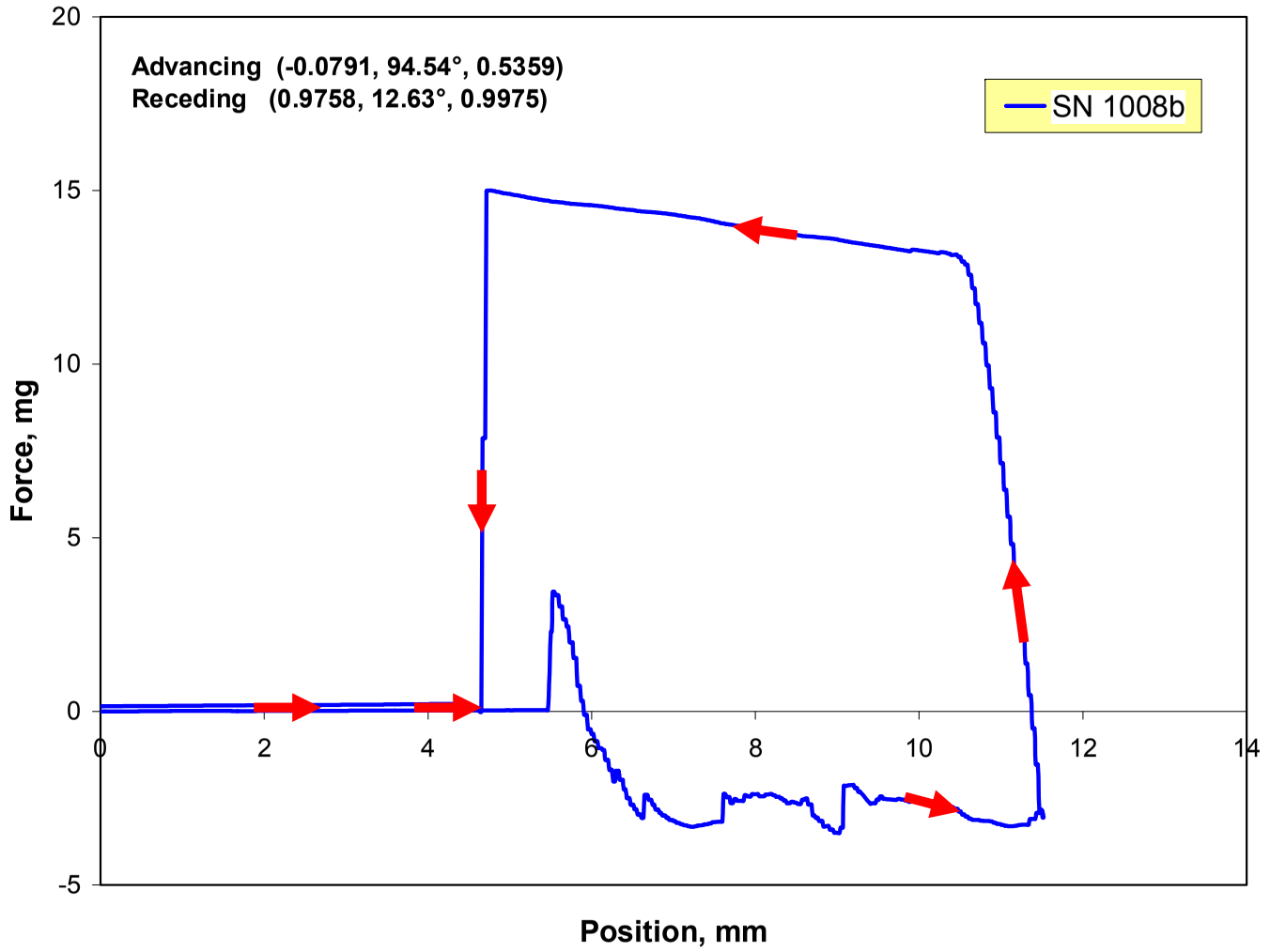

Figure 63f. Slippage of contact line in a dynamic contact angle measurement (coated PP 150/330 hollow fiber sample from S/N 1008).

Table 7. Measured Contact Angles of Hollow Fibers from DCMD Modules

Modules	Specifications	Advancing contact angle (°)	Receding contact angle (°)
[1]MXFR #4	coated PP 150/330	138.34	22.17
[1]MXFR #10	coated PP 50/280	73.13	19.31
[1]MXFR #15	noncoated PP 50/280	99.88	53.47
[2]SN 1002	coated PP 150/330	142.18	22.01
[3]SN 1008a	coated PP 150/330	95.75	14.63
[3]SN 1008b	coated PP 150/330	94.54	12.63

[1] Phase II research (Sirkar and Li, 2003).

[2] Phase III research (Sirkar and Li, 2005).

[3] Different sections of the same fiber.

4.6.6 Polymeric Hollow Fiber Heat Exchanger for Heat Recovery

A large crossflow heat exchanger was obtained from Membrana Inc. (figure 64). This polymeric solid hollow fiber-based heat exchanger (HX) has a surface area per unit volume of 22.5 cm^{-1} and a total heat exchange surface area of around 4 m^2. Heat transfer data were gathered at UTRC facilities using this hollow fiber unit built out of solid polypropylene hollow fibers of the internal diameter 430 μm and the outside diameter 580 μm. The overall dimensions of this heat exchanger are: 38 cm long, shell side housing I.D. 9.7 cm. The system studied was hot brine on one side and cold distillate on the other side.

A schematic of the internal flow pattern in this heat exchanger is provided in figure 65. Figures 66 and 67 provide information on heat transfer rate under three different conditions. Figure 68 provides the inlet and outlet temperatures of the two streams at various values of the shell side city water flow rate.

4.6.7 Pressure Drops Encountered

Generally, the pressure drop encountered in one single-pair unit in hot brine flow on the shell side was less than 3 psi at the highest flow rate. The pressure drop encountered on the distillate side per single-pair unit was up to 8.5 psi at the highest flow rate. Therefore, an assembly of a couple of modules in one leg of flow will incur significant pressure drop on the distillate side if all of the distillate flows through one module at a time in a countercurrent cascade. It will be useful to put intermediate pumps to prevent any potential leakages.

Figure 64. Photos of solid polypropylene hollow fiber heat exchanger HEPP4 (effective area 3.9 m^2 based on fiber I.D.).

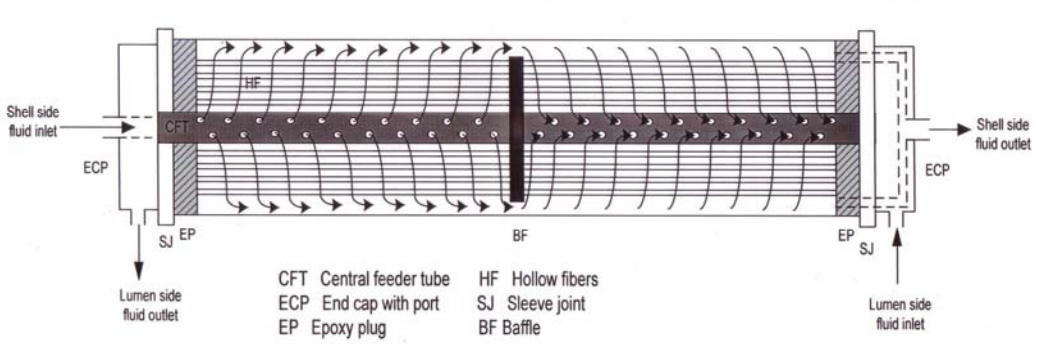

Figure 65. Schematic view of the baffled crossflow HX module.

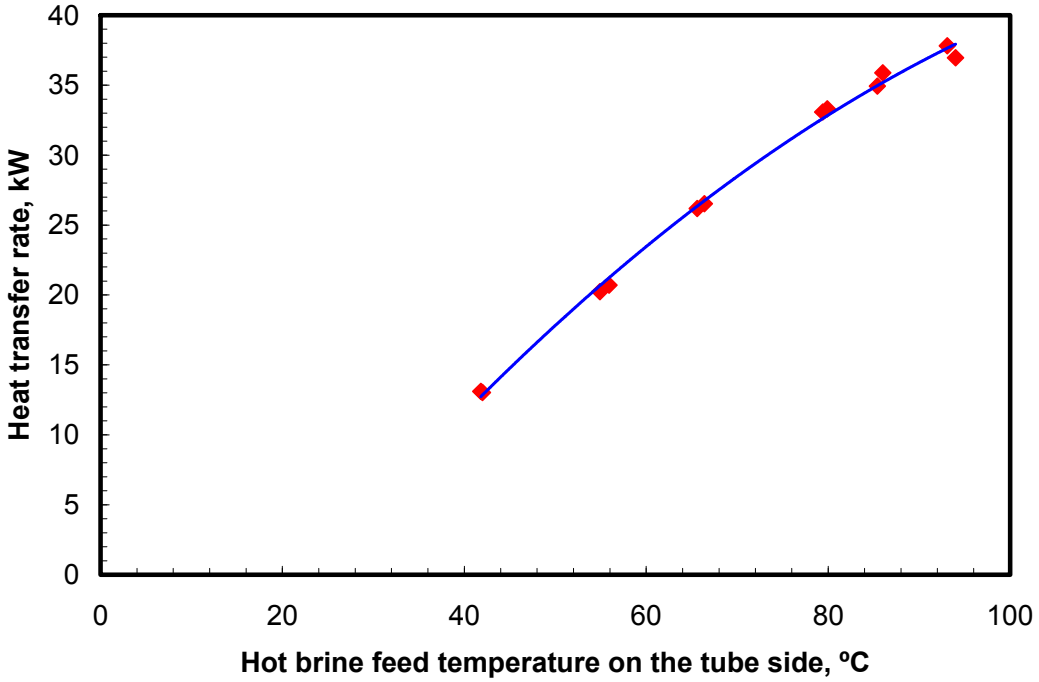

Figure 66. Variation of heat transfer rate of module HEPP4 with feed temperature of hot brine flowing on the tube side at a flow rate 20 L/min (Shell side: city water, flow rate 11.3 L/min, temperature 21.3–22.3 ºC).

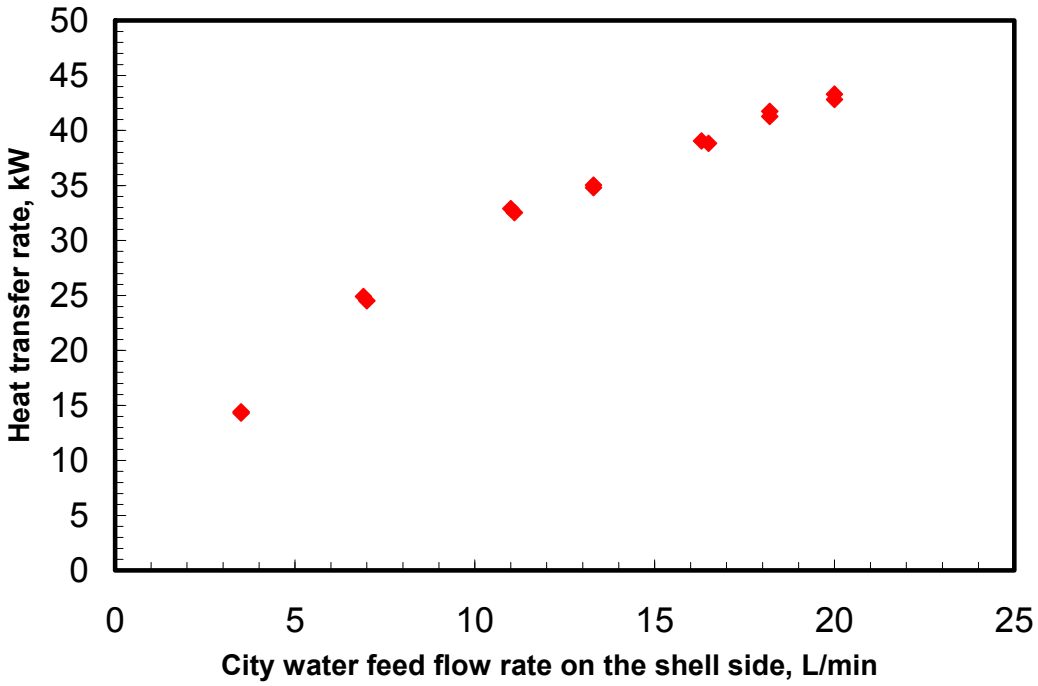

Figure 67. Variation of heat transfer rate of module HEPP4 with flow rate of city water flowing on the shell side at a temperature 20–23.4 ºC (tube side: hot brine, flow rate 20 L/min, temperature 89.6–90.7 ºC).

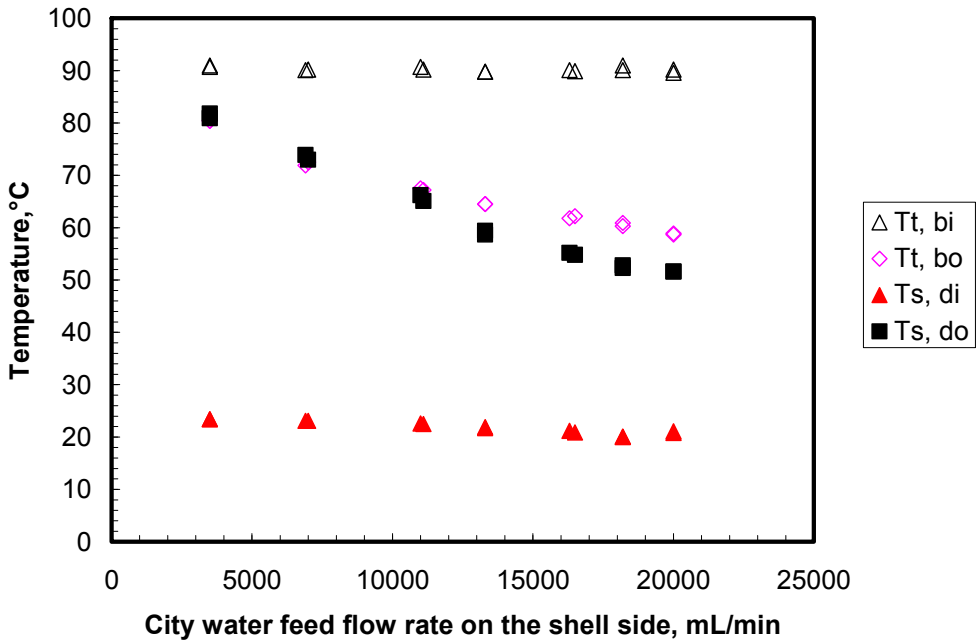

Figure 68. Variation of temperature at the inlet and outlet of module HEPP4 with flow rate of city water flowing on the shell side at a temperature 20–23.4 ºC (tube side: hot brine, flow rate 20 L/min, temperature 89.6–90.7 ºC)($T_{t,\,bi}$.- inlet temperature on the tube side; $T_{t,bo}$ – outlet temperature on the tube side; $T_{s,di}$ – inlet temperature on the shell side; $T_{s,do}$ – outlet temperature on the shell side).

4.7 TASK 7: Project the Cost of Water Production in a Large-Scale Plant Based on Pilot Plant Data and Analysis

An analysis of the cost of water production by this direct contact membrane distillation process is provided here. The schematic adopted for analysis is shown in figure 69. Note the most important point in this figure. The distillate was heated up by the DCMD process, and the brine was concentrated and cooled down. Most of the concentrated brine was recirculated, and only a small part of the brine was rejected back to the sea. The heat from the distillate was recovered via a recuperator (distillate heat recovery heat exchanger) by the brine, which consisted of the recycled brine stream and fresh seawater. The distillate coming out of the recuperator (distillate heat recovery heat exchanger) needed to be cooled further before introduction into the DCMD unit. We used the seawater heat exchanger to provide this cooling. This means that the flow rate through this HX on the brine side was much larger than the actual fresh seawater brine fed into our process. The calculations were carried out for 1 million gallons per day (mgd) distillate production rate. The methodologies employed were adopted from Ray (2001) and Sirkar and Li (2005).

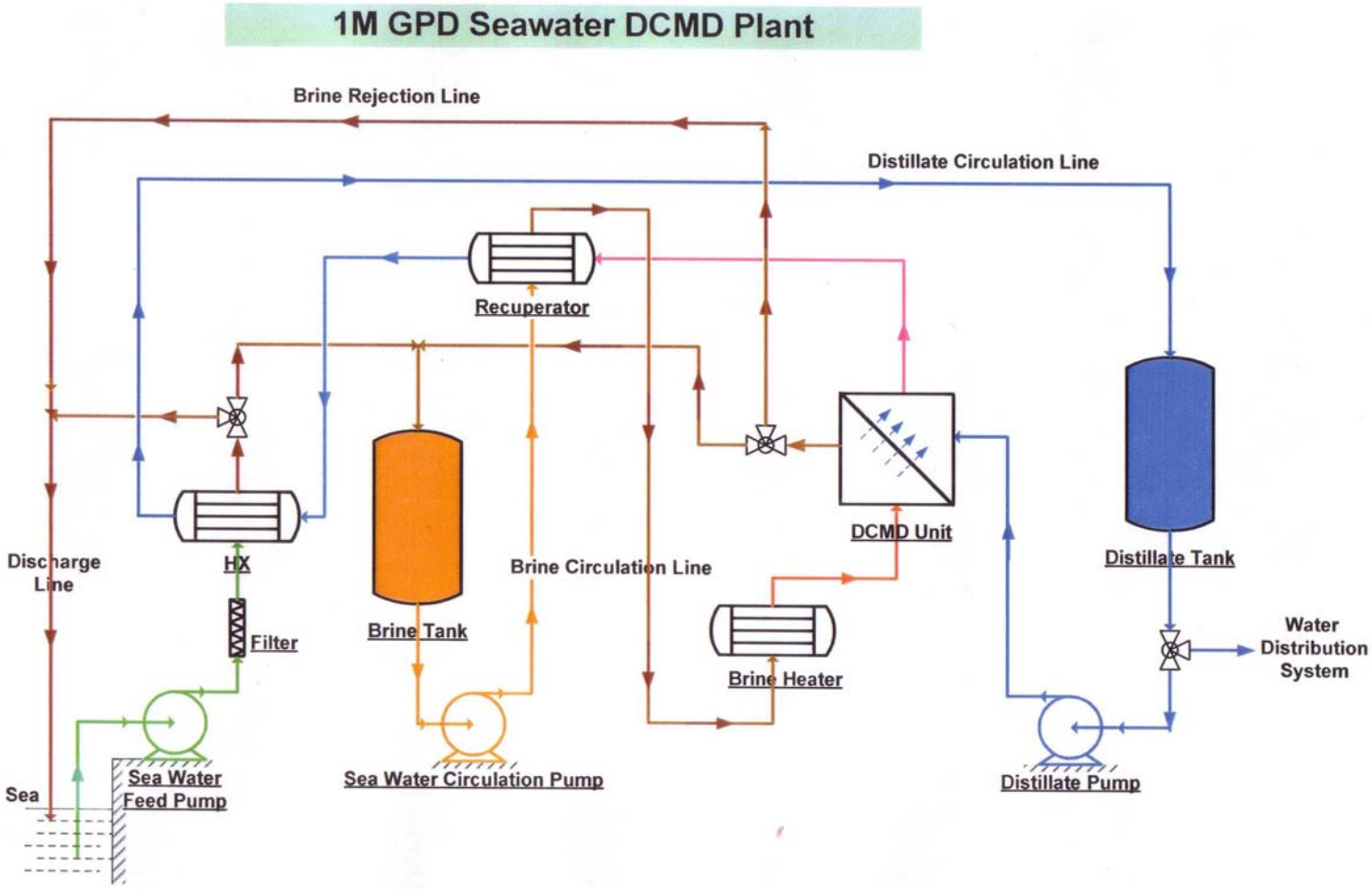

Figure 69. Flow diagram of 1-mgd seawater DCMD desalination plant with hollow fiber heat exchangers for heat recovery.

Table 8 provides the details of the mass and energy balance and the surface area required for the membrane and the heat exchanger. The mathematical model developed in section 4.6.3 was used for the DCMD calculations. Table 9 provides the cost factors employed in this economic analysis for 1-mpd DCMD seawater desalination plant. The calculation of production cost was based on the capital cost and operating cost. Note that polymeric hollow fiber heat exchangers (PHFHEs) were developed recently (Zarkadas and Sirkar, 2004; Song, Christian, Li, etc., 2006) and used for cost estimation in this desalination process (recuperator, seawater heat exchanger, and steam heater). The same cost factor and lifetime for the PHFHEs were taken as those of DCMD units.

Table 8. Mass Balance and Energy Balance for One 1-mgd DCMD Seawater Desalination Plant

DCMD Performance		
Overall product recovery (y)	%	80
Evaporation efficiency (η)	%	80
Production rate (P)	gpd	1,000,000
Production rate (P)	L/min	2,628.5
Seawater refill rate (F)	L/min	3,285.6
Seawater concentrate discharge rate (BCDR)	L/min	657.1
Seawater discharge temperature (T_{BD})	°C	25.2
Seawater circulation feed flow rate (B_i)	L/min	34,266.7
Seawater circulation outlet flow rate (B_o)	L/min	31,638.2
Seawater circulation inlet temperature ($T_{b,\,i}$)	°C	90
Seawater circulation outlet temperature ($T_{b,\,o}$)	°C	37.3
Distillate circulation feed flow rate (D_i)	L/min	26,385.4
Distillate circulation outlet flow rate (D_o)	L/min	29,013.84
Distillate circulation inlet temperature ($T_{d,\,i}$)	°C	20
Distillate circulation outlet temperature ($T_{d,\,o}$)	°C	88.5
Water vapor flux rate (N_v)	kg/m^2/h	8.1
DCMD membrane area (A_{DCMD})	m^2	19,470.2
Heat transferred (Q_{DCMD})	kJ/s	125,947.6
Recuperator		
Overall heat transfer coefficient (U_{HX1})	W/m^2/K	1,000
Energy Recovery percent for Recuperator (ERP_{HX1})	%	80.9
Overall energy recovery percent ($ERP_{overall}$)	%	82.7
Seawater inlet flow rate ($B_{HX1,i}$)	L/min	30,981.1
Seawater outlet flow rate ($B_{HX1,o}$)	L/min	30,981.1
Seawater inlet temperature ($T_{b,\,HX1,i}$)	°C	37.31
Seawater outlet temperature ($T_{b,\,HX1,o}$)	°C	84.5
Distillate inlet flow rate ($D_{HX1,i}$)	L/min	29,013.8
Distillate outlet flow rate ($D_{HX1,o}$)	L/min	29,013.8

Table 8. Mass Balance and Energy Balance for One 1-mgd DCMD Seawater Desalination Plant (continued)

Recuperator (continued)		
Distillate inlet temperature ($T_{d,\ HX1,i}$)	°C	88.5
Distillate outlet temperature ($T_{d,\ HX1,o}$)	°C	38.1
Heat transfer rate (Q_{HX1})	kJ/s	101,885.6
Log mean temperature difference ($\Delta T_{lm,HX1}$)	°C	2.0
Heat exchanger area (A_{HX1})	m^2	51,188.4
HX (Heat Exchanger)		
Overall heat transfer coefficient (U_{HX2})	$W/m^2.K$	800
Effective energy recovery percent (ERP_{HX2})	%	6.3
Seawater inlet flow rate ($B_{HX2,i}$)	L/min	52,498.3
Seawater outlet flow rate ($B_{HX2,o}$)	L/min	52,498.3
Seawater inlet temperature ($T_{b,\ HX2,i}$)	°C	15
Seawater outlet temperature ($T_{b,\ HX2,o}$)	°C	25
Distillate inlet flow rate ($D_{HX2,i}$)	L/min	29,013.8
Distillate outlet flow rate ($D_{HX2,o}$)	L/min	29,013.8
Distillate inlet temperature ($T_{d,\ HX2,i}$)	°C	38.1
Distillate outlet temperature ($T_{d,\ HX2,o}$)	°C	20
Heat transfer rate (Q_{HX2})	kJ/s	36,608.8
Log mean temperature difference ($\Delta T_{lm,\ HX2}$)	°C	8.4
Heat exchanger area (A_{HX2})	m^2	5,442.8
Effective heat recovery for system (Q'_{HX2})	kJ/s	2,291.2
Steam Heater		
Overall heat transfer coefficient (U_{HX3})	$W/m^2.K$	1,000
Seawater inlet flow rate ($B_{HX3,i}$)	L/min	34,266.7
Seawater outlet flow rate ($B_{HX3,o}$)	L/min	34,266.7
Seawater inlet temperature ($T_{b,\ HX3,i}$)	°C	78.8
Seawater outlet temperature ($T_{b,\ HX3,o}$)	°C	90
Steam inlet mass flow rate ($S_{HX3,i}$)	kg/min	682.4
Steam outlet mass flow rate ($S_{HX3,o}$)	kg/min	682.4
Steam inlet temperature ($T_{s,\ HX3,i}$)	°C	110
Steam outlet temperature ($T_{s,\ HX3,o}$)	°C	78.8
Heat transfer rate (Q_{HX3})	kJ/s	26,878.3
Temperature difference (ΔT_{HX3})	°C	15
Heat exchanger area (A_{HX3})	m^2	1,791.9
Ratio of kilogram (kg) water product to kg steam (110 °C)	–	3.85

Table 9. Cost Factors Used in Economic Analysis for 1-mgd DCMD Seawater Desalination Plant

Item	Unit	Quantity
DCMD area cost	$/m^2	20.00
Hollow fiber HX area cost	$/m^2	20.00
Electricity	$/kWh	[1]0.05
Exhaust steam	$/1,000 kg	[1]2.00 or 1.73[b] or 0.73[c]
Membrane lifetime	year	4
System lifetime (r)	year	15
Annual interest rate (i)	%	12
Downtime (Dt)	%	15
Pump efficiency	%	82

[1] Peters, M.S., K.D. Timmerhaus, R.E. West, 2003. *Plant Design and Economics for Chemical Engineers* (*5th Edition*), Table B-1, p. 898, McGraw-Hill, New York, New York.

For a comparison between RO and DCMD, the values for RO were taken from Ray (2001), which had the following assumptions: water production rate, 1-mgd; operating pressure, 1,000 psi; 30% recovery; a feed flow rate of 2.3 kilogallons (kgal) per minute; energy recovery, 30%; estimated lifetime, 3 years.

Table 10 provides the results and a comparison with the cost of RO. It appears that without considering the cost of waste heat, the total production cost of water by the DCMD process is $2.63/1,000 gal, which is much cheaper than RO ($4.48/1,000 gal). When the cost of steam is taken into account, DCMD is either competitive with RO or cheaper than RO depending on the steam cost. Three levels of steam costs were used. Note that DCMD can produce a water product of much lower salinity (less than 1 ppm in our pilot-scale studies) than single-pass RO (> 200 ppm). Therefore, DCMD would look even economically better compared with RO for the production of high-purity water.

Table 10. Summary of Representative Costs for RO Treatment and DCMD Treatment

Cost Category	RO[1]	DCMD
CAPITAL COSTS ($/gal/day)		
Direct		
Site development	0.10	0.10
Water	0.09	0.09
Utilities	0.16	0.16
Equipment [2]	3.34	2.48
Land [3]	—	—
Other	—	—
Total direct capital costs	3.69	2.83
Indirect		
Construction overhead	0.44	0.34
Contingency	0.37	0.28
Other	—	—
Total indirect capital costs	0.81	0.62
Total capital costs	4.50	3.45
OPERATING COSTS ($/1,000 gallons)		
Energy [4]	1.34	0.21
Membrane replacement	0.41	0.27
Labor and overhead	0.30	0.30
Spare parts	0.09	0.09
Chemicals	0.16	0.08
Filters	0.05	0.05
Cooling water	—	—
Exhaust steam [5]	—	$(1.96)^a$ $(1.70)^b$ $(0.72)^c$
Other (ion exchange beds)	—	—
Total operating costs	2.35	1.00^d $(2.96)^a$ $(2.70)^b$ $(1.72)^c$
Capital recovery costs [6]	2.13	1.63
Total production costs ($/1,000 gallons)	4.48	2.63^d $(4.59)^a$ $(4.33)^b$ $(3.35)^c$

[1] Quoted from Ray in *Membrane Handbook* (2001), p. 368.

[a] Calculated using steam cost $2.00/1,000 kg steam.

[b] Calculated using steam cost $ 1.73/1,000 kg steam.

[c] Calculated using steam cost $ 0.73/1,000 kg steam.

[d] Calculated without considering the steam cost.

[2] Categories of equipment costs ($/gal/day).

Table 10. Summary of Representative Costs for RO Treatment and DCMD Treatment (continued)

Component	RO	DCMD
Pretreatment①	0.5	0.3
Membrane module	0.5	0.39
Pumps②	0.8	0.05
Controls, pressure vessels, electrical subsystems, heat exchangers, power recovery system③	1.2	1.70
Shipping and installation	0.17	0.17
Equipment related engineering	0.17	0.17
Total	3.34	2.48

① Pretreatment cost of seawater for DCMD is much lower than that for RO because almost no chemical treatment is needed in DCMD application.

② Pump cost for RO is referred to from the Reclamation letter (Denver Federal Center) on June 23, 1999. The pump cost for DCMD is calculated as follows:

Seawater circulation pump

Pressure difference = 10 psi

Power requirement: $E_1 = \frac{10(psi) \times 6.9 \times 10^3 (Pa/psi) \times 0.57(m^3/s)}{0.82} = 48.1(kW)$

Capacity factor = 40 (m^3/s × kPa)

Cost of pump: \$ 1.2 × 10^4 (Peters, Timmerhaus, and West [2003]), figure12-20, page 518)

Seawater feed/cooling pump

Pressure difference = 10 psi

Power requirement: $E_2 = \frac{10(psi) \times 6.9 \times 10^3 (Pa/psi) \times 0.88(m^3/s)}{0.82} = 73.7(kW)$

Capacity factor = 60.4 (m^3/s × kPa)

Cost of pump: \$ 1.9 × 10^4 (Peters, Timmerhaus, and West (2003), figure 12-20, page 518)

Distillate circulation pump

Power requirement: $E_3 = \frac{15(psi) \times 6.9 \times 10^3 (Pa/psi) \times 0.44(m^3/s)}{0.82} = 55.6(kW)$

Capacity factor = 45.5 (m^3/s × kPa)

Cost of pump: \$ 1.9 × 10^4 (Peters, Timmerhaus, and West (2003), figure 12-20, page 518)

Total pump costs (\$/gallon/day) = $\frac{(1.2+1.9+1.6) \times 10^4}{10^6} = 0.05$

③ Here we have found that the cost of all items except energy recovery system (used in RO process) is \$0.6/gal/day. The cost calculations for heat exchangers (if needed in DCMD process) are based on the most recent experiments.

We propose here that the distillate is cooled down by seawater (15 °C).

Cost of recuperator: $\$1.02 \times 10^6$

Cost of seawater heat exchanger: $\$1.09 \times 10^5$

Cost of steam heater: $\$3.58 \times 10^4$

Total capital cost for heat exchangers: $\$(10.2+1.09+0.358) \times 10^5 = \$1.168 \times 10^6$

The cost in \$/gallon/day: 1.168×10^6(\$)/10^6(gallon/day)) = \$1.17/gallon/day

[3] Normally, the land-related costs are negligible.

Table 10. Summary of Representative Costs for RO Treatment and DCMD Treatment (continued)

[4] Energy costs include costs for pumps for feed well, high-pressure pumps, cooling, heating, pretreatment system, and instrumentation. Suppose industrial waste heat is available; the heat cost can be neglected in DCMD. The dominant energy cost in most installations is for the high-pressure pumps in RO applications; DCMD pumps are low pressure centrifugal pumps.
The representative energy costs can be calculated for a single-stage system using the equation

$$E_P = \frac{q_v \Delta P}{\eta}$$

where q_v = flow rate (m^3/s); ΔP = pressure difference (Pa); η = efficiency of pump and motor (%)

RO: consumption of energy

$$E_0 = \frac{1000(psi) \times 6.9 \times 10^3 (Pa/psi) \times 0.15(m^3/s)}{0.65} = 1592(kW)$$

Recovery of energy = 1,592(kW) × 30% = 477.6 (kW)
So the total energy consumption = 1,592(kW) – 477.6(kW) = 1,114.4 (kW)
Energy cost of 1,000 gallon water produced =

$$\frac{1114.4(kW) \times 24(hr) \times 0.05(\$)}{1000(gallon)} = 1.34(\$)/kgallon$$

Here pressure difference = 1,000 psi; 1 psi=6.9 × 10^3Pa; η = 0.65; electricity price = \$0.05/(kW· hr).

DCMD: Energy cost for pumps = $\frac{(48.1 + 73.7 + 55.6kW) \times (24h) \times (\$0.05/kWh)}{1000kgallon}$

= \$0.21 per kgal

[5] Calculation of waste heat cost for producing 1,000 gallons distillate water

(Latent heat of water: 540 cal/g; Specific heat of water: 1 cal/g/^{o}C; Specific heat of super-heated steam: 0.49 cal/g/^{o}C; Cost of exhaust steam: \$2/1,000 kg)

Cost of steam for producing 1 kgal distillate:

$$\frac{(682kg/\min) \times (24h) \times (60\min/h) \times (\$2.00/1000kg)}{1000kgallon} = \$1.96/kgallon$$

[+] Peters, M.S., K.D. Timmerhaus, R.E. West, *Plant Design and Economics for Chemical Engineers* (5th Edition), table B-1, p. 898, McGraw-Hill, New York, 2003.

[6] Capital recovery costs = $\frac{(total\ capital\ cost) \times 1000 \times i \times [1 + (i/100)]^r}{365 \times (100 - Dt) \times [(1 + i/100)^r - 1]}$

where r is system lifetime (yr), i is the annual interest rate (%), and Dt represents downtime (%). A system lifetime (exclusive of membrane replacement) of 15 years, an interest rate of 12%, and a downtime percentage of 15% are used as representative values.

4.8 TASK 8: Dismantle Pilot Plant

UTRC has decided to pay for the expense incurred to build the pilot plant. Reclamation has agreed that for an appropriate compensation to Reclamation, the pilot plant could stay at UTRC.

5. Analysis of Results and Commercial Viability of the Project

An analysis of the results obtained in the pilot plant project indicates the following:

1. The scaleup of crossflow hollow fiber membrane modules was successful. The DCMD pilot plant was operated with ease using membrane surface areas between 1.30 m^2 (14.0 ft^2) and 6.6 m^2. The membranes did not allow any salt leakage. Therefore, fiber potting problems encountered in the Phase III project were solved. However, the fluorosilicone coating on the outside of the fibers appeared to be somewhat less permeable.

2. Hot brine velocity and module configurations, especially with respect to the brine flow, are very important in determining the module productivity. Higher brine velocity leads to higher flux; the brine Reynolds numbers are in the range of about 100–290.

3. Three months' of runs with startup and shutdown on a daily basis indicated that the hollow fibers and the modules are rugged; they were exposed to hot brine coming in at 90–93 °C (194–199.4 °F).

4. Back-to-back stacking of two modules led to as much as a 1.30-m^2 membrane area. Although 9–10 modules were used requiring very limited space, efforts should be made for redesigning modules, large numbers of which have to be employed in larger-scale plants.

5. The pilot plant achieved a productivity of a 0.62-gpm (2.35-L/min) distillate production rate. The average flux at this level of production varied between 15 to 33 kg/m^2/h (8.8–19.4 gfd). Larger brine flow rate and/or a larger number of modules would have easily yielded a 1-gpm distillate production rate. The productivity limitation was introduced by the distillate cooling side capacity limitation at the site. We, therefore, proposed employing the brine source under ambient conditions to provide distillate cooling in future larger-scale operations.

6. The model developed to describe the performance of DCMD modules predicted successfully the observed performances of modules at three scales: MXFR #3 (119 cm^2); S/N 1004 (0.28 m^2); S/N 1006–1015 (0.61–0.66 m^2). Further, the model also described the performances of the pilot plant with eight modules in two parallel legs for 6% and 10% NaCl solutions. One can now employ such a model for designing larger plants with appropriate considerations.

7. An item which requires additional experimental investigation is the membrane mass transfer coefficient k_m. In fact, an increase in k_m will lead to higher fluxes; therefore, additional membrane development should focus on it.

8. The pressure drop encountered on the brine side of the membrane was minor in the range of 1–3 psi (6.9–20.7 kPa). The pressure drop encountered on the distillate side, however, was up to 8.5 psi. Intermediate pumps can be used to reduce the pressure rise when the distillate flows through a countercurrent DCMD cascade.

9. Conservative cost calculations indicate that if the steam cost for the brine heater is not too high, this DCMD process is competitive with RO. In fact, if lower levels of published low-pressure steam costs are used, DCMD may be cheaper. This process can go to much higher levels of salt concentration than RO. If the cost of the concentrated brine disposal is taken into account for inland desalination applications, the economics of DCMD-based desalination will be even better.

10. United Technologies, at whose research center the pilot plant was built and operated, has become very interested in further development and commercialization of this technology.

6. References

Adam, N.K. *The physics and chemistry of surfaces*, Dover Publications, New York, p. 383, 1968.

Banat, F.A. and J. Simandl. "Theoretical and experimental study in membrane distillation," *Desalination*, 95, 39–52, 1994.

Bhattacharyya, D., M.E. Williams, R.J. Ray, and S.B. McCray. "Reverse Osmosis: Design," in W.S. Ho and K.K. Sirkar, eds., *Membrane Handbook*, chapter. 23, Kluwer Academic, Boston, 2001.

Bureau of Reclamation, U.S. Department of the Interior. *Desalination Roadmap*, *Desalination and Water Purification Technology Roadmap – A Report of the Executive Committee*, *Desalination and Water Purification Research and Development Program Report No. 95*, Bureau of Reclamation and Sandia National Laboratories, January 2003.

Calabro, V., B.L. Jiao, and E. Drioli. "Theoretical and experimental study on membrane distillation in the concentration of orange juice," *Ind. Eng. Chem. Res.*, 33, 1803–1808, 1994.

Drioli, E., Y. Wu, and V. Calabro. "Membrane distillation in the treatment of aqueous solutions," *J. Membr. Sci.*, 33, 277–284, 1987.

Findley, M.E. "Vaporization through porous membranes," *Ind. Eng. Chem. Process Des. Dev*., 6 (2), 226, 1967.

Gore, D.W. "Gore-Tex membrane distillation," in *Proceedings of the 10th Annual Convention of Water Supply Improvement Association*, Honolulu, Hawaii, July 25–29, 1982.

Guijt, C.M., G.W. Meindersma,, T. Reith, and A.B. de Haan. "Air gap membrane distillation 1. modeling and mass transport properties for hollow fiber membranes," *Sep. Puri. Tech*., 43, 233-244, 2005.

Howe, E.D. *Fundamentals of Water Desalination*, Marcel Dekker, New York, p. 71, 1974.

Kreith, F., and M.S. Bohn. *Principles of Heat Transfer* (6th edition), Appendix 2, Brooks/Cole, A26, 2001.

Lawson, K.W., and D.R. Lloyd. Membrane Distillation, *J. Membrane Sci.*, 124, 1–25, 1997.

Li, B., and K.K. Sirkar. "Novel membrane and device for direct contact membrane distillation-based desalination process," *Ind. Eng. Chem. Res.*, 43, 5300–5309, 2004.

Li, B., and K.K. Sirkar. "Novel membrane and device for vacuum membrane distillation-based desalination process," *J. Membrane. Sci.*, 257, 60–75, 2005.

Mark, J.E. *Polymer Data Handbook*, Oxford University Press, New York, 1999.

Maron, M.J., and R.J. Lopez. *Numerical Analysis: A Practical Approach, Wadsworth*, 210–214, 1991.

Martinez-Diez, L., and F.J. Florido-Diaz. "Desalination of brine by membrane distillation, *Desalination*," 137, 267–273, 2001.

Martinez-Diez, L., and M.I. Vazquez-Gonzalez. "Temperature polarization in mass transport through hydrophobic membranes," *AIChE J*., 42 (7), 1844–1852, 1996.

Pan, C.Y., and H.W. Habgood. "Gas separation by permeation Part II: effect of permeate pressure drop and choice of permeate pressure," *The Canadian Journal of Chemical Engineering*, 56, 210–217, 1978.

Phattaranawik, J., R. Jiraratananon, A.G. and Fane. "Effects of net-type spacers on heat and mass transfer in direct contact membrane distillation and comparison with ultrafiltration studies," *J. Membrane Sci.*, 217, 193–206, 2003.

Peters, M.S., K.D. Timmerhaus, R.E. West. *Plant Design and Economics for Chemical Engineers* (5th edition), Table B-1, p. 898, McGraw-Hill, New York, 2003.

Ray, R. "Cost Estimates," in W.S. Ho and K.K. Sirkar, eds., *Membrane Handbook*, Chapter 25, Kluwer Academic Publishers, Boston, 2001.

Schneider, K., W. Hölz, and R. Wollbeck. "Membranes and modules for transmembrane distillation," *J. Membrane Sci.*, 39, 25–42, 1988.

Schofield, R.W., A.G. Fane, and C.J.D. Fell. "Heat and Mass Transfer in Membrane Distillation," *J. Membrane Sci.*, 33, 299, 1987.

Schofield, R.W., A.G. Fane, C.J.D. Fell, and R. Macoun. "Factors Affecting Flux in Membrane Distillation," *Desalination*, 77, 279–294, 1990a.

Schofield, R.W., A.G. Fane, and C.J.D. Fell. "Gas and Vapor Transport through Microporous Membranes," II. Membrane Distillation, *J. Membrane Sci.*, 53, 173, 1990b.

Schofield, R.W., A.G. Fane, and C.J.D. Fell. "Gas and vapor transport through microporous membranes," I. Knudsen-Poiseuille transition, *J. Membrane Sci.*, 53, 159–171, 1990c.

Sieder, E.N., and C.E. Tate. "Heat transfer and pressure drop of liquids in tubes," *Ind. Eng. Chem. Res.*, 28, 1429–1435, 1936.

Sirkar, K.K., "Other New Membrane Processes," in W.S. Ho and K.K. Sirkar, eds., *Membrane Handbook*, Chapter 46, Van Nostrand Reinhold: New York, 1992.

Sirkar, K.K., and B. Li. *Novel Membrane and Device for Direct Contact Membrane Distillation-Based Desalination Process: Phase II*, *Desalination and Water Purification Research and Development Program Report No. 96*, July 2003.

Sirkar, K.K. and B. Li. *Novel Membrane and Device for Direct Contact Membrane Distillation-Based Desalination Process: Phase III*, *Desalination and Water Purification Research and Development Program Report No. 99*, 2005.

Smith, J.M., H.C. Van Ness, and M.M. Abbott. *Vapor/Liquid Equilibrium: Introduction, Introduction to Chemical Engineering Thermodynamics* (6^{th} edition), McGraw-Hill Higher Education, 328-367, International Edition, 2001.

Song, L., S.O. Christian, B. Li, D.M. Zarkadas, and K.K. Sirkar. "Compact polymeric hollow fiber heat exchangers (PHFHEs): multiscale performance studies and modeling, in section Fundamental Research in Transport Processes III," #279g, AIChE Annual Meeting, San Francisco, California, 2006.

Steinbruchel, A.B., and R.D. Rhinesmith. "Design of Distilling Plants," in K.S. Spiegler and A.D.K. Laird (eds.),*Principles of Desalination*, Part A, 2^{nd} edition., Academic Press, New York, p. 114, 1980.

Van Gassel, T.J., and K. Schneider. "An energy-efficient membrane distillation process," in E. Drioli and M. Nagaki (eds.), *Membranes and Membrane Processes*, Plenum Press: New York, 343–348, 1986.

Wickramasinghe, S.R.J., M.J. Semmens, and E.L. Cussler. "Mass transfer in various hollow fiber geometries," *J. Membrane Sci.*, 69, 235-250, 1992.

Zarkadas, D.M., and K.K. Sirkar. "Polymeric hollow fiber heat exchangers: an alternative for lower temperature applications," *Ind. Eng. Chem. Res.*, 43, 8093–8106, 2004.

Žukauskas, A. "Heat transfer from tubes in crossflow," *Advance in Heat Transfer*, 18, 87–159, 1987.